ERDC/GSL TR-17-9

Geotechnical and Structures Laboratory

US Army Corps
of Engineers®
Engineer Research and
Development Center

ERDC
INNOVATIVE SOLUTIONS
for a safer, better world

# Full-Scale Accelerated Testing of Multi-axial Geogrid Stabilized Flexible Pavements

W. Jeremy Robinson, Jeb S. Tingle, and Gregory J. Norwood

June 2017



Approved for public release; distribution is unlimited.

**The U.S. Army Engineer Research and Development Center (ERDC)** solves the nation's toughest engineering and environmental challenges. ERDC develops innovative solutions in civil and military engineering, geospatial sciences, water resources, and environmental sciences for the Army, the Department of Defense, civilian agencies, and our nation's public good. Find out more at www.erdc.usace.army.mil.

To search for other technical reports published by ERDC, visit the ERDC online library at http://acwc.sdp.sirsi.net/client/default.

ERDC/GSL TR-17-9
June 2017

# Full-Scale Accelerated Testing of Multi-axial Geogrid Stabilized Flexible Pavements

W. Jeremy Robinson, P.E., Jeb S. Tingle, and Gregory J. Norwood, P.E.

*Geotechnical and Structures Laboratory*
*U.S. Army Engineer Research and Development Center*
*3909 Halls Ferry Road*
*Vicksburg, MS 39180-6199*

Final report

Approved for public release; distribution is unlimited.

Prepared for Tensar International Corporation
2500 Northwinds Pkwy #500
Alpharetta, GA 30009

Under Project Number 151098

# Abstract

The U.S. Army Engineer Research and Development Center (ERDC) constructed a full-scale test section to evaluate the performance of geogrid-stabilized highway pavements. The test section consisted of two pavements composed of 3 in. of hot mix asphalt over a crushed limestone base course over a 6 CBR subgrade. One section was stabilized with Tensar's TX5 multi-axial geogrid, and the second section was stabilized with a developmental geogrid referred to as TX8. Each section was instrumented with moisture probes, pore-water pressure probes, temperature probes, earth pressure cells, and asphalt strain gauges. Simulated truck traffic was applied using a heavy vehicle simulator (HVS) to evaluate the rutting performance and collect instrumentation response data. This report summarizes the material characterization and construction techniques, instrumentation response, and performance response of each section under simulated truck traffic. Comparisons are drawn to previous sections constructed and trafficked at ERDC without geogrids utilizing similar construction techniques and material properties.

**DISCLAIMER:** The contents of this report are not to be used for advertising, publication, or promotional purposes. Citation of trade names does not constitute an official endorsement or approval of the use of such commercial products. All product names and trademarks cited are the property of their respective owners. The findings of this report are not to be construed as an official Department of the Army position unless so designated by other authorized documents.

**DESTROY THIS REPORT WHEN NO LONGER NEEDED. DO NOT RETURN IT TO THE ORIGINATOR.**

# Contents

**Abstract** ..... ii

**Figures and Tables** ..... v

**Preface** ..... vii

**Unit Conversion Factors** ..... viii

**1 Introduction** ..... 1

1.1 Background ..... 1
1.2 Objective ..... 1
1.3 Scope ..... 1

**2 Test Plan and Layout** ..... 2

**3 Materials** ..... 4

3.1 Subgrade ..... 4
3.2 Base course ..... 6
3.3 Asphalt ..... 8
3.4 Geogrids ..... 9

**4 Instrumentation** ..... 10

4.1 Earth pressure cells ..... 10
4.2 Asphalt strain gauges ..... 12
4.3 Single-depth deflectometer ..... 13

**5 Pavement Characterization** ..... 15

5.1 As-built properties ..... 15
5.2 Dynamic cone penetrometer ..... 16
5.3 Falling weight deflectometer ..... 16

**6 Traffic Testing** ..... 20

**7 Results** ..... 22

7.1 Surface deformations ..... 22
7.2 Falling weight deflectometer ..... 25
7.3 Earth pressure cells ..... 26
7.4 Single-depth deflectometers ..... 29
7.5 Asphalt strain gauges ..... 30

**8 Post-Traffic Forensics** ..... 32

**9 Analysis** ..... 37

**10 Conclusions and Recommendations** ..... 38

References ..... 39

Appendix A: Earth Pressure Cell Responses ..... 41

Appendix B: Single-Depth Deflectometer Responses ..... 57

Appendix C: Asphalt Strain Gauge Responses ..... 73

Report Documentation Page

# Figures and Tables

## Figures

Figure 1. Test section profile view. 2
Figure 2. Subgrade particle-size analysis. 4
Figure 3. Clay subgrade moisture-density relationship. 5
Figure 4. Clay subgrade CBR/moisture content relationship. 6
Figure 5. Crushed limestone base particle-size analysis. 7
Figure 6. Limestone base moisture/density relationship. 7
Figure 7. Plan view of instrumentation layout. 10
Figure 8. Profile view of instrumentation layout. 11
Figure 9. Earth pressure cell installation in subgrade. 11
Figure 10. Asphalt strain gauge adhered to crushed stone base. 12
Figure 11. Asphalt strain gauge covered with HMA prior to paving. 13
Figure 12. Single-depth deflectometer installation. 14
Figure 13. As-built DCP results for Item 1 Station 25, West. 17
Figure 14. As-built DCP results for Item 2 Station 25, East. 18
Figure 15. As-built ISM values. 19
Figure 16. Dual-wheel tandem axle configuration. 20
Figure 17. Normally distributed traffic pattern. 21
Figure 18. Measurement of maximum rut depth. 22
Figure 19. Accumulated rut depth with traffic. 23
Figure 20. Permanent surface deformation with traffic. 24
Figure 21. ISM change with traffic. 25
Figure 22. Base damage index with traffic. 26
Figure 23. Peak subgrade earth pressure cell response during trafficking. 28
Figure 24. Peak base earth pressure cell response during trafficking. 29
Figure 25. Peak subgrade deflection during trafficking. 30
Figure 26. Peak asphalt tensile strain during trafficking. 31
Figure 27. Item 1 excavated geogrid. 33
Figure 28. Item 2 excavated geogrid. 34
Figure 29. Item 1 indentations in subgrade. 34
Figure 30. Item 2 indentations in subgrade. 35
Figure 31. Post-traffic pavement cross section in Item 1. 35
Figure 32. Post-traffic pavement cross section in Item 2. 36
Figure 33. Post-traffic pavement cross section in unstabilized section. 36

## Tables

Table 1. Hot-mix asphalt properties. 8
Table 2. Geogrid physical properties. 9
Table 3. As-built section properties. 15
Table 4. Maximum rut depth measurements. 24
Table 5. Permanent surface deformation measurements. 24
Table 6. Predicted and measured earth pressure cell responses. 27
Table 7. Predicted and measured single-depth deflectometer responses. 29
Table 8. Predicted and measured asphalt strain gauge responses. 31
Table 9. Post-traffic physical data. 32
Table 10. Effective stabilized layer structural coefficient. 37

# Preface

This study was conducted for Tensar International Corporation located at Alpharetta, Georgia. Dr. Mark H. Wayne, Tensar, provided technical guidance and review during the project. Mr. Jeb S. Tingle was the ERDC program manager.

The work described in this report was performed by the Airfields and Pavements Branch (GMA) of the Engineering Systems and Materials Division (GM), U.S. Army Engineer Research and Development Center, Geotechnical and Structures Laboratory (ERDC-GSL). At the time of publication, Dr. Timothy W. Rushing was Chief, CEERD-GMA; Dr. Gordon W. McMahon was Chief, CEERD-GM; and Ms. Pamela G. Kinnebrew, CEERD-GZT, was Technical Director for Military Engineering. The Deputy Director of ERDC-GSL was Dr. William P. Grogan, and the Director was Mr. Bartley P. Durst.

COL Bryan S. Green was the Commander of ERDC, and Dr. David W. Pittman was the Director.

# Unit Conversion Factors

| Multiply | By | To Obtain |
|---|---|---|
| cubic feet | 0.02831685 | cubic meters |
| cubic inches | 1.6387064 E-05 | cubic meters |
| cubic yards | 0.7645549 | cubic meters |
| degrees Fahrenheit | (F-32)/1.8 | degrees Celsius |
| feet | 0.3048 | meters |
| gallons (U.S. liquid) | 3.785412 E-03 | cubic meters |
| inches | 0.0254 | meters |
| miles per hour | 0.44704 | meters per second |
| mils | 0.0254 | millimeters |
| pounds (force) | 4.448222 | newtons |
| pounds (force) per foot | 14.59390 | newtons per meter |
| pounds (force) per inch | 175.1268 | newtons per meter |
| pounds (force) per square foot | 47.88026 | pascals |
| pounds (force) per square inch | 6.894757 | kilopascals |
| pounds (mass) | 0.45359237 | kilograms |
| pounds (mass) per cubic foot | 16.01846 | kilograms per cubic meter |
| pounds (mass) per cubic inch | 2.757990 E+04 | kilograms per cubic meter |
| pounds (mass) per square foot | 4.882428 | kilograms per square meter |
| pounds (mass) per square yard | 0.542492 | kilograms per square meter |
| square feet | 0.09290304 | square meters |
| square inches | 6.4516 E-04 | square meters |
| tons (force) | 8,896.443 | newtons |
| tons (force) per square foot | 95.76052 | kilopascals |
| yards | 0.9144 | meters |

# 1 Introduction

## 1.1 Background

With increased material costs and reduced budgets, transportation officials are often tasked with applying innovative solutions to pavement design and construction projects. The inclusion of geosynthetics in pavement structures has been utilized as a means of reducing costs and/or extending pavement service life. These products have been shown to be effective in overcoming challenging subsurface conditions, in reducing overall pavement thickness, and in reducing labor and equipment requirements. As new geosynthetic products are developed, full-scale performance data are needed to provide quantifiable benefits to pavement designers.

## 1.2 Objective

The objective of this effort was to construct and traffic full-scale flexible pavement sections to provide performance data for comparing the effectiveness of Tensar's multi-axial geogrids to an unstabilized flexible pavement section. The test items constructed were similar to previously tested unstabilized and stabilized flexible pavement sections allowing for performance comparisons. A secondary objective was to record pavement response data for the verification of mechanistic performance models for Tensar's geogrid stabilization products currently on the market and for the validation of the SpectraPave4Pro™ software used to design the test items.

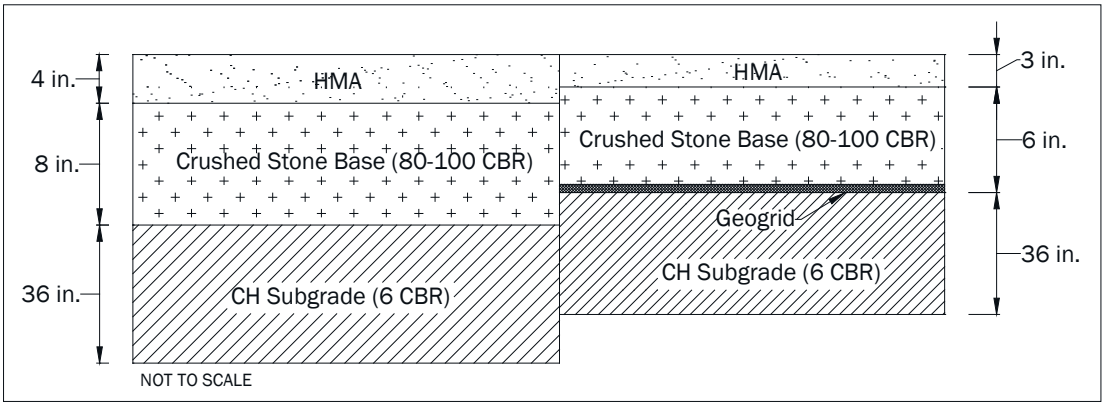
## 1.3 Scope

The scope of this project included the construction and trafficking of a full-scale test section comprised of a geogrid-stabilized base course. The U.S. Army Engineer Research and Development Center (ERDC) constructed the full-scale test section as designed by Tensar under shelter in its Hangar 2 Pavement Test Facility. During construction, quality control data were collected to verify layer properties and to ensure that the project objectives were accomplished. The test items were trafficked with ERDC's Heavy Vehicle Simulator (HVS). Pavement performance data were collected at selected intervals during trafficking for use in comparing the performance of the test items with the geogrid-stabilized base course to the historical test item with an unstabilized base course. In addition, instrumentation response data were collected and reported to support the verification of mechanistic pavement performance models.

# 2 Test Plan and Layout

The structural design of the test section was developed by Tensar Corporation. The test items were constructed utilizing similar materials and construction techniques as previous unstabilized and stabilized sections (Norwood and Tingle 2014) to extend the usefulness of performance comparisons. A profile view of the stabilized and unstabilized test section (Norwood and Tingle 2014) is shown in Figure 1. Each test item consisted of a 10-ft-wide by 50-ft-long testing area. For this study, two test items were constructed with each item stabilized with a different multi-axial geogrid. Item 1 was stabilized with TX5 multi-axial geogrid, and Item 2 was stabilized with a developmental grid identified as TX8. The TX5 multi-axial geogrid was previously tested but due to a temperature control malfunction in the HVS, temperatures rose outside the established control range and the section was reconstructed and retested. The subgrade for the test items was constructed with nominal 36 in. of high-plasticity clay (CH) placed to achieve the target California Bearing Ratio (CBR) value of 6%. A CBR of 6% was selected to provide a test section with moderate subgrade strength. The 6-in.-thick aggregate base course consisted of a crushed limestone, stabilized by placing a multi-axial geogrid at the base-subgrade interface. The test-section surface consisted of a 3-in.-thick hot mix asphalt (HMA) layer. All construction and traffic testing occurred under ERDC's Hangar 2 pavement testing facility, minimizing the potential for moisture variations due to environmental factors.

Figure 1. Test section profile view.



The structural design of the test section was developed by Tensar Corporation following the guidelines set forth in the American Association of State Highway and Transportation Officials (AASHTO) 1993 design guide (AASHTO 1993) and their SpectraPave4Pro™ software. The geogrid-stabilized items were assigned a structural number of 2.92 with an estimated service life of 580,000 equivalent single axle loads (ESALs).

The test items contained a suite of instrumentation consisting of asphalt strain gauges, earth pressure cells, single-depth deflectometers, moisture probes, pore-water pressure transducers, and temperature probes.

The test item was trafficked with ERDC's Heavy Vehicle Simulator (HVS) simulating normal highway loadings. The configuration used for testing consisted of a tandem-axle dual wheel gear loaded to a nominal load of 20,000 lb. Tire pressures were maintained at 120 psi throughout testing. The equivalent axle load factor for this configuration is 2.08. Therefore, one pass of the HVS was equal to 2.08 equivalent standard axle loads (ESALs).

The traffic loading was applied at a target test chamber temperature of 77° Fahrenheit, with an allowable temperature range of 72-82° Fahrenheit. The HVS is equipped with automated software that halts traffic and alerts the operator if the temperature falls outside the prescribed range.

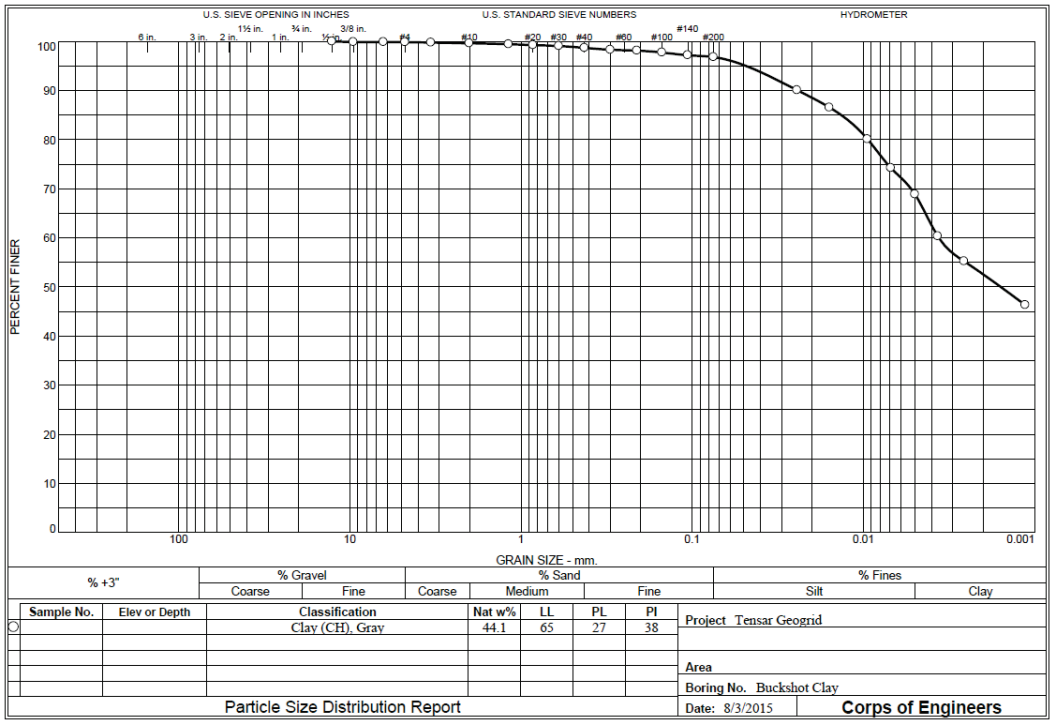
# 3 Materials

Laboratory tests were performed to characterize each component layer material. The material characterization results are presented in the following paragraphs.

## 3.1 Subgrade

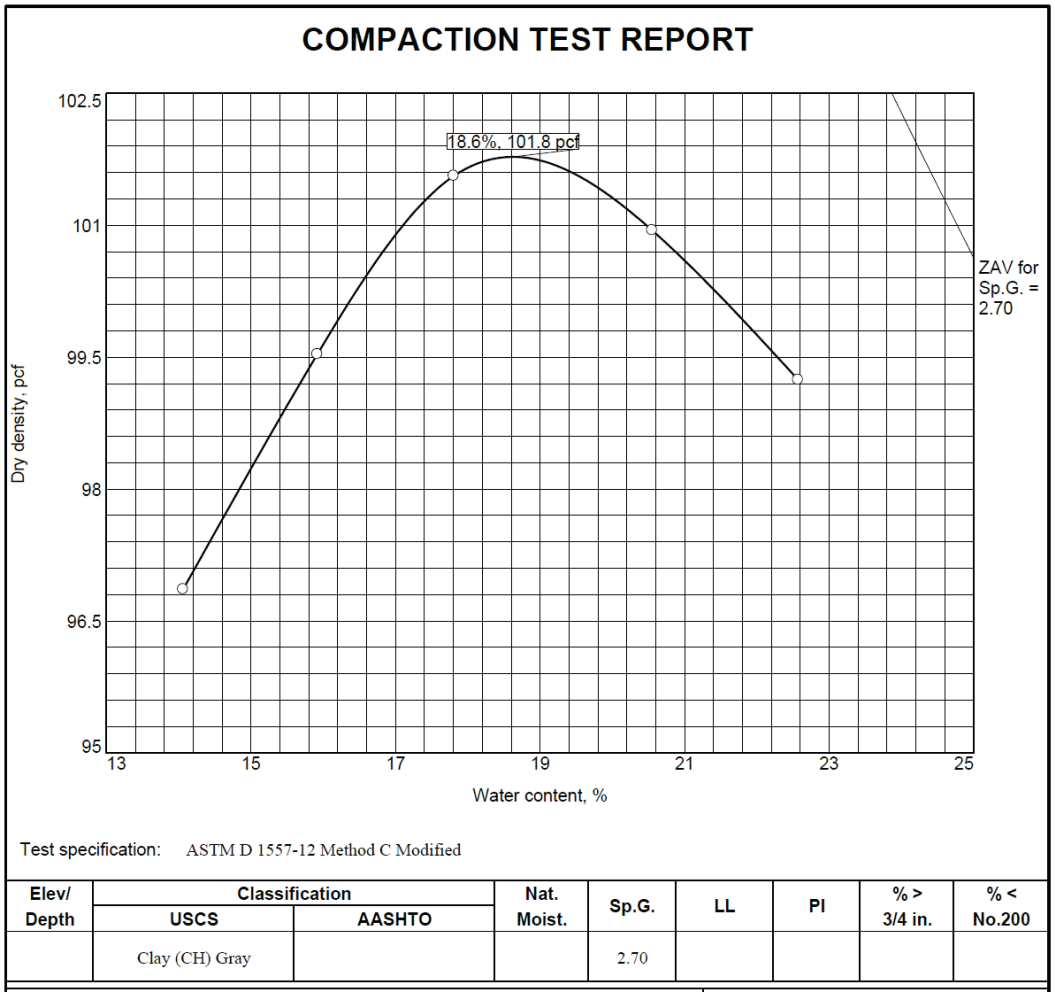
A locally sourced high-plasticity clay was used to construct the nominal 36-in.-thick test-section subgrade. A particle size analysis, shown in Figure 2, indicated the material consisted of 96.8% fines passing the No. 200 sieve. The soil had a liquid limit (LL) of 65%, a plastic limit (PL) of 27%, and a plasticity index (PI) of 37%, as determined by ASTM D4318. According to the Unified Soil Classification System (USCS), the soil was classified as a high-plasticity clay (CH) and an A-7-6 according to the American Association of State and Highway Transportation Officials (AASHTO) classification system.

Figure 2. Subgrade particle-size analysis.



Modified proctor compaction tests (ASTM D1557) were performed to determine the relationship between moisture content and dry density. Maximum dry density was found to be 101.8 pcf at an optimum moisture content of 18.6%. Graphical results of the moisture-density relationship test are shown in Figure 3.

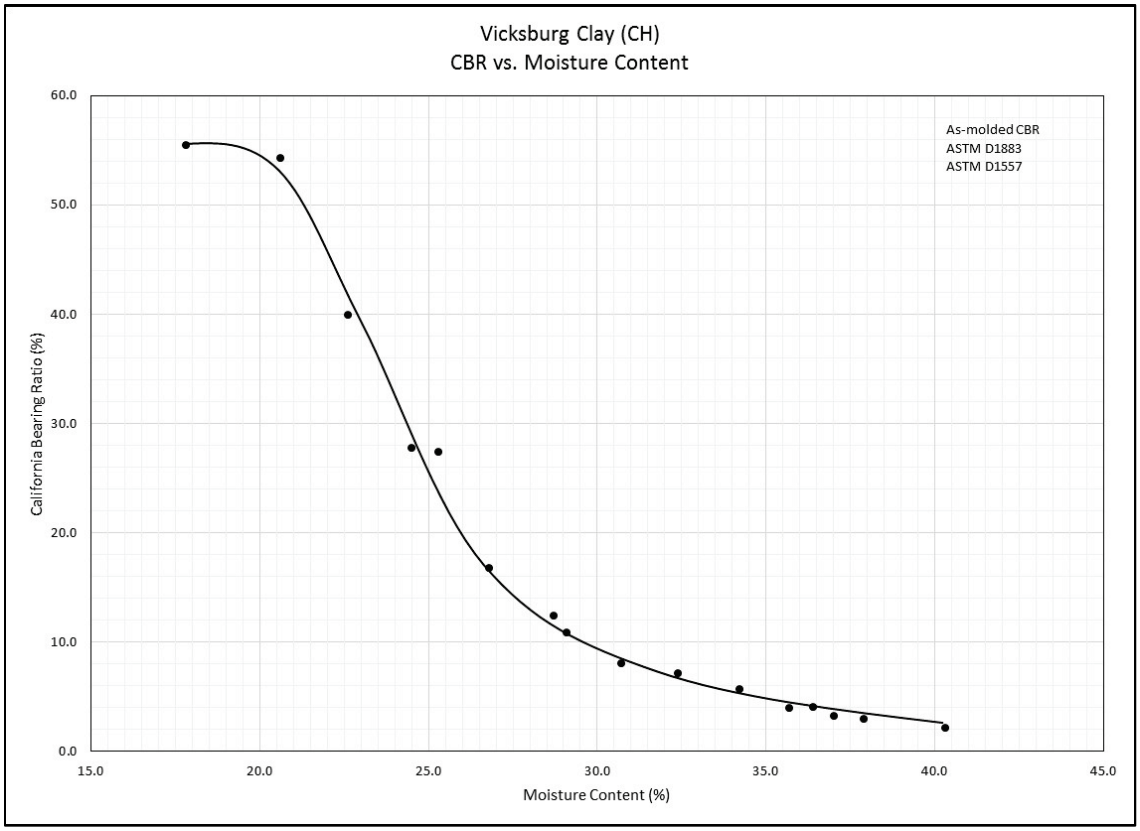
Figure 3. Clay subgrade moisture-density relationship.




| Elev/ Depth | Classification | | Nat. Moist. | Sp.G. | LL | PI | % > 3/4 in. | % < No.200 |
|---|---|---|---|---|---|---|---|---|
| | USCS | AASHTO | | | | | | |
| | Clay (CH) Gray | | | 2.70 | | | | |

To determine an in-place moisture content at the targeted 6 CBR, a suite of laboratory CBR tests (ASTM D1883) were performed. These tests were conducted at moisture contents ranging from approximately 17% to approximately 40%. A target in-place moisture content of 33% was selected based upon the relationship between moisture content and CBR. The relationship between CBR and moisture content is presented graphically in Figure 4.

Figure 4. Clay subgrade CBR/moisture content relationship.




## 3.2 Base course

Locally available crushed limestone was used to construct the flexible aggregate base course. The gradation for the crushed limestone is shown in Figure 5. ASTM procedure D2487 was used to determine that the base course was comprised of 71.5% gravel, 23.3% sand, and 5.2% non-plastic fines passing the No. 200 sieve. The coefficient of curvature (Cc) was calculated as 2.71, and the coefficient of uniformity (Cu) was 21.16. The crushed limestone aggregate base was classified as a well-graded gravel with silt and sand (GW-GM) according to the USCS and an A-1-a according to the AASHTO procedure. Modified proctor compaction tests (Figure 6) were performed in accordance with ASTM D1557 Method C Modified. The maximum dry density was 146.7 pcf at an optimum moisture content of 5.9%.

Figure 5. Crushed limestone base particle-size analysis.

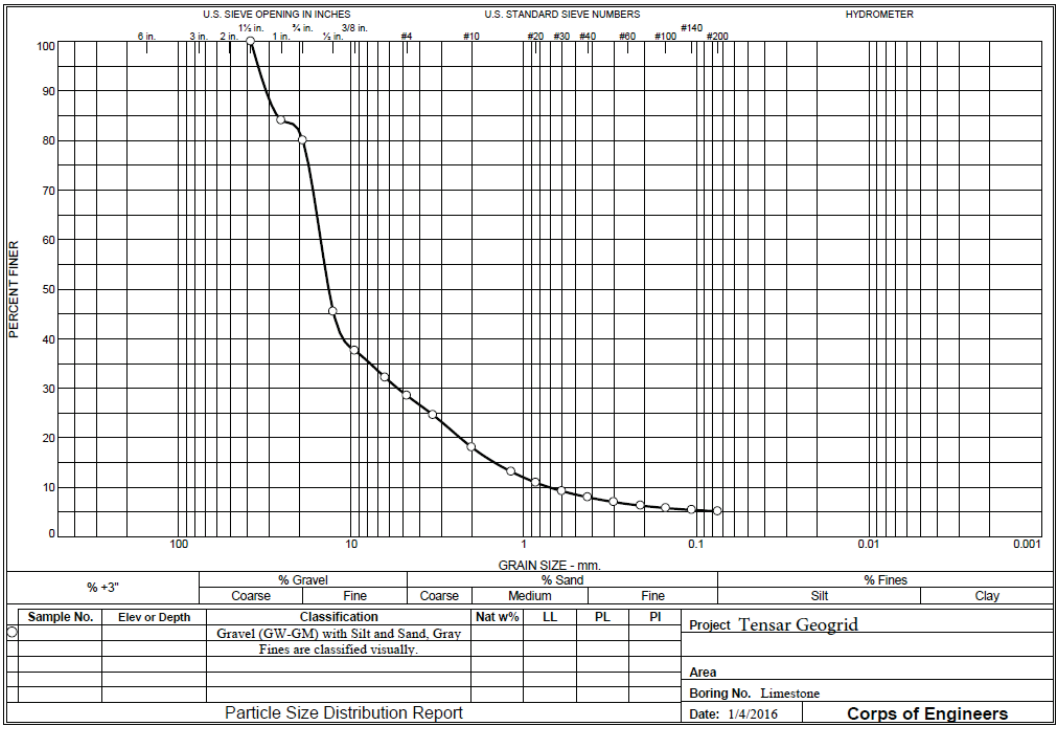
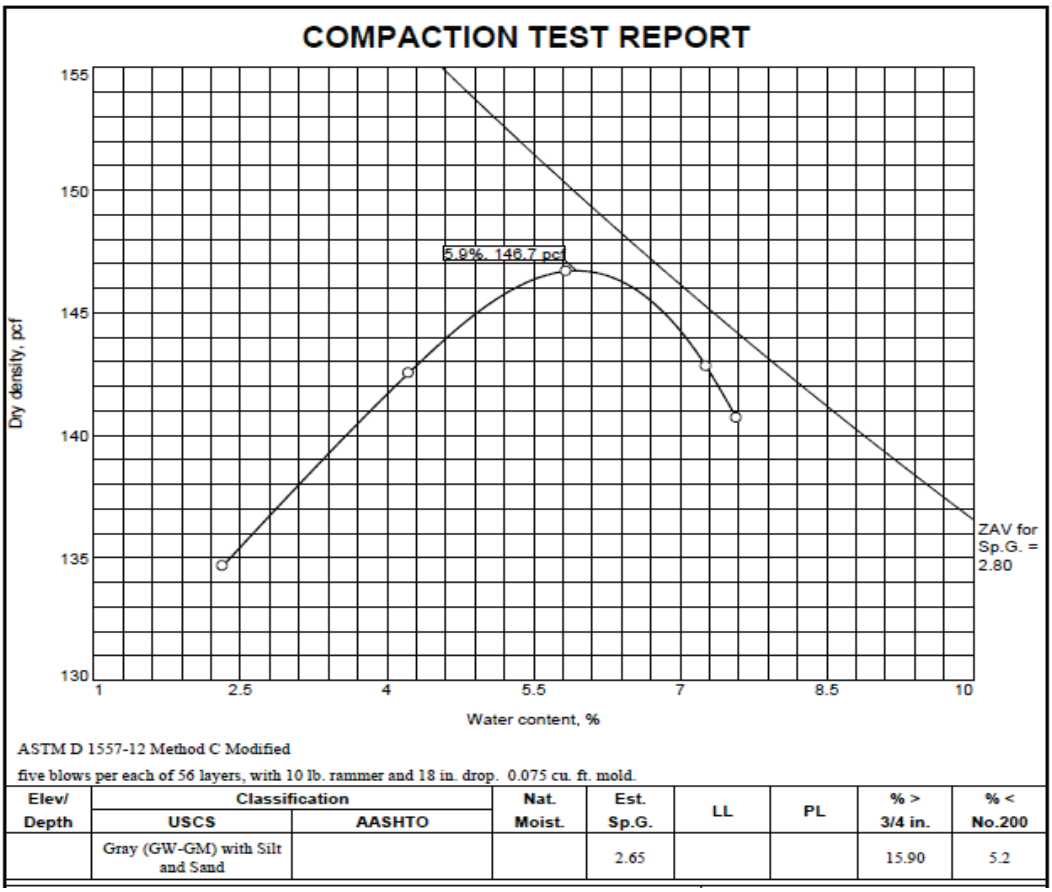



Figure 6. Limestone base moisture/density relationship.



## 3.3 Asphalt

A 9.5-mm nominal maximum aggregate size (NMAS) HMA surface mixture was selected for placement of the final wearing surface on both test items. The asphalt mixture was one that is representative of the local highway mix used on medium-traffic-level roadways in Mississippi. Mixture properties were adjusted to closely replicate those used in previous geogrid evaluation studies. Pertinent mixture properties, including control values (Norwood and Tingle 2014) are presented in Table 1.

Table 1. Hot-mix asphalt properties.

| Test Property | | Item 1 & Item 2 | Control 4-in. Nominal AC Unstabilized Base (Norwood and Tingle 2014) |
|---|---|---|---|
| $N_{design}$ | | 75 | 75 |
| Binder Grade | | PG 67-22 | PG 67-22 |
| Mixing Temp (°F) | | 310 | 310 |
| Compaction Temp (°F) | | 300 | 292 |
| Percent Passing (%) | 1.0 in. (25.0 mm) | 100 | 100 |
| | 3/4 in. (19.0 mm) | 100 | 100 |
| | 1/2 in. (12.5 mm) | 100 | 100 |
| | 3/8 in. (9.5 mm) | 93 | 95 |
| | #4 (4.75 mm) | 57 | 54 |
| | #8 (2.36 mm) | 38 | 34 |
| | #16 (1.18 mm) | 27 | 27 |
| | #30 (0.60 mm) | 22 | 20 |
| | #50 (0.30 mm) | 12 | 7 |
| | #100 (0.15 mm) | 7 | 5 |
| | #200 (0.075 mm) | 5.1 | 3.8 |
| RAP (%) | | 20 | 15 |
| RAP AC (%) | | 5.0 | 5.5 |
| $G_{sb}$ | | 2.510 | 2.6 |
| $P_b$ (%) | | 5.7 | 5.7 |
| $G_{mm}$ | | 2.361 | 2.429 |
| VMA (%) | | 15.1 | 15.4 |
| VFA (%) | | 73.5 | 74.0 |
| $P_{200}/P_{be}$ | | 1.02 | 0.76 |

## 3.4 Geogrids

The geogrids evaluated in this study were both multi-axial geogrid products manufactured from a punched and drawn polypropylene sheet. The geogrids have a hexagonal structure forming a series of triangular apertures. Nominal index properties provided for each geogrid are presented in Table 2.

Table 2. Geogrid physical properties.

| Index Property | TX5 (Item 1) | | | TX8 (Item 2) | | |
|---|---|---|---|---|---|---|
| | Longitudinal | Diagonal | Transverse | Longitudinal | Diagonal | Transverse |
| Rib pitch, mm (in.) | 40 (1.60) | 40 (1.60) | -- | 33 (1.30) | 33 (1.30) | -- |
| Mid-rib depth, mm (in.) | -- | 1.3 (0.05) | 1.2 (0.05) | -- | 1.6 (0.06) | 1.2 (0.05) |
| Mid-rib width, mm (in.) | -- | 0.9 (0.04) | 1.2 (0.05) | -- | 0.4 (0.02) | 0.7 (0.03) |

# 4 Instrumentation

Instrumentation was installed in the subgrade, base course, and HMA surface course to monitor pavement response during test-section trafficking. Sensors used to capture the pavement response included earth pressure cells (EPCs), single-depth deflectometers (SDDs), and asphalt strain gauges (ASGs). Pore-water pressure, temperature sensors, and moisture sensors were installed to monitor environmental parameters. Figure 7 and Figure 8 show the plan and profile view of the typical instrumentation layout for each traffic lane, respectively.

## 4.1 Earth pressure cells

Vertical stresses in the base course and subgrade were measured using 9-in.-diam Geokon EPCs. EPCs provide a quantitative measurement of the vertical distribution of the stresses within each traffic lane during testing. Cells with a maximum pressure range of 100 psi were installed in the subgrade, and 200-psi EPCs were installed in the base course. The EPCs in the base course were located 2 in. below the top of the base, while the EPCs placed in the subgrade were located 2 in. below the top of the subgrade. Figure 9 shows an EPC being installed 2 in. below the surface of the subgrade at the interface with the base course.

Figure 7. Plan view of instrumentation layout.

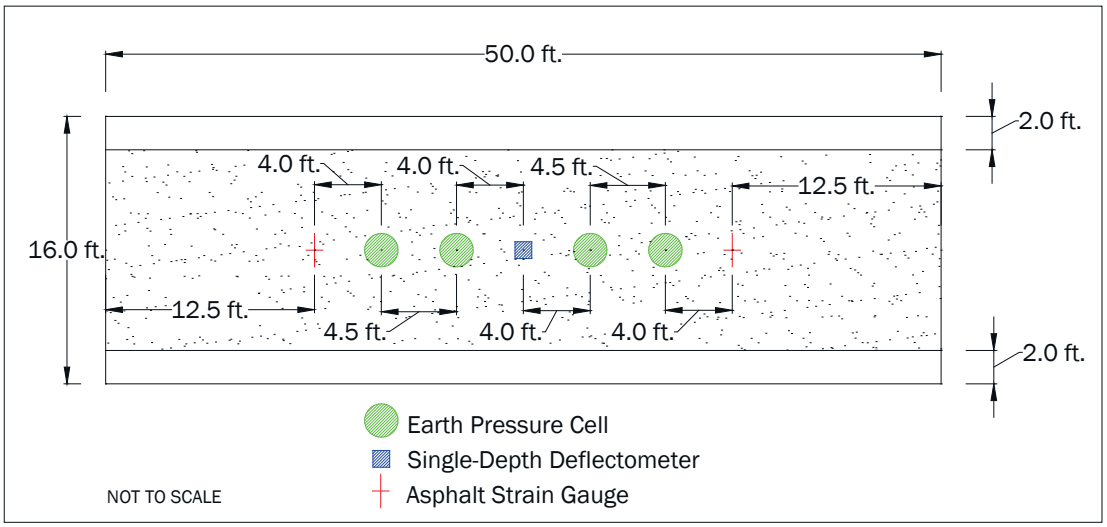


Figure 8. Profile view of instrumentation layout.

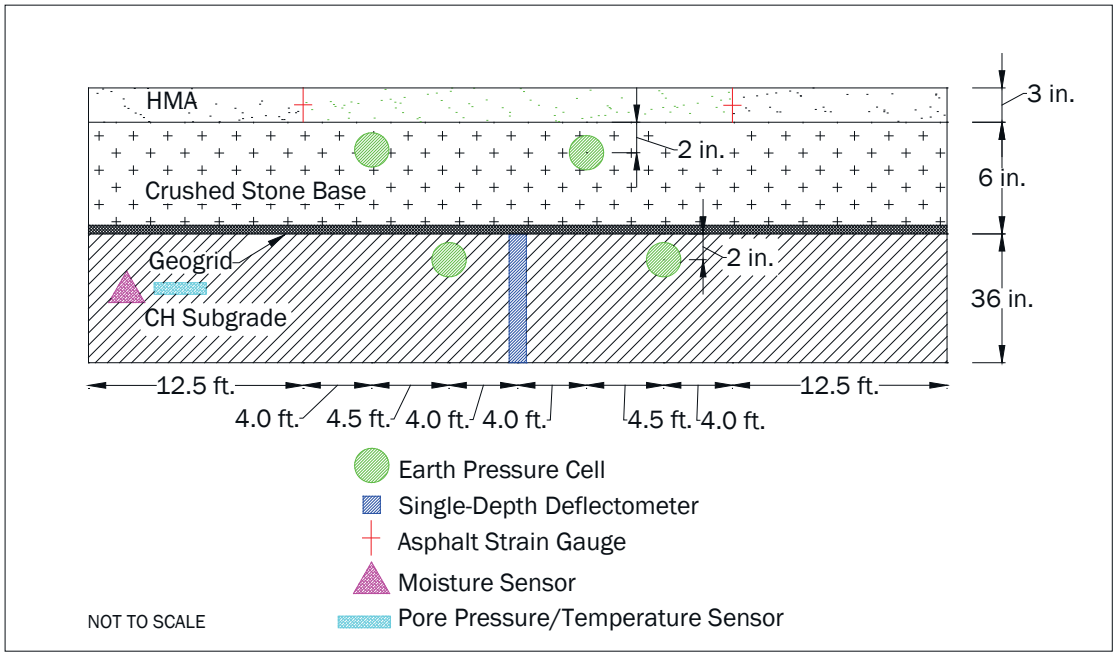



Figure 9. Earth pressure cell installation in subgrade.



## 4.2 Asphalt strain gauges

Tensile strain at the bottom of an HMA layer provides a quantitative measure of the pavement response during trafficking. The tensile strain at the bottom of the asphalt is a key response parameter linked to fatigue damage in the HMA layer. For this study, strain at the bottom of the HMA surface was measured using dynamic asphalt strain gauges (ASGs) in both the transverse and longitudinal directions. The ASGs were manufactured by Tokyo Sokki and are capable of measuring a range of ±5,000 microstrain. The gauges were adhered to the surface of the base course with a heated asphalt binder, and HMA from the asphalt paver was placed as cover over each of the gauges immediately prior to paving of the entire test section. This process is shown in Figure 10 and Figure 11, respectively.

Figure 10. Asphalt strain gauge adhered to crushed stone base.

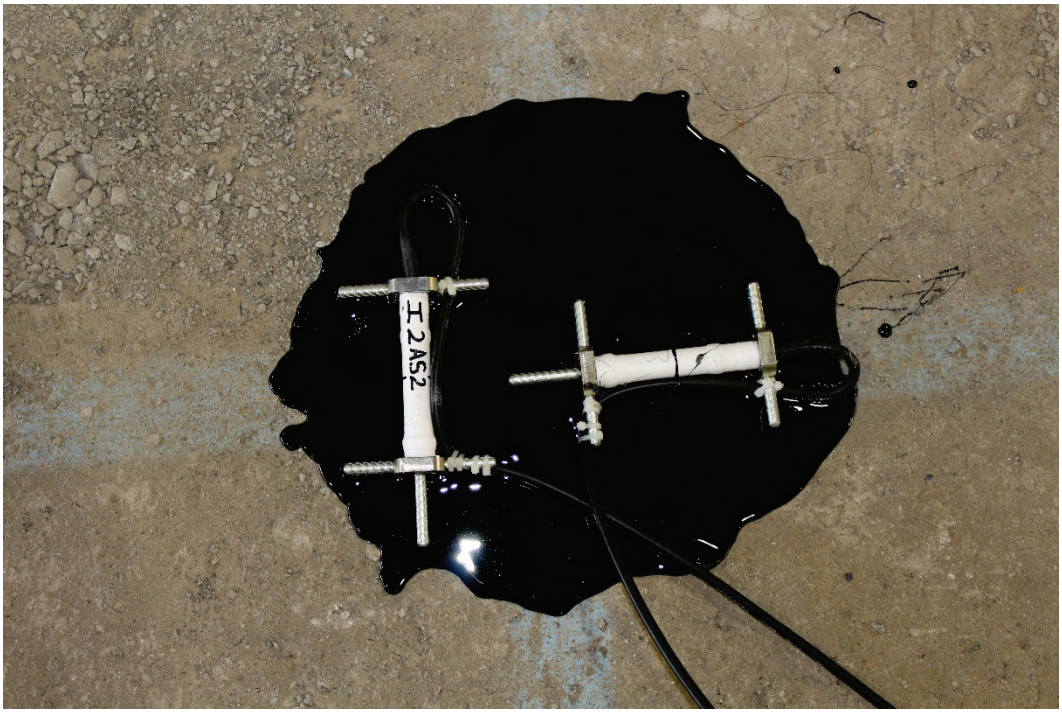


Figure 11. Asphalt strain gauge covered with HMA prior to paving.



## 4.3 Single-depth deflectometer

Measurements of deformations in the subgrade are used to quantify the stabilization benefits of a geogrid as well as assisting with the validation of the failure mechanism within the pavement structure. Potential reductions in vertical stresses at the subgrade should also be reflected as reductions in the deformation. In theory for pavements with similar structural components, the geogrid-stabilized pavement should show lower deflections than the unstabilized pavement at a given traffic level.

Vertical deflections in the subgrade were measured using single-depth deflectometers (SDDs). One SDD was placed in the middle of each test item along the centerline of traffic. The SDD was placed such that the shaft was anchored at a depth of 8 ft from the top of the subgrade. A linear velocity displacement transducer (LVDT) with a range of ±2 in. was placed in the housing such that it was in contact with both the anchor rod and the surface plate as shown in Figure 12. Thus, the LVDT measured movement of the plate 2 in. below the base-subgrade interface relative to the control point located at a depth of 8 ft.

Figure 12. Single-depth deflectometer installation.



# 5 Pavement Characterization

## 5.1 As-built properties

Quality control tests were performed during construction of each material lift to ensure target values were achieved and to monitor material consistency. Dry density and moisture content were measured using a nuclear moisture density device in accordance with ASTM D6938-15 to verify the uniformity of each material lift. Field in-place CBR tests were performed in general accordance with ASTM D4429-09a on each compacted lift to ensure target values were achieved. To further characterize the strength of the completed base and subgrade layers, Dynamic Cone Penetrometer (DCP) tests were performed in accordance with ASTM D6951-09. Asphalt cores were obtained from each test item, and core densities were determined in accordance with AASHTO T166.

As-built material properties of the base and subgrade are summarized in Table 3. Also included are the as-built control section properties from a previous test-section construction that included a comparable unstabilized control section (Norwood and Tingle 2014).

Table 3. As-built section properties.

| Property | Item 1<br>TX5 Stabilized Base | Item 2<br>TX8 Stabilized Base | Control<br>4-in. Nominal AC<br>Unstabilized Base<br>(Norwood and<br>Tingle 2014) |
|---|---|---|---|
| CH Subgrade Properties | | | |
| Wet Density (pcf) | 116.5 ± 1.0 | 116.6 ± 1.0 | 116.9 |
| Dry Density (pcf) | 88.5 ± 1.1 | 88.7 ± 1.2 | 88.9 |
| Nuclear Moisture Content (%) | 31.6 ± 0.8 | 31.6 ± 1.1 | 30.0 |
| Oven-Dried Moisture (%) | 32.7 ± 1.3 | 32.6 ± 1.2 | 34.1 |
| In-Place CBR (%) | 5.9 ± 0.2 | 5.9 ± 0.2 | 5.9 |
| Crushed Limestone Properties | | | |
| Wet Density (pcf) | 138.8 ± 1.6 | 141.5 ± 1.8 | 143.0 |
| Dry Density (pcf) | 134.5 ± 1.5 | 137.2 ± 1.7 | 138.1 |
| Nuclear Moisture Content (%) | 3.3 ± 0.1 | 3.3 ± 0.2 | 3.6 |
| Oven-Dried Moisture (%) | 3.0 ± 0.3 | 3.2 ± 0.2 | 2.4 |
| In-Place CBR (%) | 98.6 ± 9.1 | 100(+) ± 4.9 | 95.3 |
| Thickness (in.) | 5.82 ± 0.36 | 5.90 ± 0.33 | 7.7 |

| Property | Item 1<br>TX5 Stabilized Base | Item 2<br>TX8 Stabilized Base | Control<br>4-in. Nominal AC<br>Unstabilized Base<br>(Norwood and<br>Tingle 2014) |
|---|---|---|---|
| Hot-Mix Asphalt Properties | | | |
| Density (% of $G_{mm}$) | 93.4 ± 0.5 | 93.2 ± 1.0 | -- |
| Thickness (in.) | 3.20 ± 0.21 | 3.22 ± 0.11 | 4.0* |

*Nominal thickness reported

## 5.2 Dynamic cone penetrometer

A series of dynamic cone penetrometer (DCP) tests were performed to further characterize the strength of the unbound pavement layers. DCP tests were performed after construction of the base and subgrade layers on both sides of the traffic lane, following the procedures described by ASTM D 6951-09. Measured values of the DCP index (millimeters of penetration per hammer blow) were converted to CBR strength using the relationship developed by Webster et al. (1992, 1994). As-built DCP results are shown for Item 1 Station 25 West in Figure 13 and Item 2 Station 25 East in Figure 14.

## 5.3 Falling weight deflectometer

Falling weight deflectometer tests were performed on the surface of both test items after construction and prior to trafficking. The measured impulse stiffness modulus (ISM) was used to evaluate the stiffness of the constructed pavement section and provide a baseline for subsequent comparison under traffic. The ISM is the ratio of the applied load to the measured plate deflection with higher values representing a stiffer pavement structure. Additionally, the ISM values were compared to values obtained from previous test sections to verify the validity of performance comparisons. As-built ISM values for Item 1, Item 2, and the unstabilized control (Norwood and Tingle 2014) are presented in Figure 15. As-built ISM values for each test item were found to be relatively consistent along the length of each test item. Minor differences were observed in the test items with Item 2 having a slightly higher ISM value than Item 1. Both stabilized items were found to have lower ISM values than the unstabilized item. This was anticipated as the unstabilized item had an additional 2 in. of base course and 1 in. of HMA.

Figure 13. As-built DCP results for Item 1 Station 25, West.

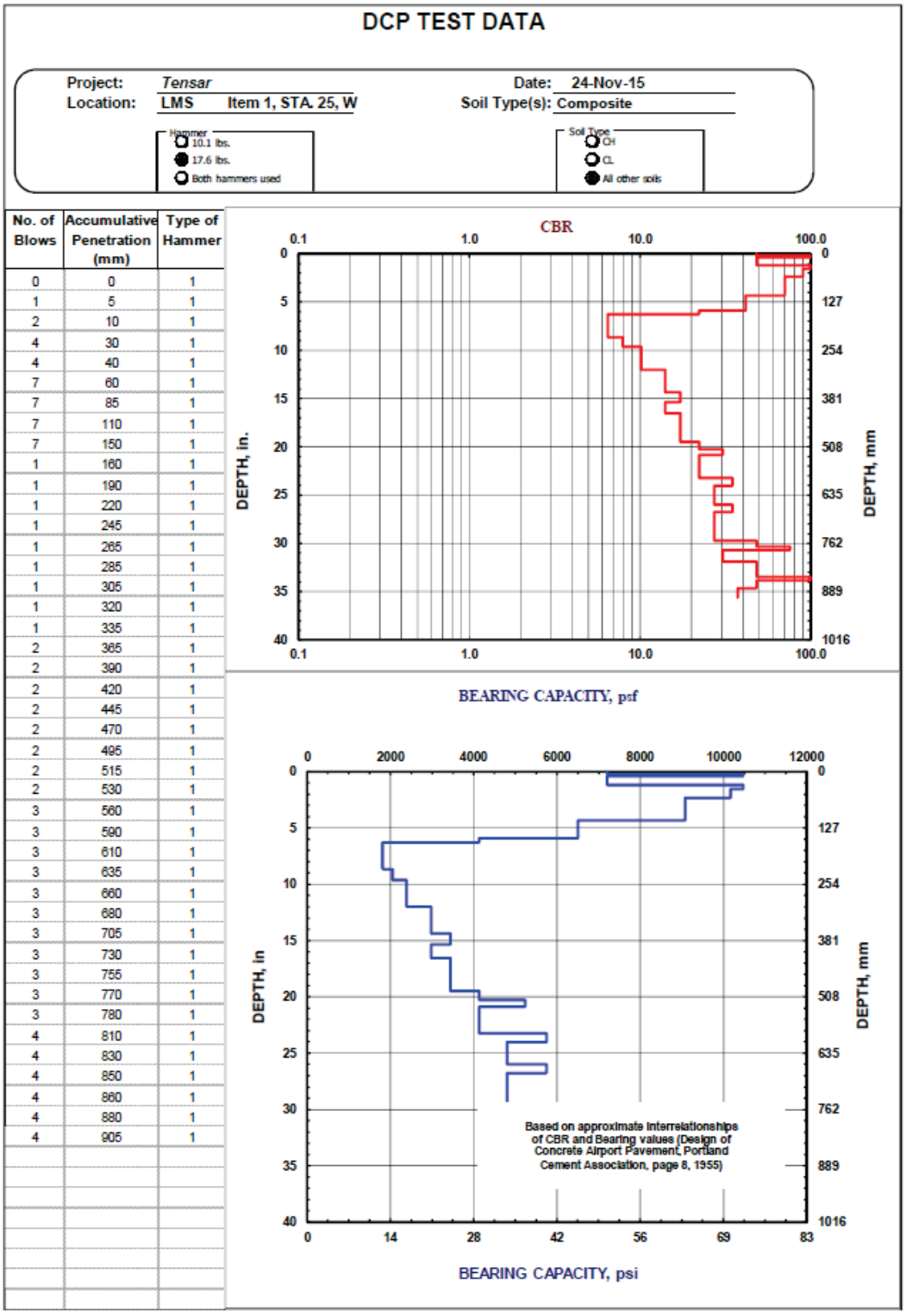


Figure 14. As-built DCP results for Item 2 Station 25, East.

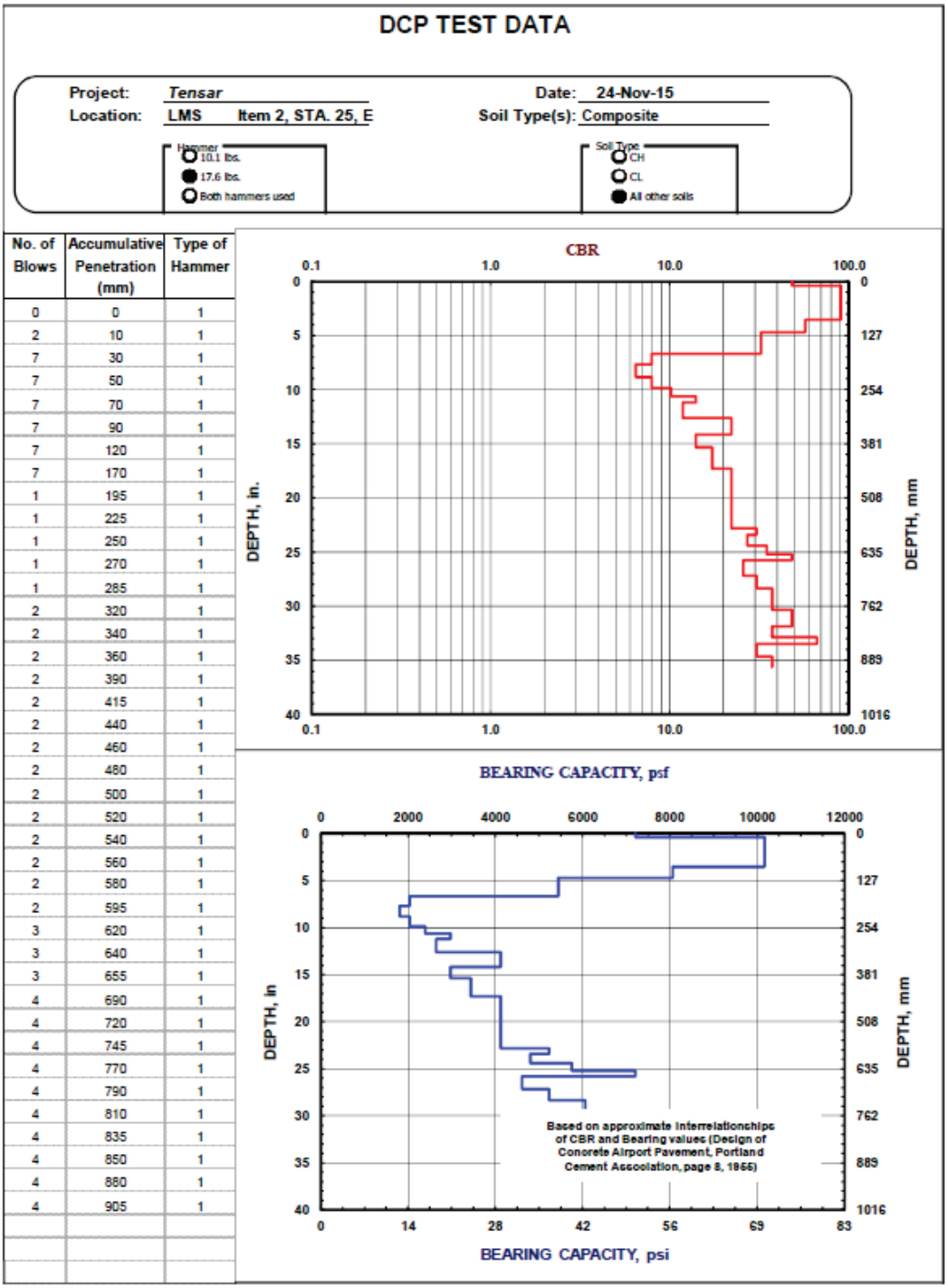
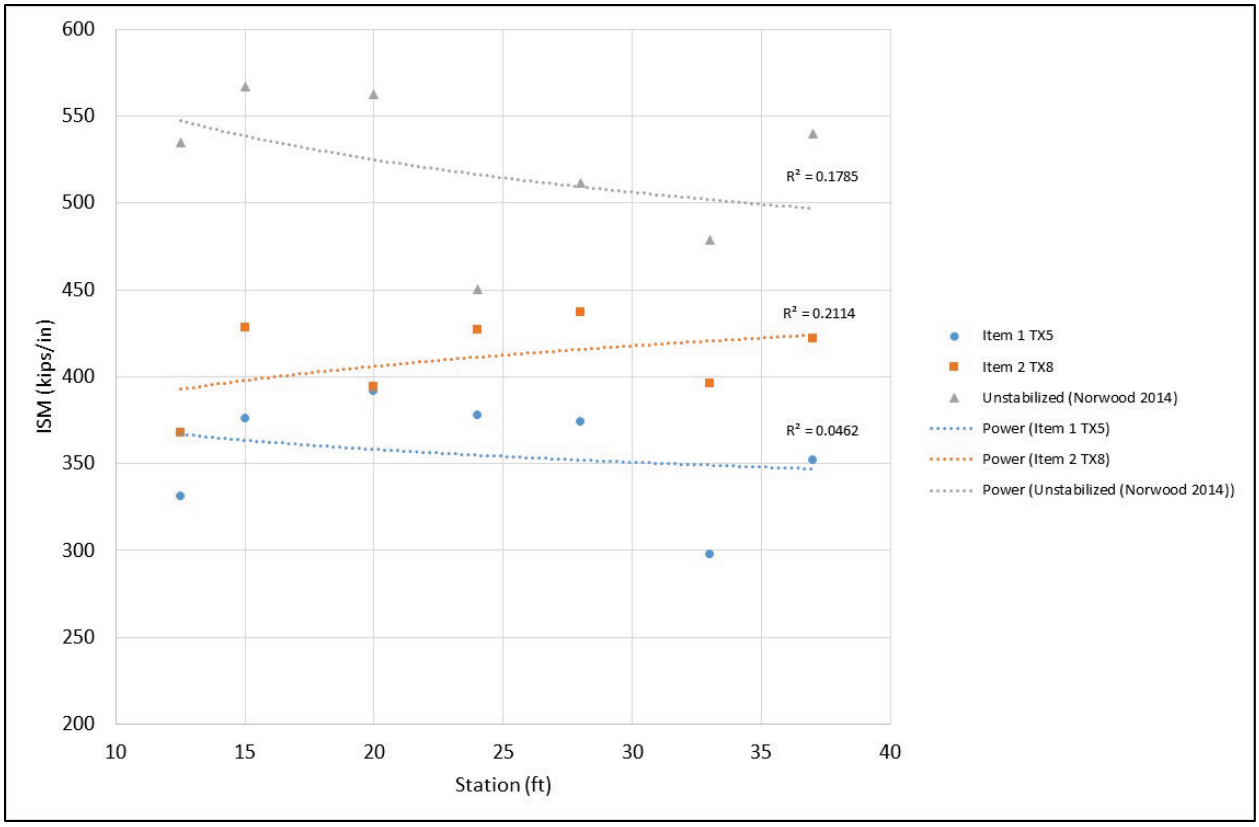


Figure 15. As-built ISM values.



# 6 Traffic Testing

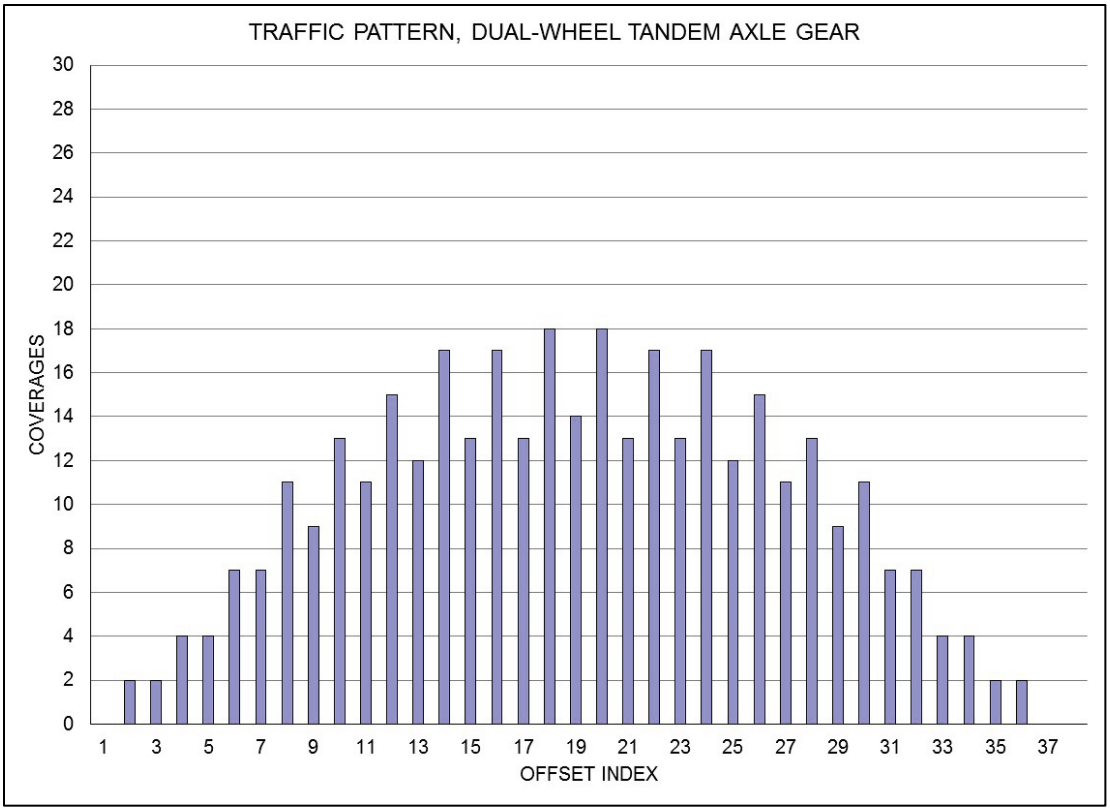
Traffic testing on both test items was performed utilizing a dual-wheel tandem axle gear (Figure 16) on the ERDC HVS. The gear configuration was loaded to a 20,000-lb nominal load and was verified prior to testing by weighing each axle with portable aircraft wheel scales. Tire pressures were monitored and maintained at 120 psi throughout traffic testing. The equivalent single axle load factor for this configuration was 2.08; therefore, each pass of the HVS was equal to 2.08 equivalent single axle loads (ESALS). The environmental chamber was maintained at a target pavement temperature of 77°F with an allowable range of ±5°F during trafficking to minimize the effect of temperature variation on rutting performance.

Each test item was trafficked utilizing a normally distributed bi-directional traffic pattern shown in Figure 17. The lateral offset indices refer to 1-in. increments along which the axle shifts laterally, resulting in a total lateral wander of approximately 3 feet. A 3-ft-wide wander pattern was utilized to mimic previous studies and to duplicate observations in other test sections.

Figure 16. Dual-wheel tandem axle configuration.



Figure 17. Normally distributed traffic pattern.



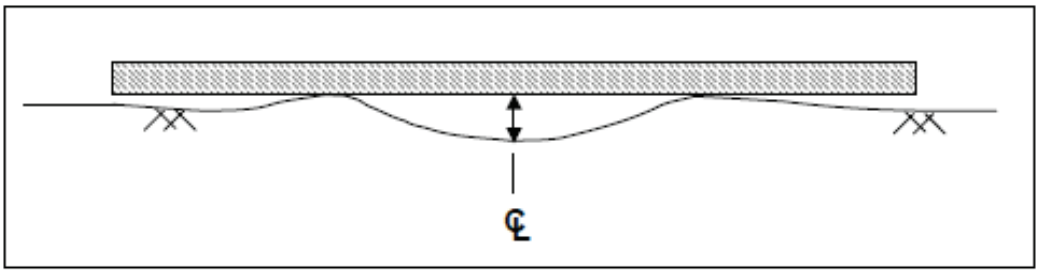
# 7 Results

Failure of the flexible pavement test items was defined as 1 in. of rutting. This failure definition was based on the concept of pavement serviceability and the fact that pavement serviceability begins to decrease exponentially in flexible pavements after 1 in. of rutting. Results are presented to document the changes in vertical alignment and instrumentation response at each traffic interval. Included within each results section are the responses documented from the unstabilized control section presented by Norwood and Tingle (2014).

## 7.1 Surface deformations

Surface deformation and rut depth measurements were made at predetermined traffic levels throughout the testing period. Surface deformation measurements represent changes in elevation and were made along the centerline and designated cross-sections of each test item. Surface deformation measurements were made utilizing robotic total station equipment to an accuracy of 0.08 in. Rut depth measurements were made by placing a metal straight edge across the traffic lane at designated cross sections and measuring the maximum rut depth using a machined depth wedge to an accuracy of 1/16 in. The maximum rut depth includes permanent surface deformation and upheaval along the edge of the traffic pattern. A schematic of the maximum rut depth measurement procedure is shown in Figure 18.

Figure 18. Measurement of maximum rut depth.




Maximum rut depths are presented in Figure 19 and Table 4. These values represent the maximum rut depth of 50% of the traffic lane. Maximum rut depth measurements were taken at stations 12.5, 18.75, 25.0, 31.25, and 37.5 of each test item, and the average of the maximum rut depth

measurements was reported. The test results indicate the stabilized test items displayed approximately 50-60% less rutting than the unstabilized control item despite the reduced base and surface layer thicknesses of the stabilized sections compared to the control section. Minimal differences in rutting were observed in Item 1 and Item 2, with Item 2 outperforming Item 1 at most traffic levels.

Surface deformation measurements presented in Figure 20 and Table 5 were obtained by averaging elevation measurements taken at 1-ft increments along the centerline of the trafficked area. Measurements made at the outer 5 feet of the traffic centerline were excluded from the averaging calculations due to the potential for non-representative deformations caused by the change of direction of the HVS carriage. The test results indicate that the stabilized test items displayed approximatley 30-35% less surface deformation than the unstabilized control item. Minimal differences in surface deformation were observed between Item 1 and Item 2, with Item 2 outperforming Item 1 at most traffic levels.

It should be noted that while a reduction in rutting and permanent deformation were observed in the stabilized items when compared to the unstabilized item, the overall magnitude of differences in the distress would be considered relatively small in practice.

Figure 19. Accumulated rut depth with traffic.

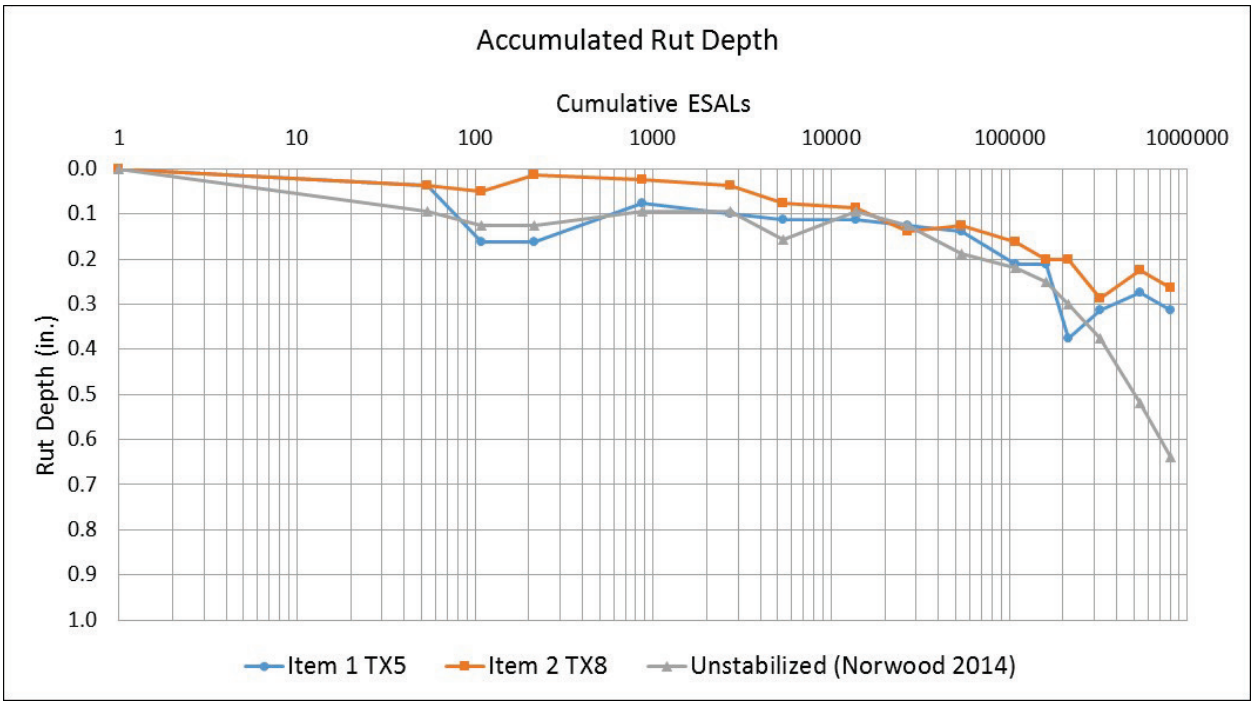


Table 4. Maximum rut depth measurements.

| Test Item | Pavement Structure | ESALS | | | | | | | | |
|---|---|---|---|---|---|---|---|---|---|---|
| | | 54 | 108 | 216 | 865 | 27,040 | 54,080 | 162,240 | 324,480 | 811,200 |
| Item 1 | 3-in. HMA 6-in. base stabilized, TX5 | 0.038 | 0.163 | 0.163 | 0.075 | 0.125 | 0.138 | 0.213 | 0.313 | 0.313 |
| Item 2 | 3-in. HMA 6-in. base stabilized, TX8 | 0.038 | 0.050 | 0.013 | 0.025 | 0.138 | 0.125 | 0.200 | 0.288 | 0.263 |
| Control | 4-in. HMA 8-in. base unstabilized | 0.094 | 0.125 | 0.125 | 0.094 | 0.125 | 0.188 | 0.250 | 0.375 | 0.640 |

Figure 20. Permanent surface deformation with traffic.

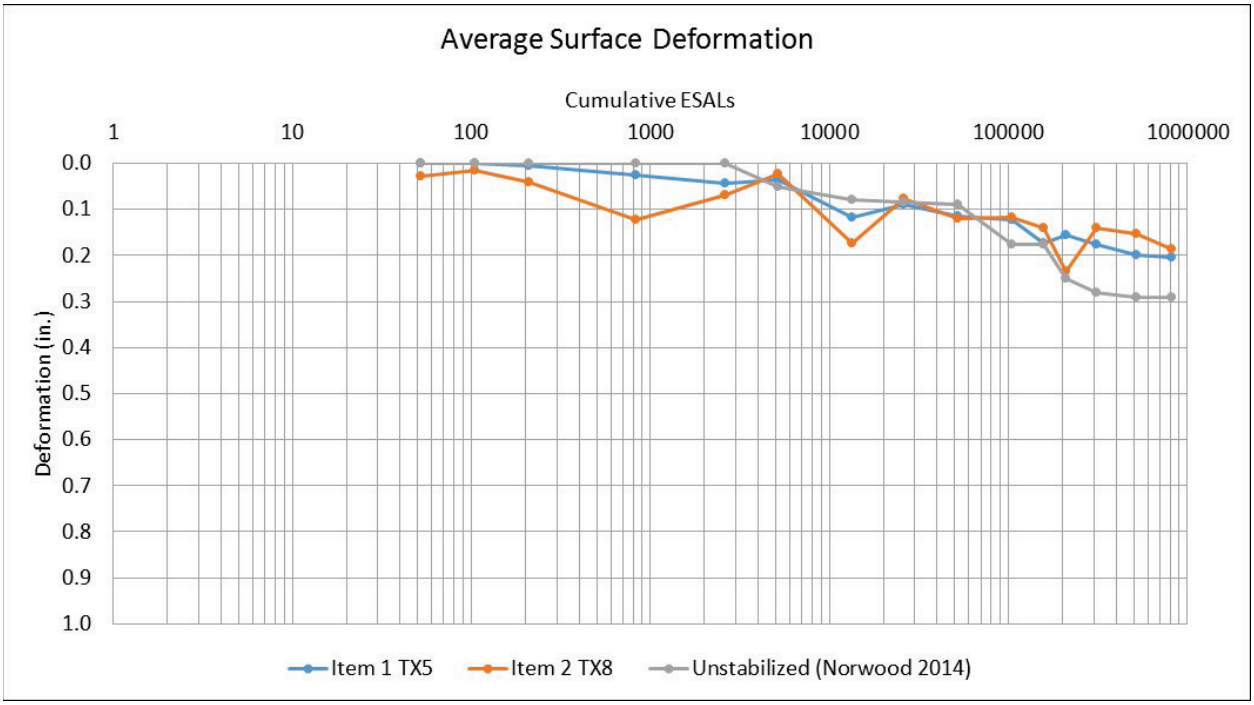


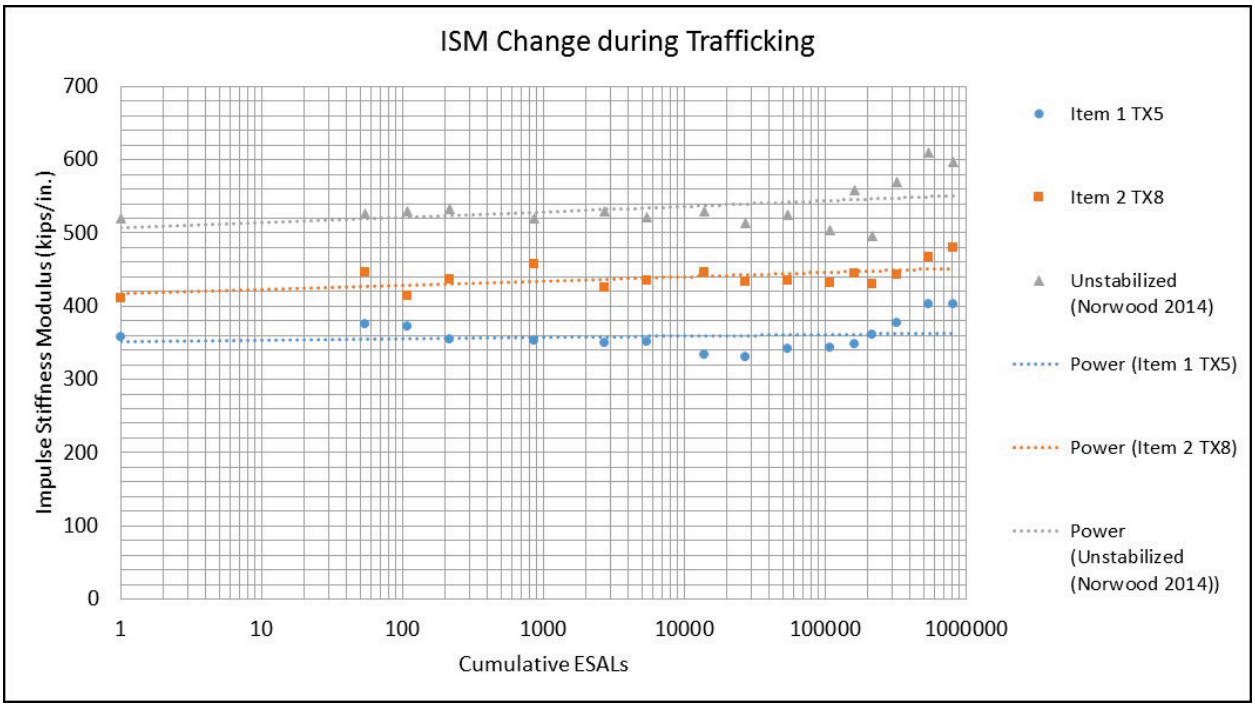

Table 5. Permanent surface deformation measurements.

| Test Item | Pavement Structure | ESALS | | | | | | | | |
|---|---|---|---|---|---|---|---|---|---|---|
| | | 54 | 108 | 216 | 865 | 27,040 | 54,080 | 162,240 | 324,480 | 811,200 |
| Item 1 | 3-in. HMA 6-in. base stabilized, TX5 | 0.000 | 0.000 | 0.005 | 0.025 | 0.090 | 0.115 | 0.175 | 0.176 | 0.203 |
| Item 2 | 3-in. HMA 6-in. base stabilized, TX8 | 0.027 | 0.016 | 0.040 | 0.124 | 0.077 | 0.121 | 0.141 | 0.140 | 0.187 |
| Control | 4-in. HMA 8-in. base unstabilized | 0.000 | 0.000 | 0.000 | 0.000 | 0.085 | 0.090 | 0.175 | 0.280 | 0.290 |

## 7.2 Falling weight deflectometer

FWD data were collected at specified traffic intervals to monitor pavement structure stiffness. The ISM, which is the applied load divided by the measured load plate deflection, was used as the basis for comparison. FWD data were collected at Stations 12.5, 15, 20, 24, 28, and 37 at each designated traffic interval. Average as-built ISM values for Item 1 and Item 2 were 357 kips/in. and 410 kips/in., respectively. The average as-built ISM value for the control section was 521 kips/in. The increased stiffness of the unstabilized section was expected due to the additional 2 in. of base course and additional 1 in. of HMA. Change in ISM values with traffic for each test item are presented in Figure 21.

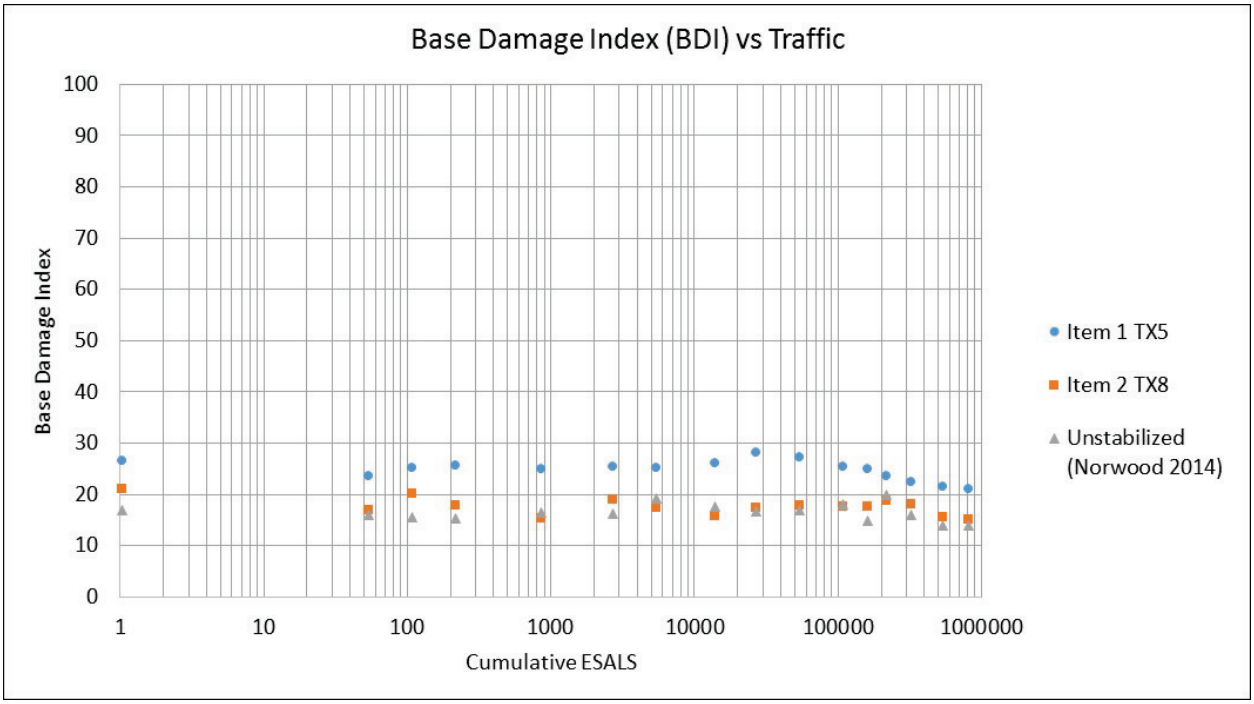
Figure 21. ISM change with traffic.




Under cumulative traffic loading, little change was observed in stiffness of the stabilized test items. A slight upward trend was noted at approximately 108,000 ESALS for each item trafficked that may have been a result of layer densification under sustained trafficking. The final ISM value for Item 1 was 402 kips/in., representing an increase of 45 kips/in. or approximately 13%. The final ISM value for Item 2 was 480 kips/in., representing an increase of 70 kips/in. or approximately 17%.

The Base Damage Index (BDI) was calculated as the difference between the measured deflection at the load plate (D1) and the measured deflection at a 12-in. offset (D2) to determine the relative stiffness of the aggregate base course. Figure 22 presents a plot of the calculated average BDI for each section at each traffic interval. The test results indicate the base stiffness values for Item 1 were lower than the unstabilized item throughout the duration of trafficking. The increased stiffness of the unstabilized section was expected due to the additional 2 in. of base course. Base stiffness values in Item 2 were found to be generally the same as those calculated for the unstabilized section.

Figure 22. Base damage index with traffic.




## 7.3 Earth pressure cells

Earth pressure cells were installed near the top of the base and near the top of the subgrade as described previously to collect dynamic stress response during trafficking. Locations and installation depths for each test item are presented in Table 6.

Predicted stresses within the pavement structure were calculated using the Pavement Engineering Utility Version 7 (PSEVEN). PSEVEN is a software tool developed at the ERDC for the analysis, design and evaluation of pavement structures. This tool implements pavement criteria and

procedures contained in Department of Defense Unified Facilities Criteria (UFC) 3-260-02. PSEVEN can be used for the analysis of flexible, rigid, unsurfaced, and mat-surfaced pavements. Required pavement thicknesses, allowable loads and allowable passes are computed for one or more ground vehicles and aircraft. PSEVEN is able to use vehicle geometrical and load data from the standard database supplied with the pavement engineering and design software package PCASE 2.09. Custom vehicles can be created and managed to add vehicles not included in the standard vehicles database. PSEVEN can also be used to design and analyze pavements using the layered elastic theory. Other features of PSEVEN include: frost calculations, minimum thickness of asphalt surfaces, and Aircraft Classification Numbers. The calculated stresses using PSEVEN are presented in Table 6 with the measured responses recorded at the beginning of the traffic testing.

Table 6. Predicted and measured earth pressure cell responses.

| Location | | | As-built HMA Thickness (in.) | As-built Base Thickness (in.) | EPC depth from surface (in.) | Predicted Stress (psi) | Measured Stress (psi) | Measured vs. Predicted (psi) |
|---|---|---|---|---|---|---|---|---|
| Item 1 | Station 15 | Subgrade | 3.72 | 5.52 | 11.24 | 7.7 | 6.3 | -1.4 |
| Item 1 | Station 28 | Subgrade | 3.24 | 5.76 | 11.00 | 8.2 | 7.6 | -0.6 |
| Item 1 | Station 20 | Base | 3.24 | 6.12 | 5.24 | 32.7 | 33.9 | 1.2 |
| Item 1 | Station 33 | Base | 3.12 | 5.64 | 5.12 | 32.7 | 30.5 | -2.2 |
| Item 2 | Station 15 | Subgrade | 3.24 | 5.60 | 10.84 | 8.3 | 7.3 | -1.0 |
| Item 2 | Station 28 | Subgrade | 3.24 | 5.88 | 11.12 | 8.1 | 13.0 | 4.9 |
| Item 2 | Station 20 | Base | 3.12 | 5.76 | 5.12 | 33.4 | 28.1 | -5.3 |
| Item 2 | Station 33 | Base | 3.36 | 6.12 | 5.36 | 30.9 | 33.1 | 2.2 |

Dynamic response was measured for approximately 10 minutes of traffic after each designated data collection point to allow for HVS wheel wander and to account for any minor instrumentation misalignments during construction. The response data set were plotted and the maximum pressure reading was selected to represent the response at the designated traffic interval. Collecting data in this manner and selecting the maximum response assisted in ensuring the HVS wheel load was directly over the pressure cell(s). Earth pressure cell response data for the 10-minute test for each designated traffic interval are presented in Appendix A.

The maximum earth pressure cell response value from each 10-minute test were collected for the subgrade and base course. Changes in the EPC response values installed in the subgrade for Item 1 and Item 2 are shown in Figure 23. Changes in the EPC response values installed in the base course for Item 1 and Item 2 are shown in Figure 24.

Subgrade and base earth pressure cell response values in the stabilized sections were found to be generally equivalent to measured responses in the unstabilized section. A slight upward trend was observed in subgrade pressure with increasing traffic that may be due to densification and stiffening over time.

Figure 23. Peak subgrade earth pressure cell response during trafficking.

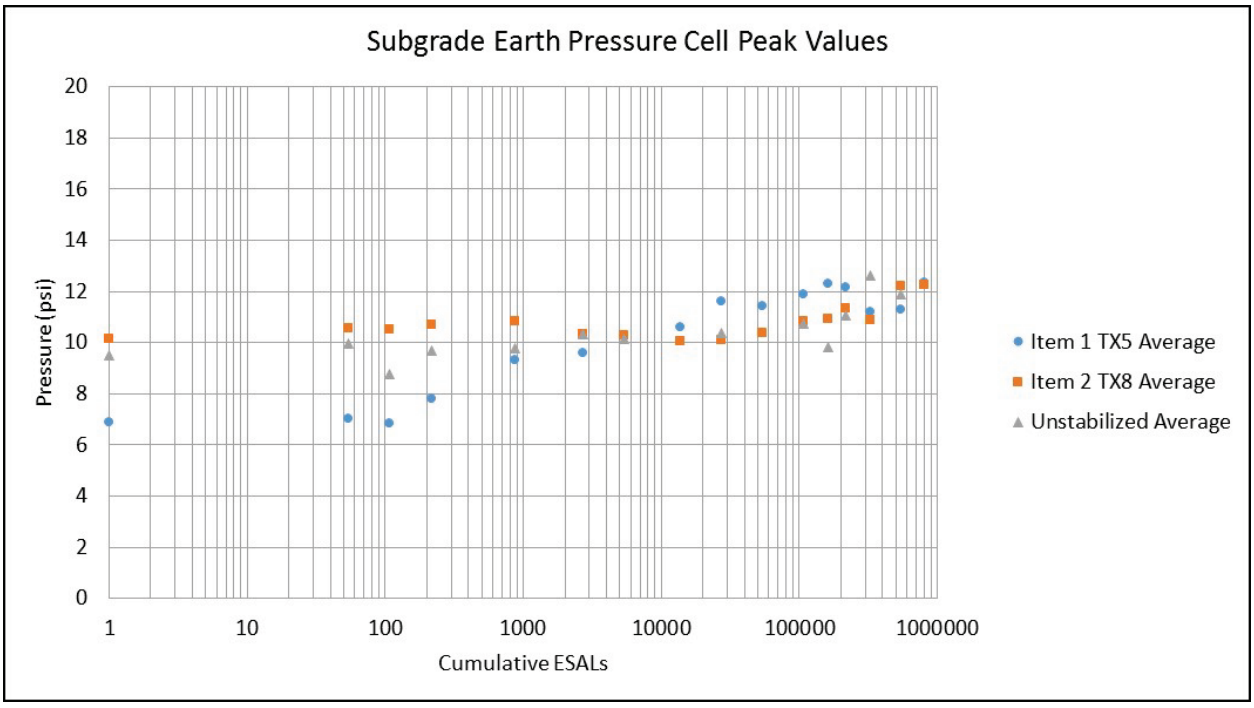
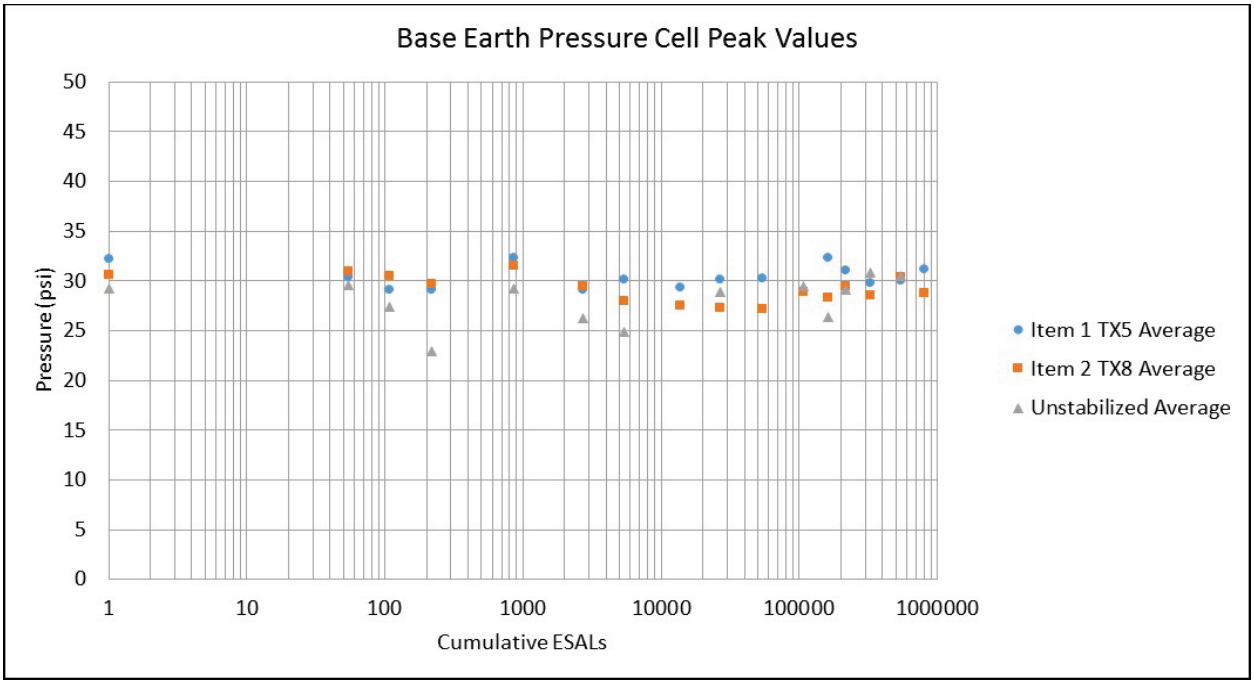


Figure 24. Peak base earth pressure cell response during trafficking.




## 7.4 Single-depth deflectometers

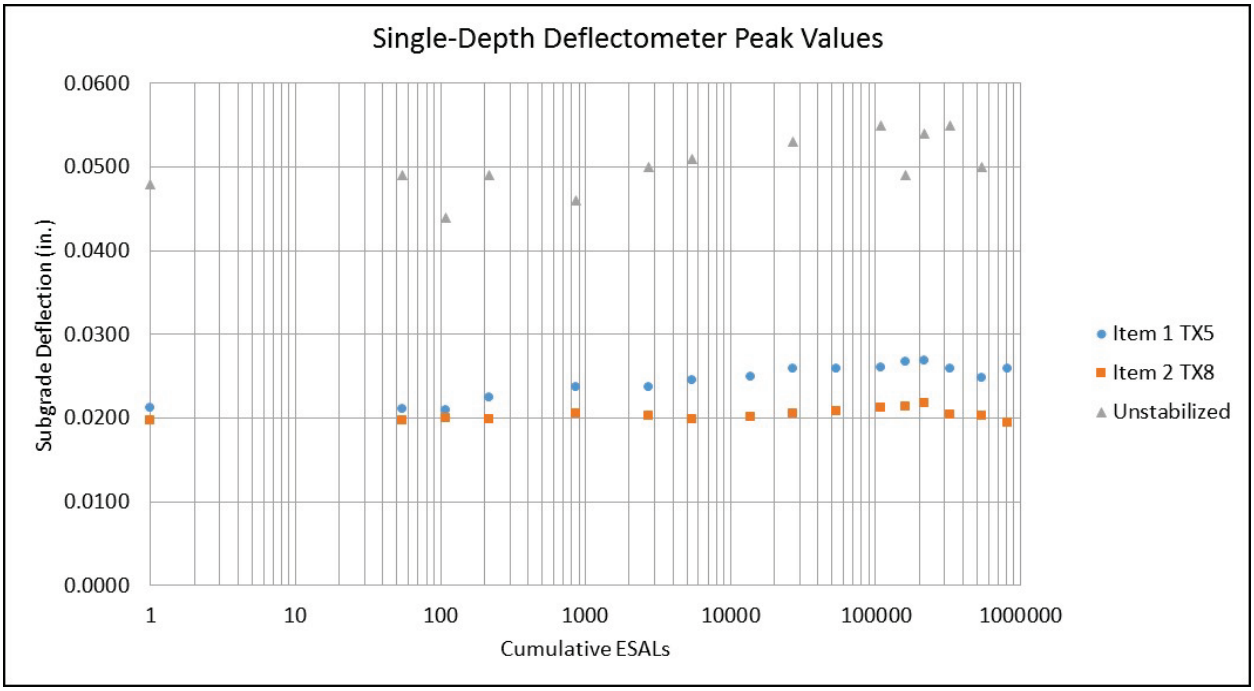
Single-depth deflectometers were installed near the center of each test item (approximately Station 24). The gauges had a measurement range of ±2 inches and were installed at the top of the subgrade to give an estimate of deflections experienced by the subgrade. Single-depth deflectometer response data for the 10-minute test for each designated traffic interval are presented in Appendix B. Installation depths, predicted deflection values using PSEVEN, and measured deflection values for each test item are presented in Table 7.

Table 7. Predicted and measured single-depth deflectometer responses.

| Location | | | As-built HMA Thickness (in.) | As-built Base Thickness (in.) | SDD depth from surface (in.) | Predicted deflection(in.) | Measured deflection (in.) | Measured vs. Predicted (in.) |
|---|---|---|---|---|---|---|---|---|
| Item 1 | Station 24 | Subgrade | 3.12 | 5.88 | 11.00 | 0.029849 | 0.021309 | -0.00854 |
| Item 2 | Station 24 | Subgrade | 3.12 | 5.76 | 10.88 | 0.030039 | 0.019779 | -0.01026 |

Peak deflection values were obtained from the 10-minute test after each designated traffic interval. SDD peak value changes with traffic are shown in Figure 25. Measured deflections in the stabilized items were approximately ½ of that observed in the unstabilized section. This may be indicative of base stiffening due to aggregate interlock at the geogrid/aggregate interface.

Figure 25. Peak subgrade deflection during trafficking.




It is noted that the measured deflection values were lower than the PSEVEN predicted values in both test items, a possible indication of base course stiffening provided by the geogrids.

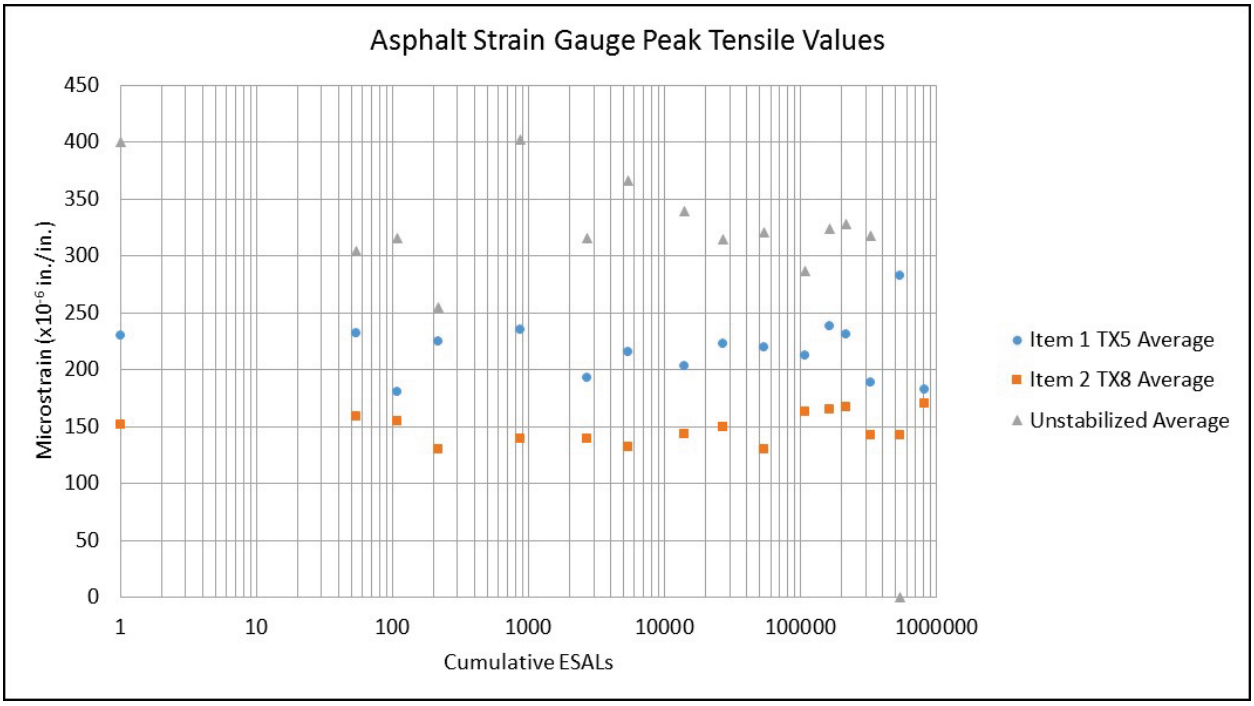
## 7.5 Asphalt strain gauges

Asphalt strain gauges (ASGs) were installed at Stations 12.5 and 37 in each item for this study. Two strain gauges were placed at each location with one oriented in the transverse direction and one oriented in the longitudinal direction. Response data were collected for a 10-minute interval at each designated data collection point, as with all other instrumentation. Dynamic asphalt strain response data are presented in Appendix C. Installation depths, predicted strain values, and measured strain values are presented in Table 8. Peak tensile strain response values are presented in Figure 26. It is noted that the measured peak tensile strain responses for the unstabilized section were much higher than that measured in the stabilized sections. This phenomena was not anticipated as higher peak strain values were expected with a 1 in. reduction in asphalt thickness. Different asphalt strain gauges were utilized for this study due to construction survivability concerns identified in previous work. It is believed the difference in gauge manufacturer could be a cause of the observed peak asphalt strain gauge responses. It is recommended caution be exercised when comparing these data.

Table 8. Predicted and measured asphalt strain gauge responses.

| Location/Orientation | | | As-built HMA Thickness (in.) | As-built Base Thickness (in.) | ASG depth from surface (in.) | Predicted Microstrain (x $10^{-6}$ in./in.) | Measured Microstrain (x $10^{-6}$ in./in.) | Measured vs. Predicted (x $10^{-6}$ in./in.) |
|---|---|---|---|---|---|---|---|---|
| Item 1 | Station 12.5 | Transverse | 3.36 | 5.94 | 3.36 | 216 | 158 | -58 |
| Item 1 | Station 12.5 | Longitudinal | 3.36 | 5.94 | 3.36 | 263 | 250 | -13 |
| Item 1 | Station 37 | Transverse | 2.88 | 5.88 | 2.88 | 228 | 167 | -61 |
| Item 1 | Station 37 | Longitudinal | 2.88 | 5.88 | 2.88 | 269 | 260 | -9 |
| Item 2 | Station 12.5 | Transverse | 3.30 | 5.58 | 3.30 | 222 | 146 | -76 |
| Item 2 | Station 12.5 | Longitudinal | 3.30 | 5.58 | 3.30 | 269 | 175 | -94 |
| Item 2 | Station 37 | Transverse | 3.36 | 6.24 | 3.36 | 213 | 153 | -60 |
| Item 2 | Station 37 | Longitudinal | 3.36 | 6.24 | 3.36 | 259 | 143 | -116 |

Figure 26. Peak asphalt tensile strain during trafficking.



# 8 Post-Traffic Forensics

After the conclusion of traffic testing, each test item was trenched in two locations to investigate the method of pavement failure and characterize material properties. Trench locations were selected to correspond with the locations of minimum and maximum rutting in each item, as determined by review of both the rutting and surface deformation data. Each trench was approximately 3 ft wide and extended across the full traffic lane. Excavation began by saw cutting the HMA surface and carefully removing it to avoid disturbing the underlying base course. Measurements of each layer thickness were made at each trench location. In-field CBR tests, nuclear density measurements, and moisture content determinations were performed on each layer both within the wheel path and outside the wheel path. Results of tests performed in the trench locations for each item are shown in Table 9.

Table 9. Post-traffic physical data.

| Property | Item 1 TX5 Stabilized Base | Item 2 TX8 Stabilized Base | Control 4-in. Nominal AC Unstabilized Base (Norwood and Tingle 2014) |
|---|---|---|---|
| CH Subgrade Properties | | | |
| Wet Density (pcf) | 116.9 | 117.9 | 113.9 |
| Dry Density (pcf) | 89.1 | 89.1 | 88.6 |
| Nuclear Moisture Content (%) | 31.2 | 32.3 | 28.1 |
| Oven-Dried Moisture (%) | 32.7 | 32.3 | 30.1 |
| In-Place CBR (%) | 11.1 | 9.8 | 11.0 |
| Crushed Limestone Properties | | | |
| Wet Density (pcf) | 140.5 | 142.6 | ** |
| Dry Density (pcf) | 136.7 | 138.7 | ** |
| Nuclear Moisture Content (%) | 2.8 | 2.9 | ** |
| Oven-Dried Moisture (%) | 2.2 | 1.7 | ** |
| In-Place CBR (%) | 100+ | 100+ | ** |

**Values not reported due to base disturbance during excavation

The test results indicate there was a minor increase in dry density of the subgrade, while the moisture content was relatively constant. A 2.2 pcf increase was measured in the base course dry density for Item 1 and a 1.5 pcf increase in base course density was measured for Item 2. Base course moisture contents for Items 1 and 2 decreased by 0.8% and 1.5%, respectively. An increase in subgrade CBR in the wheelpath was observed in both test sections, which was found to be consistent with observations made by Norwood and Tingle (2014).

The base course was carefully excavated to expose the underlying geogrid for visual inspection as shown in Figure 27 and Figure 28. Visual investigation revealed indentations were present in the subgrade of both test items (Figure 29 and Figure 30), indicating aggregate strike-through and interlock with the geogrid. Visual inspection indicated the geogrid was intact and no damage was sustained during construction or trafficking.

Visual inspection of the subsurface layers was performed to determine rutting behavior in each test section. The excavated areas are shown in Figure 31 through Figure 33 with orange markers used to delineate each layer interface. No significant permanent deformation was observed in the subgrade of both test items. Visual inspection indicated that the accumulated deformation was limited to the HMA and base-course layers.

Figure 27. Item 1 excavated geogrid.

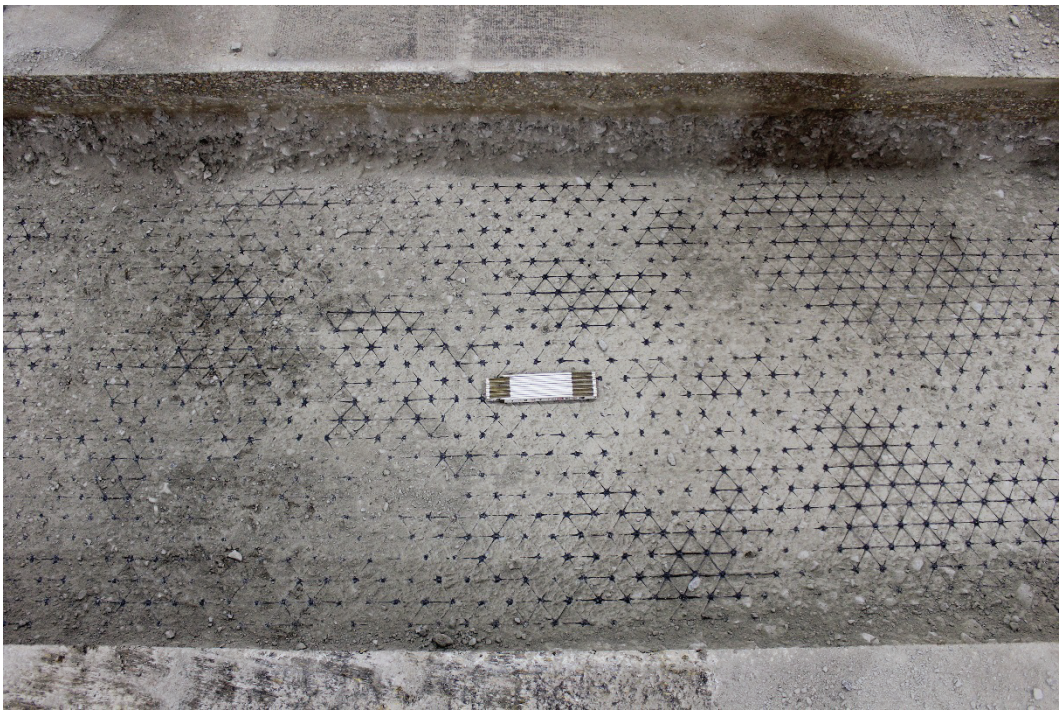


Figure 28. Item 2 excavated geogrid.

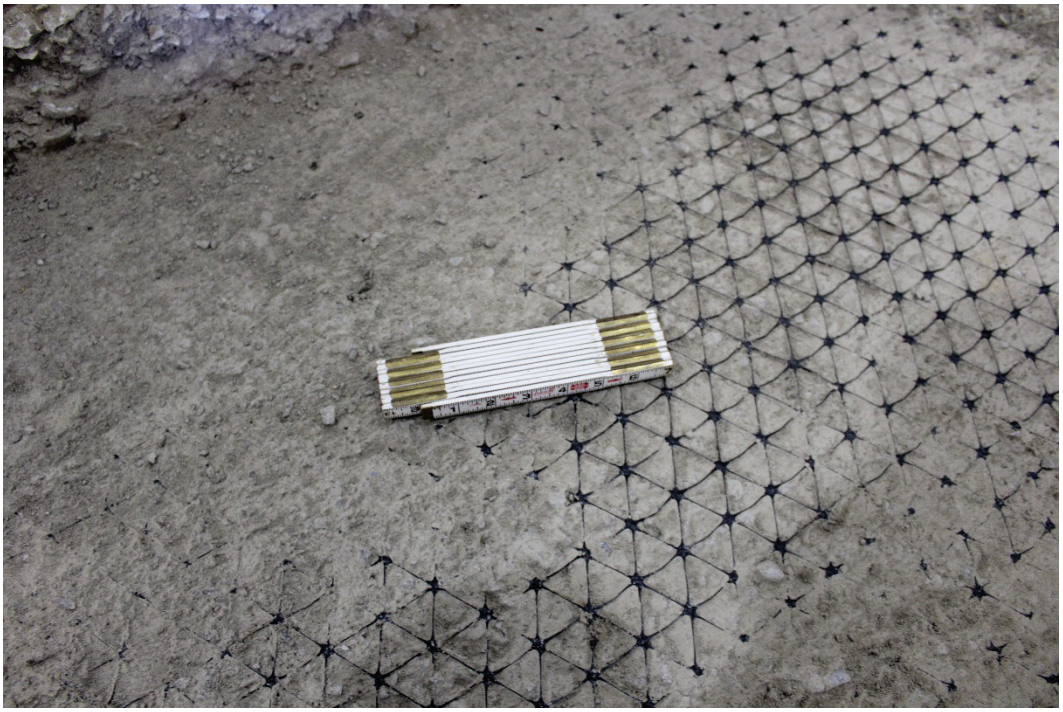


Figure 29. Item 1 indentations in subgrade.

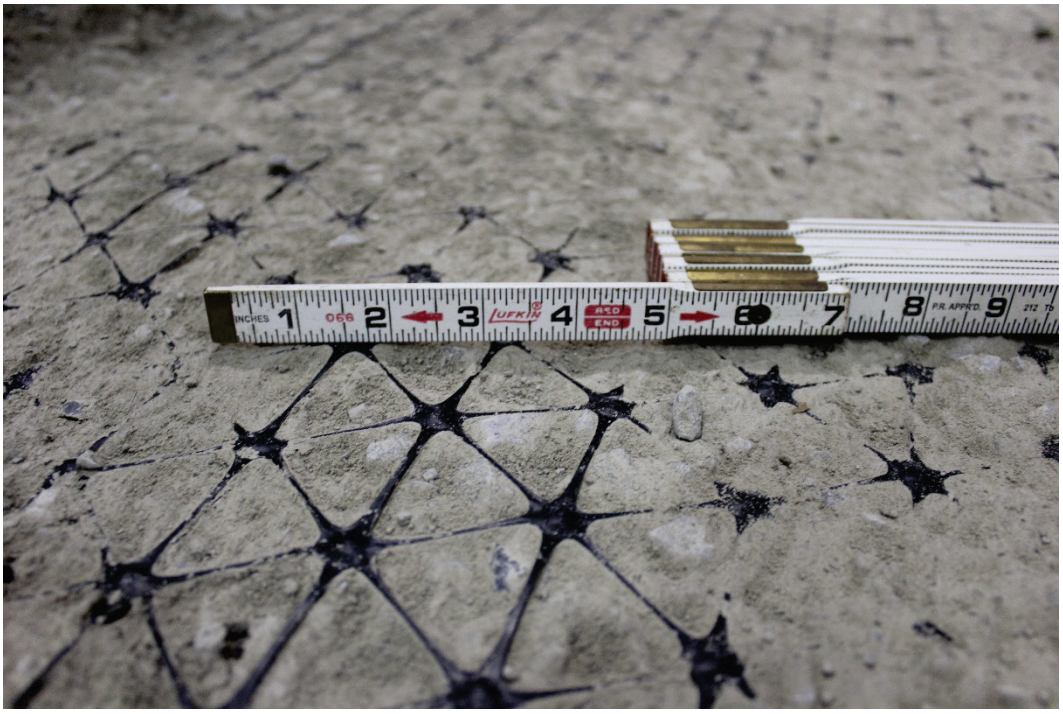


Figure 30. Item 2 indentations in subgrade.

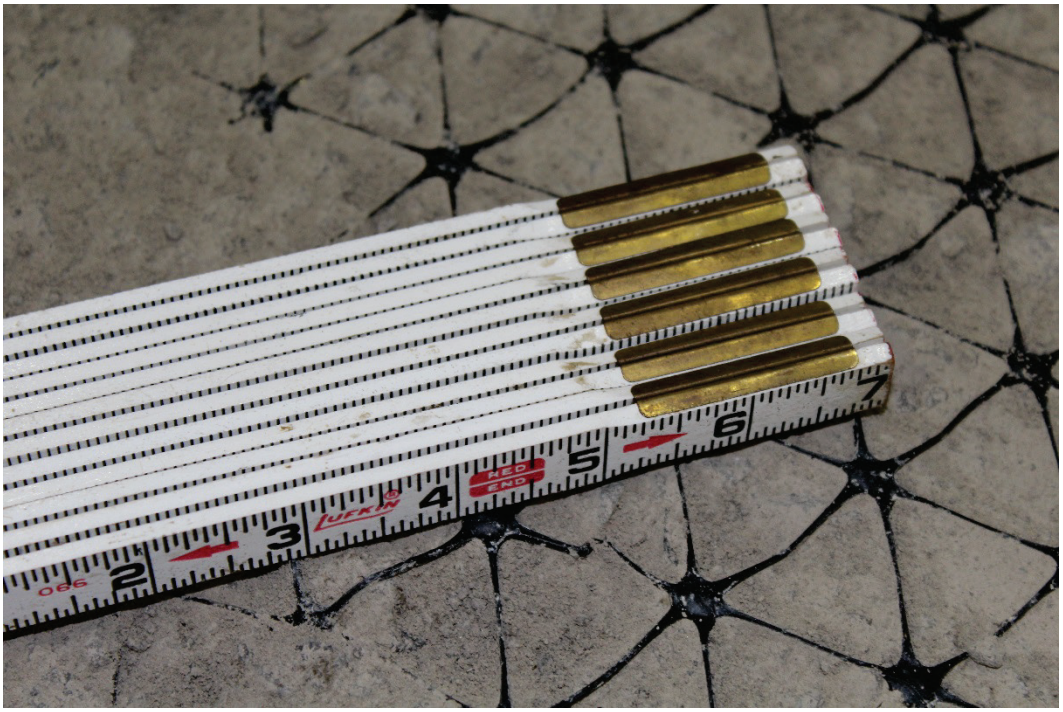


Figure 31. Post-traffic pavement cross section in Item 1.

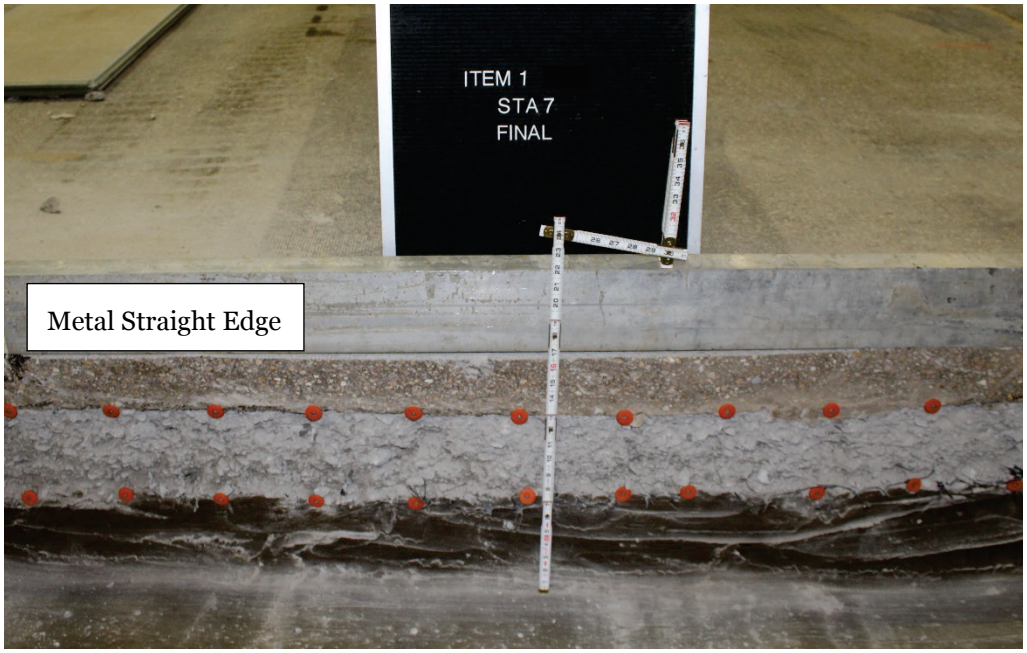


Figure 32. Post-traffic pavement cross section in Item 2.

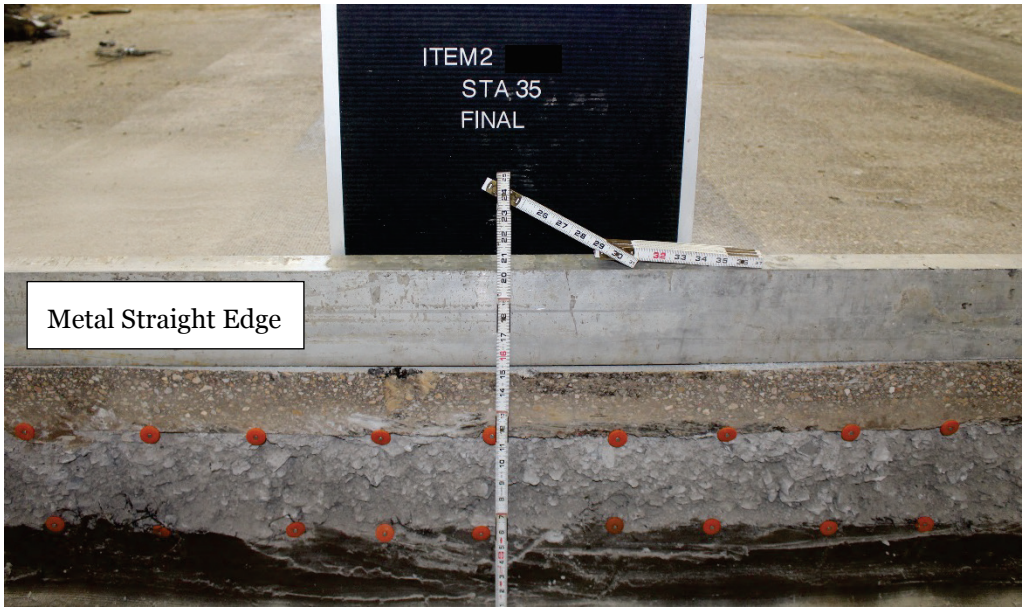



Figure 33. Post-traffic pavement cross section in unstabilized section.



# 9 Analysis

In order to provide a measure of the performance benefit of each geogrid, an analysis was performed to calculate the effective structural number of the stabilized and unstabilized test items. The analysis results are discussed in the following paragraph.

In order to quantify the structural contribution of the geogrid, an effective structural number was calculated using the AASHTO Pavement Design Guide (1993). The effective structural number was calculated using the applied ESALs and the as-built layer thicknesses to compute the structural coefficient of the base-course layer. The effective structural coefficient provides a means of comparing test sections of varying layer thicknesses. Table 10 summarizes the effective base coefficient for each test section. A 90% reliability and an asphalt structural coefficient of 0.44 was selected for the calculations. The calculations indicate the different geogrid items had nearly the same effective structural coefficient, with both items displaying a significant increase in structural capacity over the unstabilized control item. It should be noted that none of the test sections reached the failure criteria (1 in. of rutting); therefore, the structural coefficients presented should be considered conservative estimates.

Table 10. Effective stabilized layer structural coefficient.

| | Item 1 | Item 2 | Unstabilized |
|---|---|---|---|
| Design Base Thickness (in.) | 6 | 6 | 8 |
| Design Asphalt Thickness (in.) | 3 | 3 | 4 |
| Unstabilized Design Structural Number | 2.16 | 2.16 | 2.88 |
| As-Built Base Thickness (in.) | 5.8 | 5.9 | 7.7 |
| As-Built Asphalt Thickness (in.) | 3.20 | 3.22 | 4 |
| Unstabilized As-Built Structural Number | 2.22 | 2.24 | 2.84 |
| Passes to 1-in. rutting (ESALs) | 811,200+ | 811,200+ | 811,200+ |
| Effective Structural Number | 3.08+ | 3.08+ | 3.08+ |
| Effective Base Coefficient (1-in. rutting) | 0.29+ | 0.28+ | 0.17+ |
| Passes to ½-in. rutting (ESALs) | 811,200+ | 811,200+ | 500,000 |
| Effective Structural Number | 3.08+ | 3.08+ | 2.86 |
| Effective Base Coefficient (1/2-in. rutting) | 0.29+ | 0.28+ | 0.14 |

# 10 Conclusions and Recommendations

A full-scale test section was constructed and trafficked to evaluate the performance of geogrid-stabilized highway pavements. The construction and traffic data were analyzed to assess both the relative performance of two multi-axial geogrid stabilized pavement sections and their performance as compared to an unstabilized pavement section from a previous related study (Norwood and Tingle 2014). The following conclusions are a result of this study:

1. The pavement test sections were constructed in a uniform manner with minor variability utilizing similar material and construction techniques used in previous geosynthetic stabilized test sections. The uniformity of construction and materials allow for meaningful comparisons between test sections to be made.
2. As-built ISM values for the stabilized items were found to be less than those for the unstabilized items, which was expected due to a reduced pavement section.
3. Subgrade and base earth pressure cell response values in the stabilized sections were found to be generally equivalent to measured responses in the unstabilized section. A slight upward trend was observed in subgrade pressure with increasing traffic that may be due to densification and stiffening over time.
4. Measured deflections in the stabilized items were approximately ½ of that observed in the unstabilized section. This may be indicative of base stiffening due to aggregate interlock at the geogrid/aggregate interface.
5. Asphalt strain gauge response in the stabilized sections were less than that measured in the unstabilized section, however, differing gauge manufacturers were utilized. It is recommended that caution be exercised when comparing these data.
6. Both geogrid stabilized pavement sections improved the rutting resistance when compared to the unstabilized test section.
7. Minimal differences in rutting performance were observed between the two stabilized test sections.
8. The calculated effective base structural coefficient of the geogrid stabilized pavement sections was higher than the unstabilized structural coefficient, suggesting incorporation of a multi-axial geogrid in a flexible pavement base course provides a significant structural benefit.

# References

American Society for Testing and Materials (ASTM). 2010. *Standard test methods for liquid limit, plastic limit, and plasticity index of soils*. Designation: D 4318-10e1. West Conshohocken, PA.

American Society for Testing and Materials (ASTM). 2011. *Standard practice for classification of soils for engineering purposes (Unified Soil Classification System)*. Designation: D 2487-11. West Conshohocken, PA.

American Society for Testing and Materials (ASTM). 2012. *Standard test methods for laboratory compaction characteristics of soil using modified effort (56,000 ft-blf/ft³ (2,700 kN-m/m³))*. Designation: D 1557-12e1. West Conshohocken, PA.

American Society for Testing and Materials (ASTM). 2016. *Standard test method for California Bearing Ratio (CBR) of laboratory-compacted soils*. Designation: D 1883-16. West Conshohocken, PA.

American Society for Testing and Materials (ASTM). 2015. *Standard test methods for in-place density and water content of soil and soil-aggregate by nuclear methods (shallow depth)*. Designation: D 6938-15. West Conshohocken, PA.

American Society for Testing and Materials (ASTM). 2009. *Standard test method for CBR (California Bearing Ratio) of soils in place*. Designation: D 4429-09a. West Conshohocken, PA.

American Society for Testing and Materials (ASTM). 2015. *Standard test method for use of the dynamic cone penetrometer in shallow pavement applications*. Designation: D 6951/6951M-09. West Conshohocken, PA.

Association of American Highway and Transportation Officials (AASHTO). 2012. *Standard specification for classification of soils and soil-aggregate mixtures for highway construction purposes*. AASHTO M 145. Washington, DC: Association of American Highway and Transportation Officials.

Association of American Highway and Transportation Officials (AASHTO). 2013. *Standard method of test for bulk specific gravity ($G_{mb}$) of compacted hot mix asphalt (HMA) using saturated surface-dry specimens*. AASHTO T 166. Washington, DC: Association of American Highway and Transportation Officials.

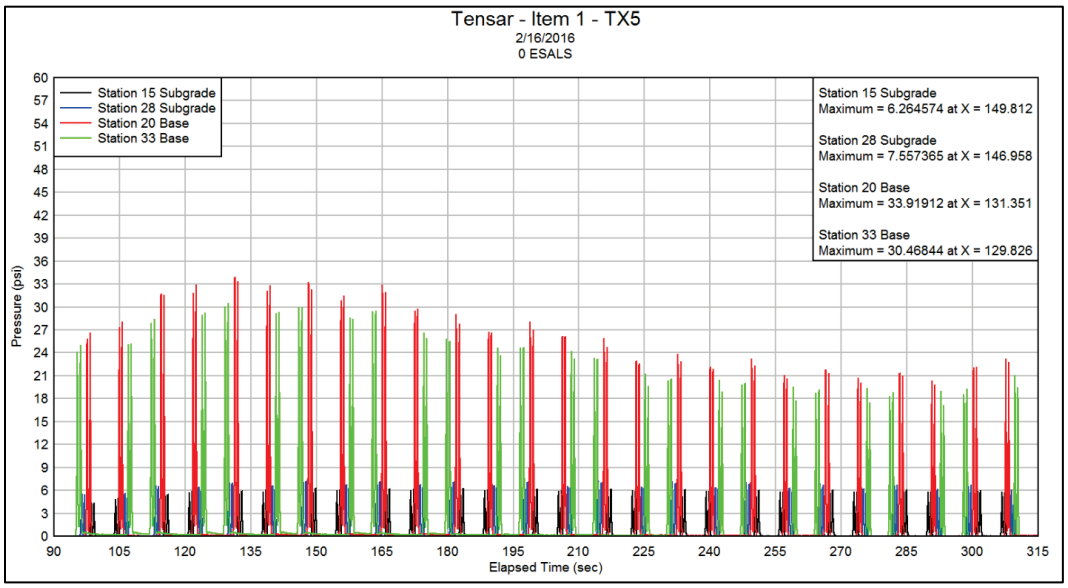
Association of American Highway and Transportation Officials (AASHTO). 1993. *AASHTO guide for design of pavement structures*. Washington, DC: Association of American Highway and Transportation Officials.

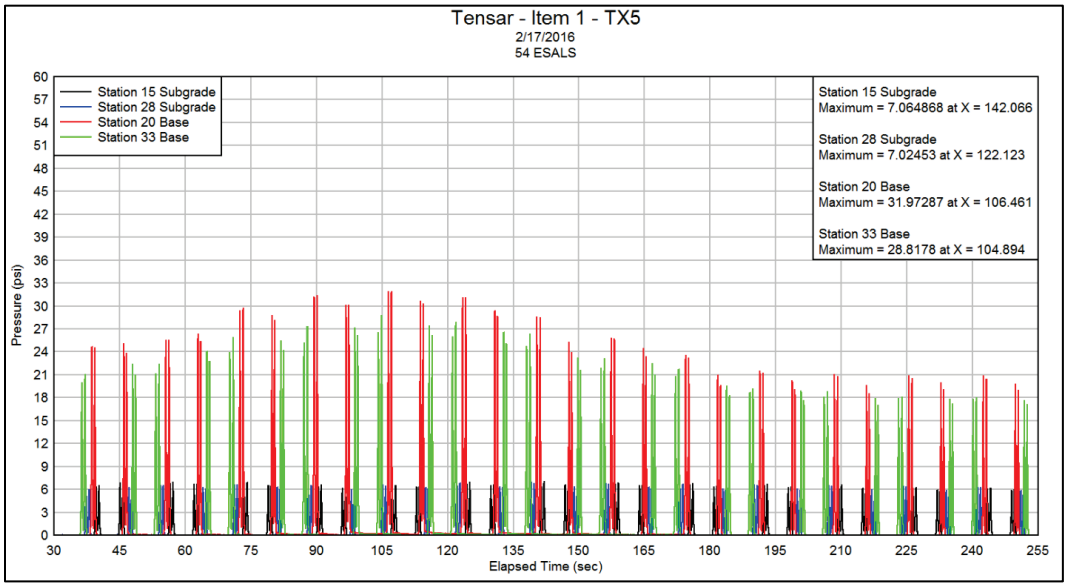
Norwood, G. J., and J. S. Tingle. 2014. *Performance of geogrid-stabilized flexible pavements*. ERDC/GSL-TR-14-28. Vicksburg, MS: U.S. Army Engineer Research and Development Center.

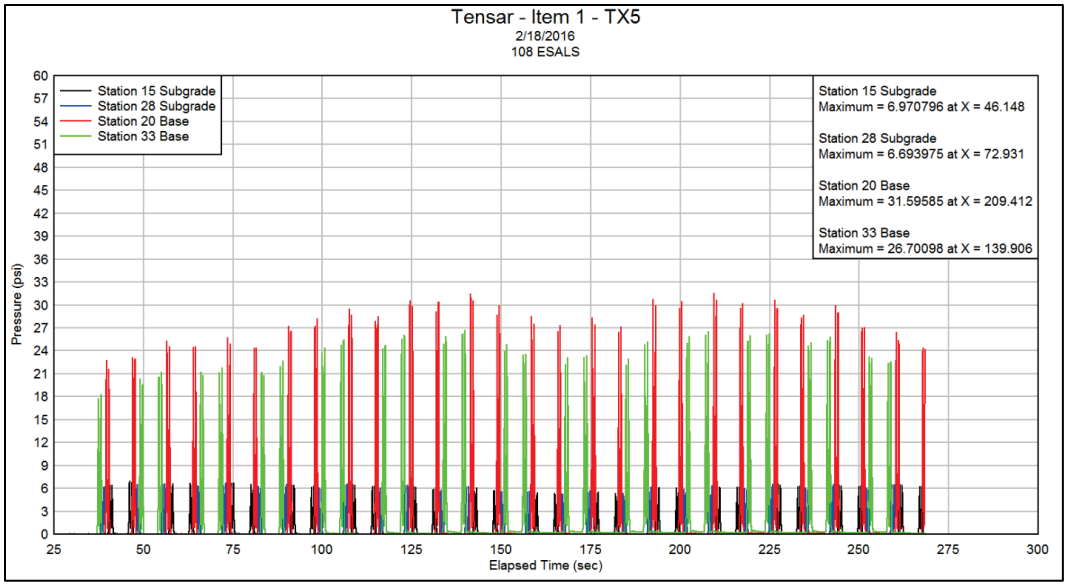
Webster, S. L., R. H. Grau, and T. P. Williams. 1992. *Description and application of dual-mass dynamic cone penetrometer*. Instruction Report GL-92-3. Vicksburg, MS: U.S. Army Engineer Waterways Experiment Station.

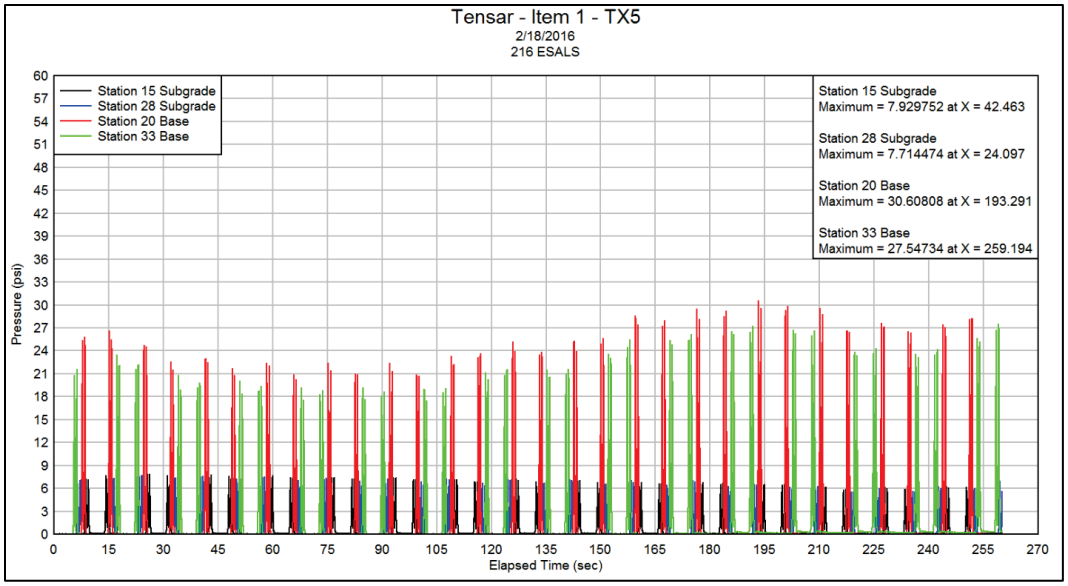
Webster, S. L., R. W. Brown, and J. R. Porter. 1994. *Force projection site evaluation using the electrical cone penetrometer (ECPO) and the dynamic cone penetrometer (DCP)*. Technical Report GL-94-17. Vicksburg, MS: U.S. Army Engineer Waterways Experiment Station.

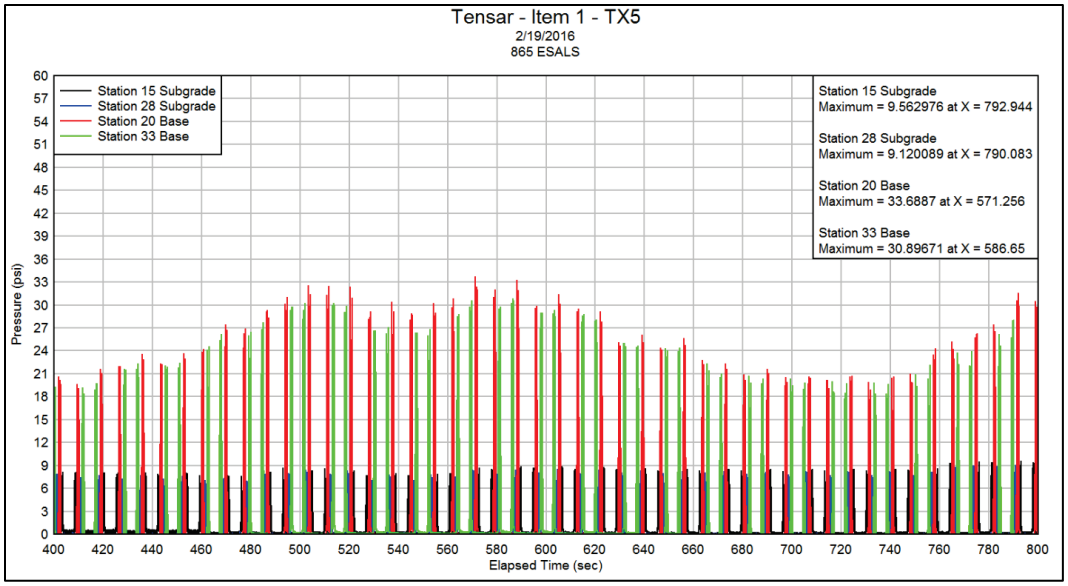
# Appendix A: Earth Pressure Cell Responses

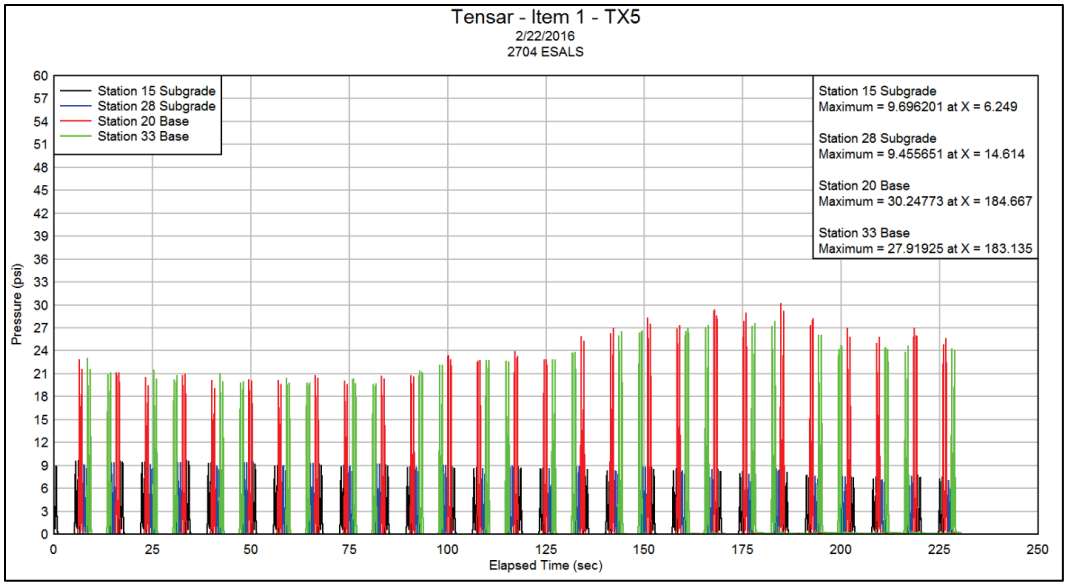


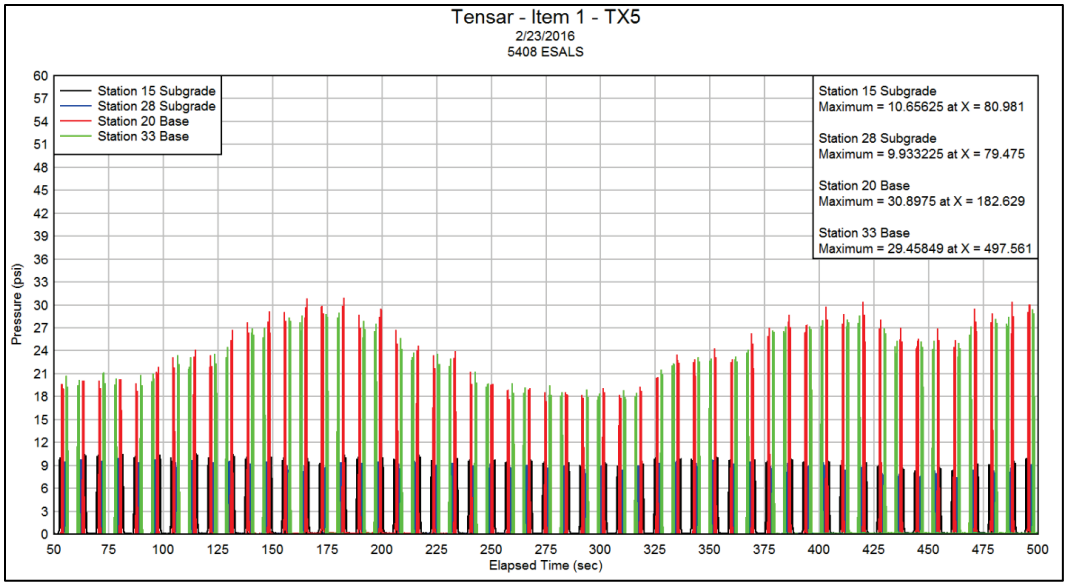



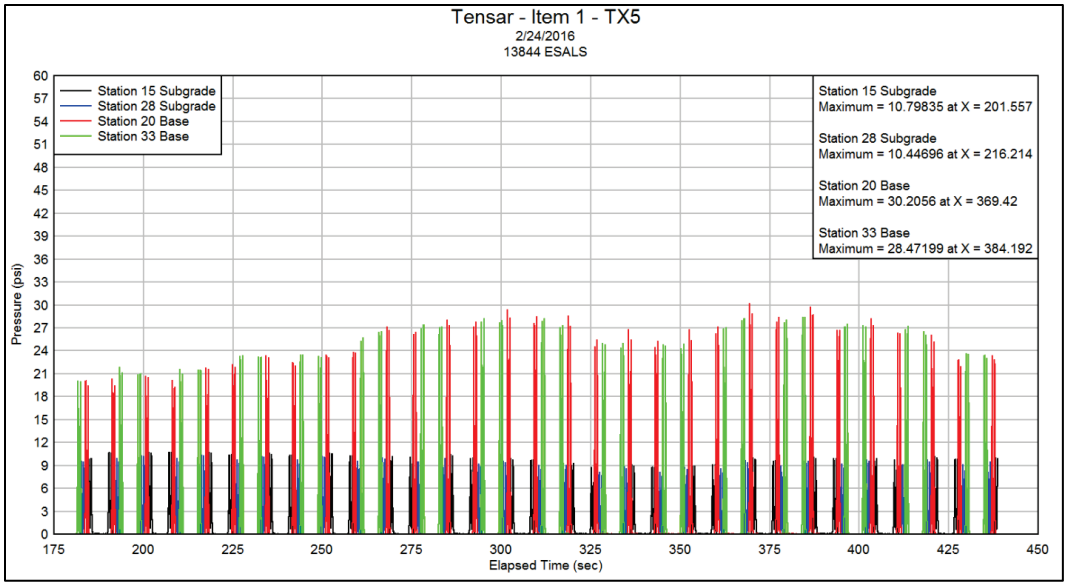

Tensar - Item 1 - TX5
2/18/2016
108 ESALS
Station 15 Subgrade
Station 28 Subgrade
Station 20 Base
Station 33 Base
Station 15 Subgrade
Maximum = 6.970796 at X = 46.148
Station 28 Subgrade
Maximum = 6.693975 at X = 72.931
Station 20 Base
Maximum = 31.59585 at X = 209.412
Station 33 Base
Maximum = 26.70098 at X = 139.906
Pressure (psi)
Elapsed Time (sec)

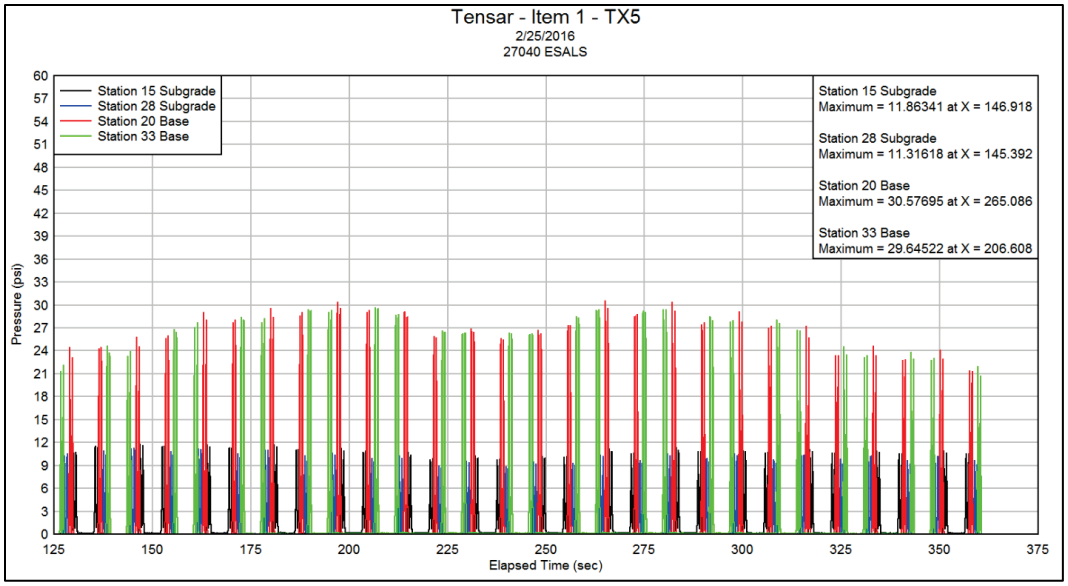

Tensar - Item 1 - TX5
2/18/2016
216 ESALS
Station 15 Subgrade
Station 28 Subgrade
Station 20 Base
Station 33 Base
Station 15 Subgrade
Maximum = 7.929752 at X = 42.463
Station 28 Subgrade
Maximum = 7.714474 at X = 24.097
Station 20 Base
Maximum = 30.60808 at X = 193.291
Station 33 Base
Maximum = 27.54734 at X = 259.194
Pressure (psi)
Elapsed Time (sec)

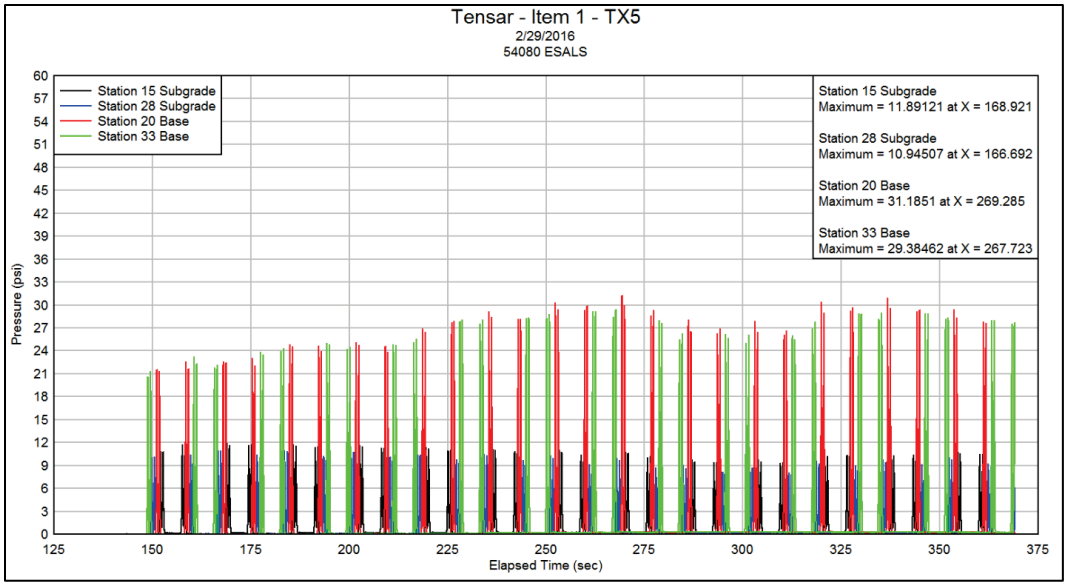

Tensar - Item 1 - TX5
2/19/2016
865 ESALS
Station 15 Subgrade
Station 28 Subgrade
Station 20 Base
Station 33 Base
Station 15 Subgrade
Maximum = 9.562976 at X = 792.944
Station 28 Subgrade
Maximum = 9.120089 at X = 790.083
Station 20 Base
Maximum = 33.6887 at X = 571.256
Station 33 Base
Maximum = 30.89671 at X = 586.65
Pressure (psi)
Elapsed Time (sec)

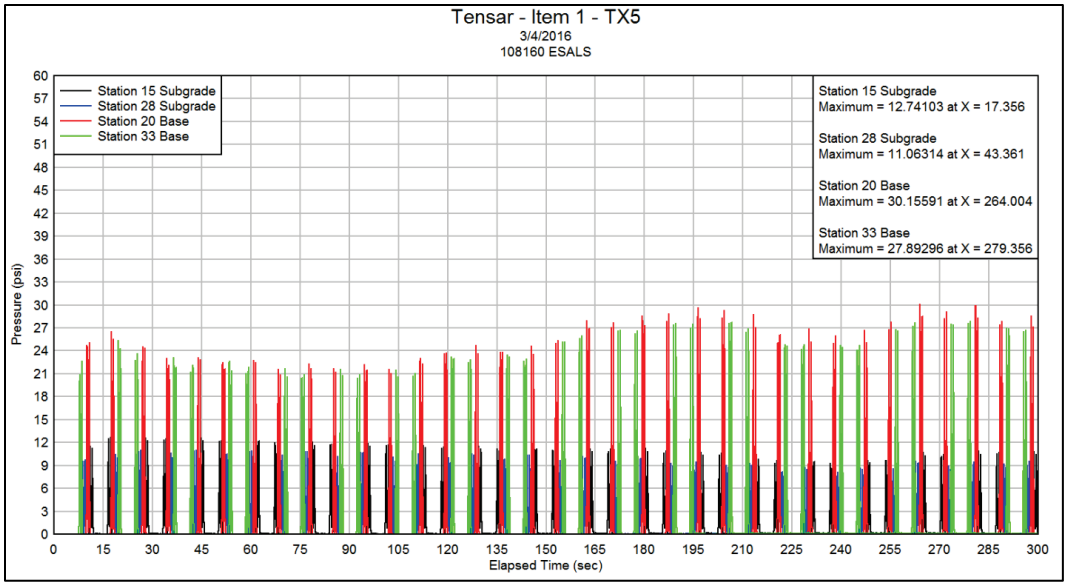

Tensar - Item 1 - TX5
2/22/2016
2704 ESALS
Station 15 Subgrade
Station 28 Subgrade
Station 20 Base
Station 33 Base
Station 15 Subgrade
Maximum = 9.696201 at X = 6.249
Station 28 Subgrade
Maximum = 9.455651 at X = 14.614
Station 20 Base
Maximum = 30.24773 at X = 184.667
Station 33 Base
Maximum = 27.91925 at X = 183.135
Pressure (psi)
Elapsed Time (sec)

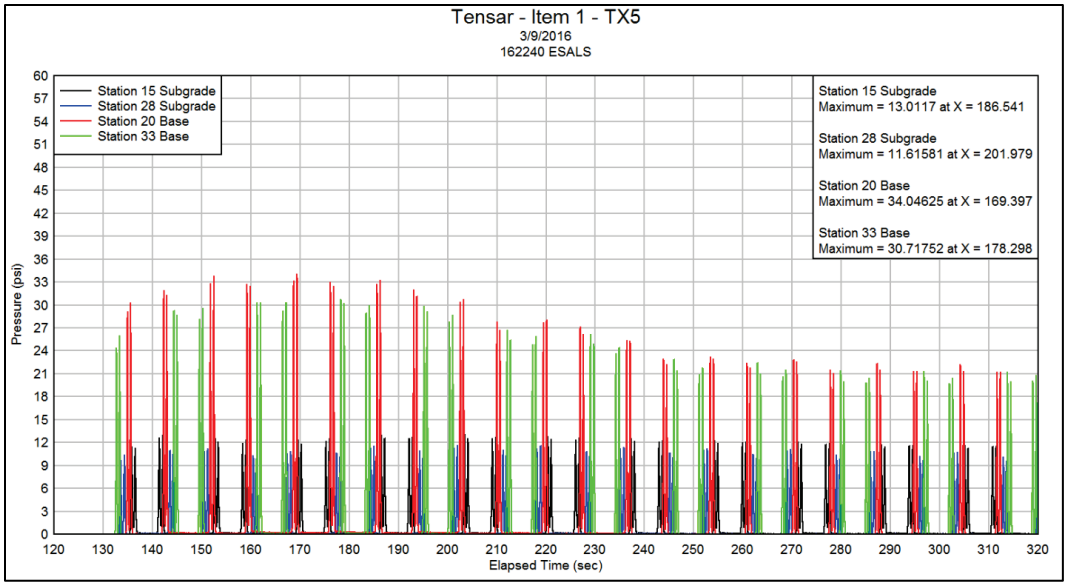

Tensar - Item 1 - TX5
2/23/2016
5408 ESALS
Station 15 Subgrade
Station 28 Subgrade
Station 20 Base
Station 33 Base
Station 15 Subgrade
Maximum = 10.65625 at X = 80.981
Station 28 Subgrade
Maximum = 9.933225 at X = 79.475
Station 20 Base
Maximum = 30.8975 at X = 182.629
Station 33 Base
Maximum = 29.45849 at X = 497.561
Pressure (psi)
Elapsed Time (sec)

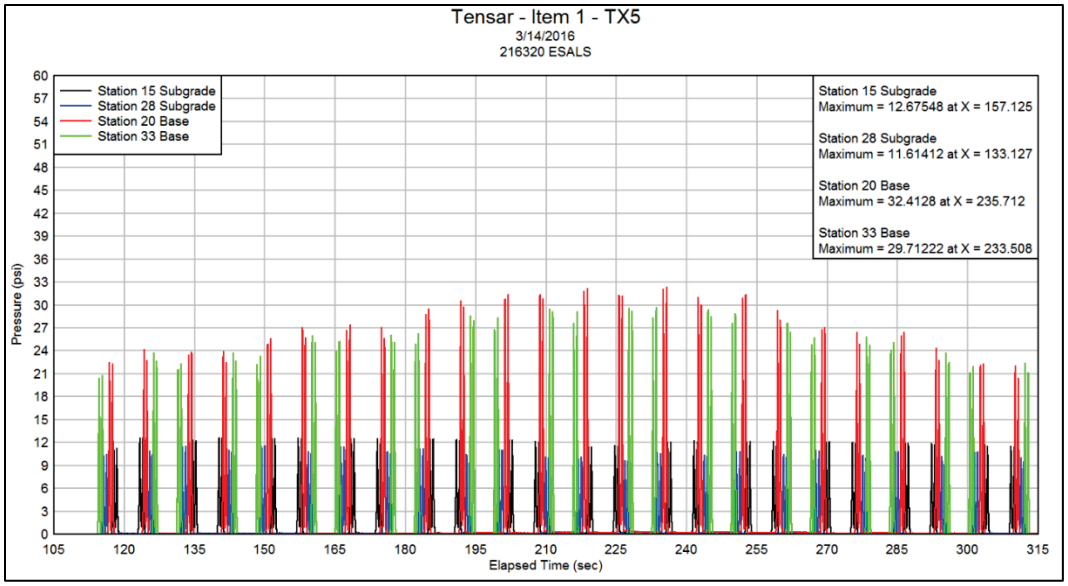

Tensar - Item 1 - TX5
2/24/2016
13844 ESALS
Station 15 Subgrade
Station 28 Subgrade
Station 20 Base
Station 33 Base
Station 15 Subgrade
Maximum = 10.79835 at X = 201.557
Station 28 Subgrade
Maximum = 10.44696 at X = 216.214
Station 20 Base
Maximum = 30.2056 at X = 369.42
Station 33 Base
Maximum = 28.47199 at X = 384.192
Pressure (psi)
Elapsed Time (sec)

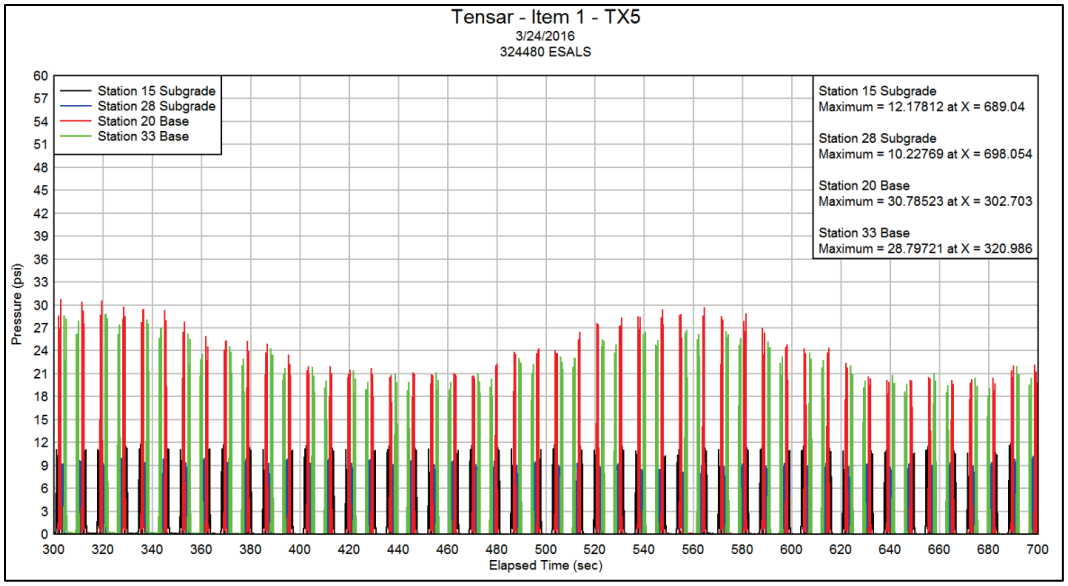

Tensar - Item 1 - TX5
2/25/2016
27040 ESALS
Station 15 Subgrade
Station 28 Subgrade
Station 20 Base
Station 33 Base
Station 15 Subgrade
Maximum = 11.86341 at X = 146.918
Station 28 Subgrade
Maximum = 11.31618 at X = 145.392
Station 20 Base
Maximum = 30.57695 at X = 265.086
Station 33 Base
Maximum = 29.64522 at X = 206.608
Pressure (psi)
Elapsed Time (sec)

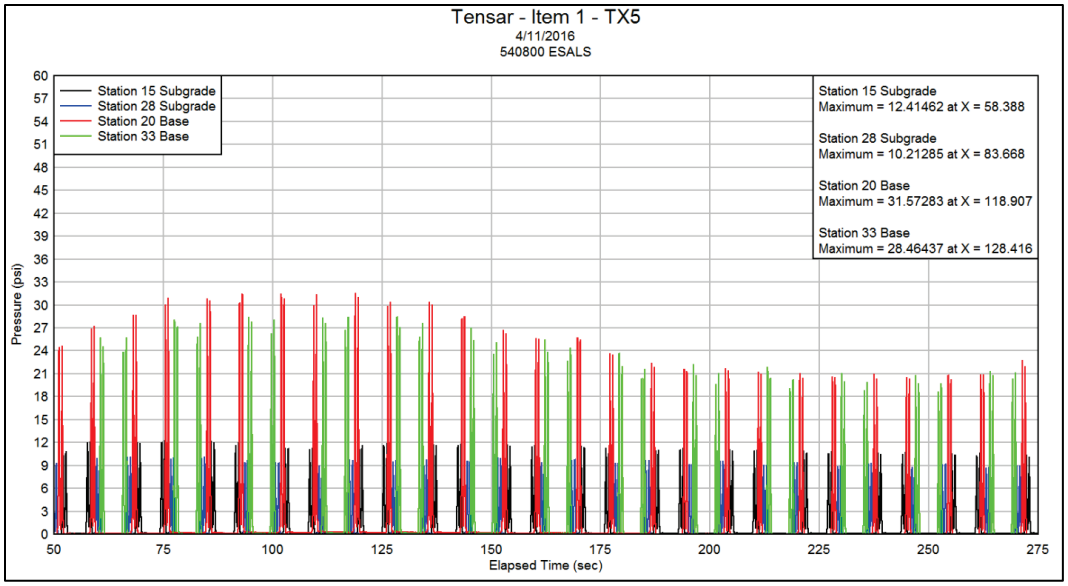

Tensar - Item 1 - TX5
2/29/2016
54080 ESALS
Station 15 Subgrade
Station 28 Subgrade
Station 20 Base
Station 33 Base
Station 15 Subgrade
Maximum = 11.89121 at X = 168.921
Station 28 Subgrade
Maximum = 10.94507 at X = 166.692
Station 20 Base
Maximum = 31.1851 at X = 269.285
Station 33 Base
Maximum = 29.38462 at X = 267.723
Pressure (psi)
Elapsed Time (sec)

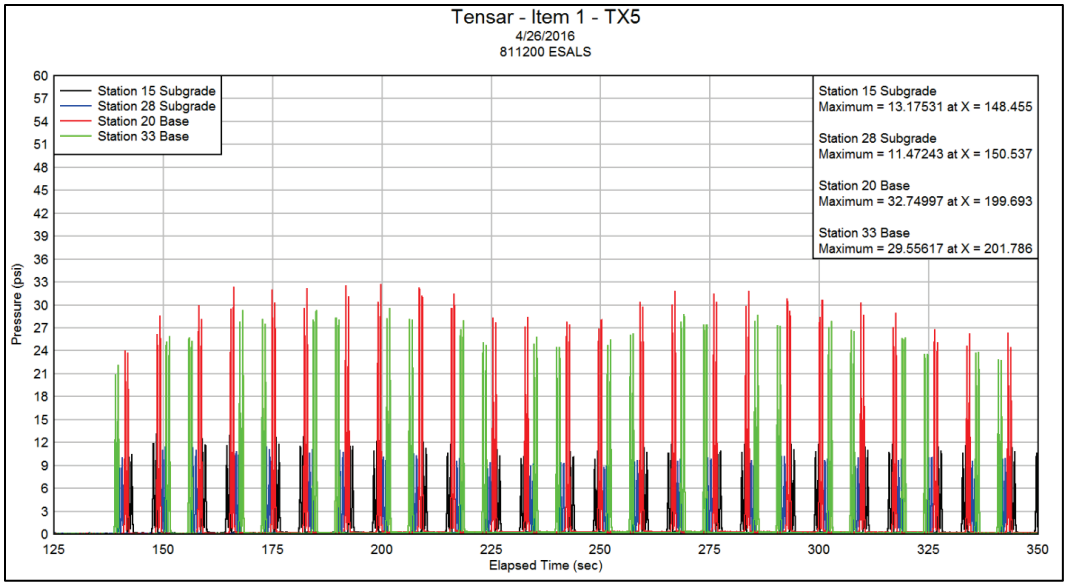

Tensar - Item 1 - TX5
3/4/2016
108160 ESALS
Station 15 Subgrade
Station 28 Subgrade
Station 20 Base
Station 33 Base
Station 15 Subgrade
Maximum = 12.74103 at X = 17.356
Station 28 Subgrade
Maximum = 11.06314 at X = 43.361
Station 20 Base
Maximum = 30.15591 at X = 264.004
Station 33 Base
Maximum = 27.89296 at X = 279.356
Pressure (psi)
Elapsed Time (sec)

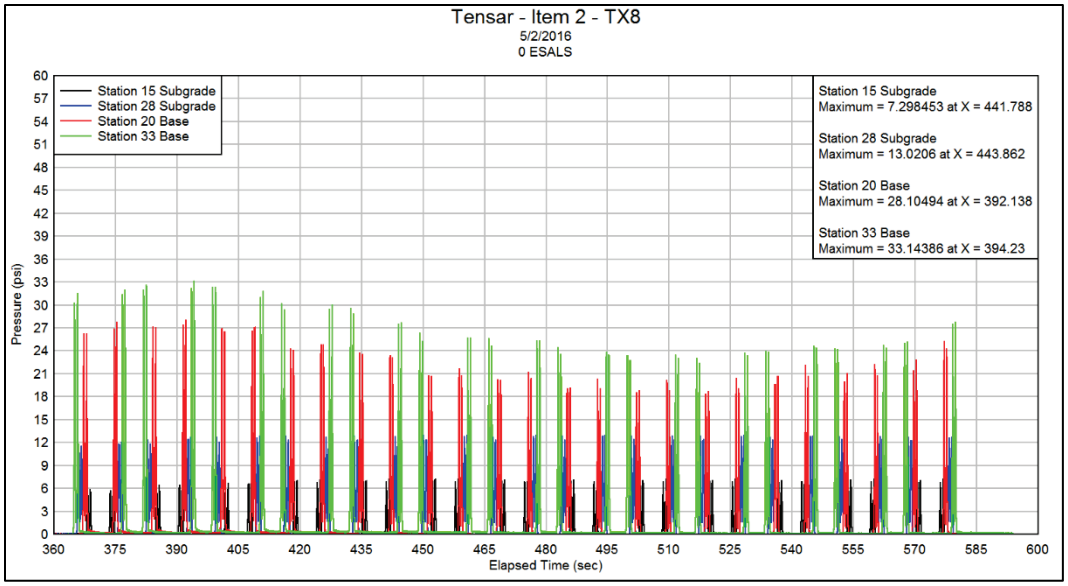

Tensar - Item 1 - TX5
3/9/2016
162240 ESALS
Station 15 Subgrade
Station 28 Subgrade
Station 20 Base
Station 33 Base
Station 15 Subgrade
Maximum = 13.0117 at X = 186.541
Station 28 Subgrade
Maximum = 11.61581 at X = 201.979
Station 20 Base
Maximum = 34.04625 at X = 169.397
Station 33 Base
Maximum = 30.71752 at X = 178.298
Pressure (psi)
Elapsed Time (sec)

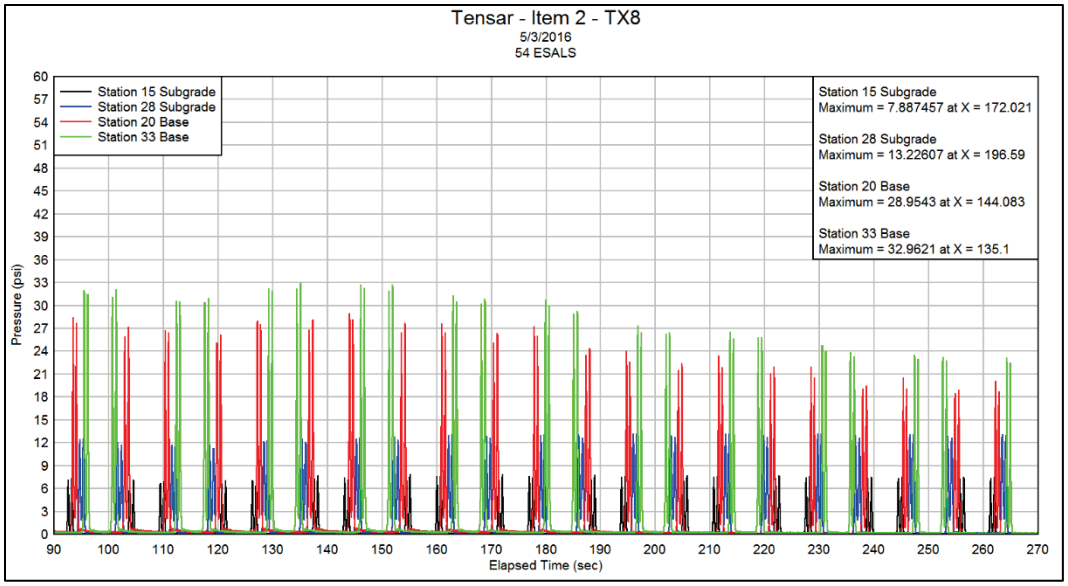

Tensar - Item 1 - TX5
3/14/2016
216320 ESALS
Station 15 Subgrade
Station 28 Subgrade
Station 20 Base
Station 33 Base
Station 15 Subgrade
Maximum = 12.67548 at X = 157.125
Station 28 Subgrade
Maximum = 11.61412 at X = 133.127
Station 20 Base
Maximum = 32.4128 at X = 235.712
Station 33 Base
Maximum = 29.71222 at X = 233.508
Pressure (psi)
Elapsed Time (sec)

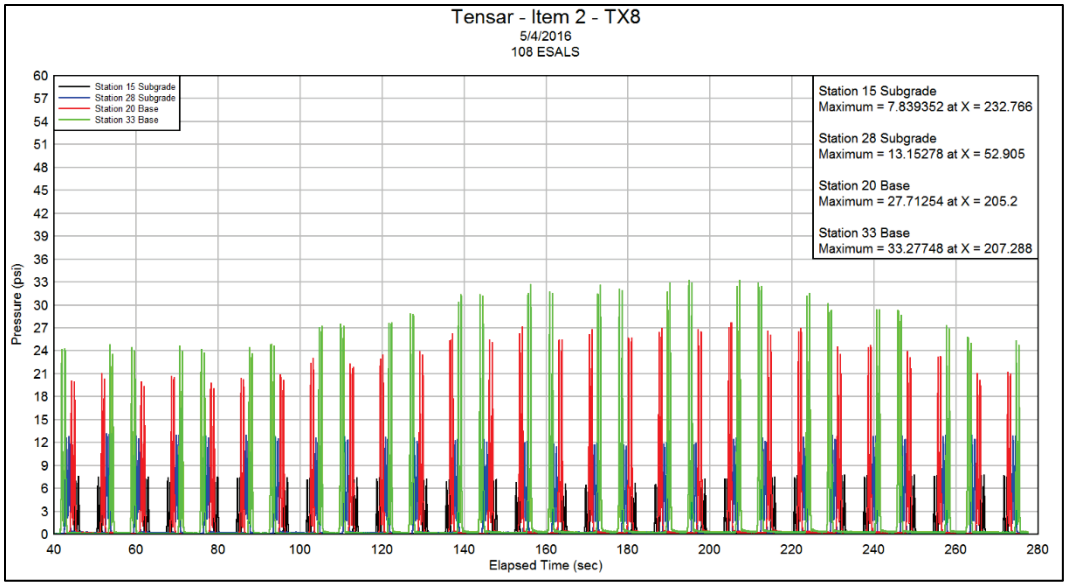

Tensar - Item 1 - TX5
3/24/2016
324480 ESALS
Station 15 Subgrade
Station 28 Subgrade
Station 20 Base
Station 33 Base
Station 15 Subgrade
Maximum = 12.17812 at X = 689.04
Station 28 Subgrade
Maximum = 10.22769 at X = 698.054
Station 20 Base
Maximum = 30.78523 at X = 302.703
Station 33 Base
Maximum = 28.79721 at X = 320.986
Pressure (psi)
Elapsed Time (sec)

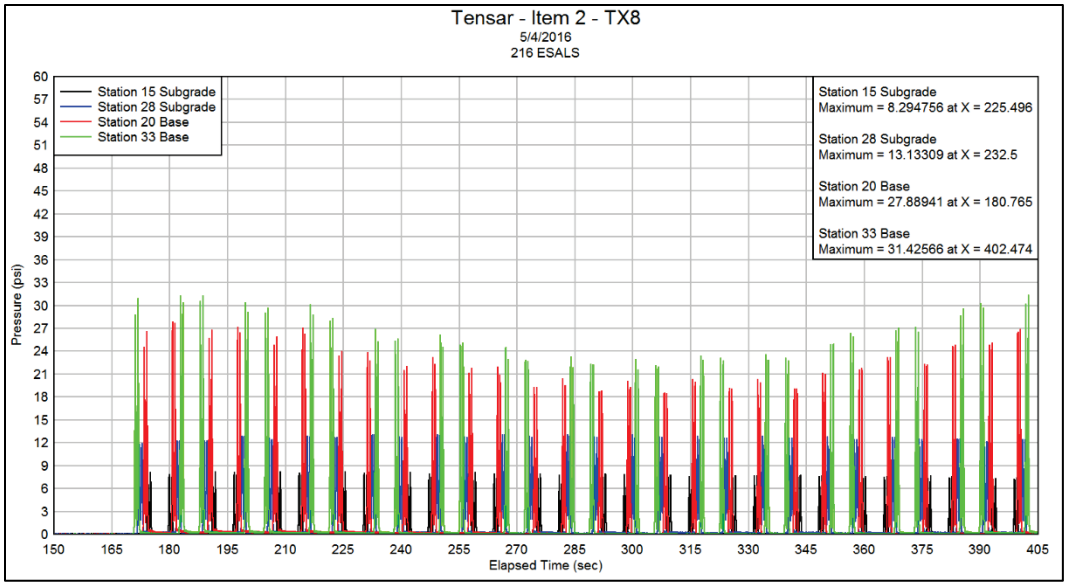

Tensar - Item 1 - TX5
4/11/2016
540800 ESALS
Station 15 Subgrade
Station 28 Subgrade
Station 20 Base
Station 33 Base
Station 15 Subgrade
Maximum = 12.41462 at X = 58.388
Station 28 Subgrade
Maximum = 10.21285 at X = 83.668
Station 20 Base
Maximum = 31.57283 at X = 118.907
Station 33 Base
Maximum = 28.46437 at X = 128.416
Pressure (psi)
Elapsed Time (sec)

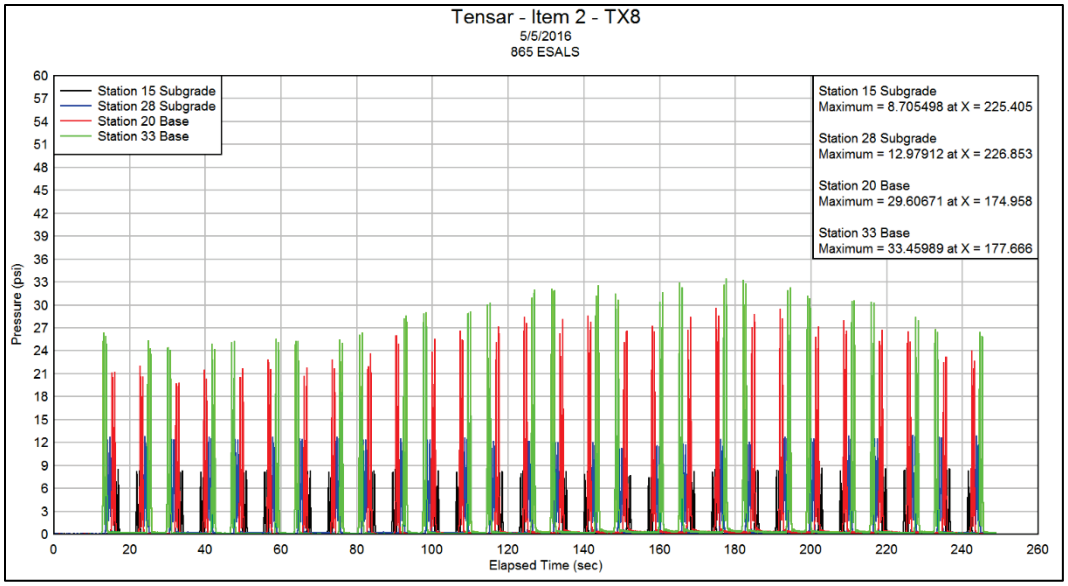

Tensar - Item 1 - TX5
4/26/2016
811200 ESALS
Station 15 Subgrade
Station 28 Subgrade
Station 20 Base
Station 33 Base
Station 15 Subgrade
Maximum = 13.17531 at X = 148.455
Station 28 Subgrade
Maximum = 11.47243 at X = 150.537
Station 20 Base
Maximum = 32.74997 at X = 199.693
Station 33 Base
Maximum = 29.55617 at X = 201.786
Pressure (psi)
Elapsed Time (sec)

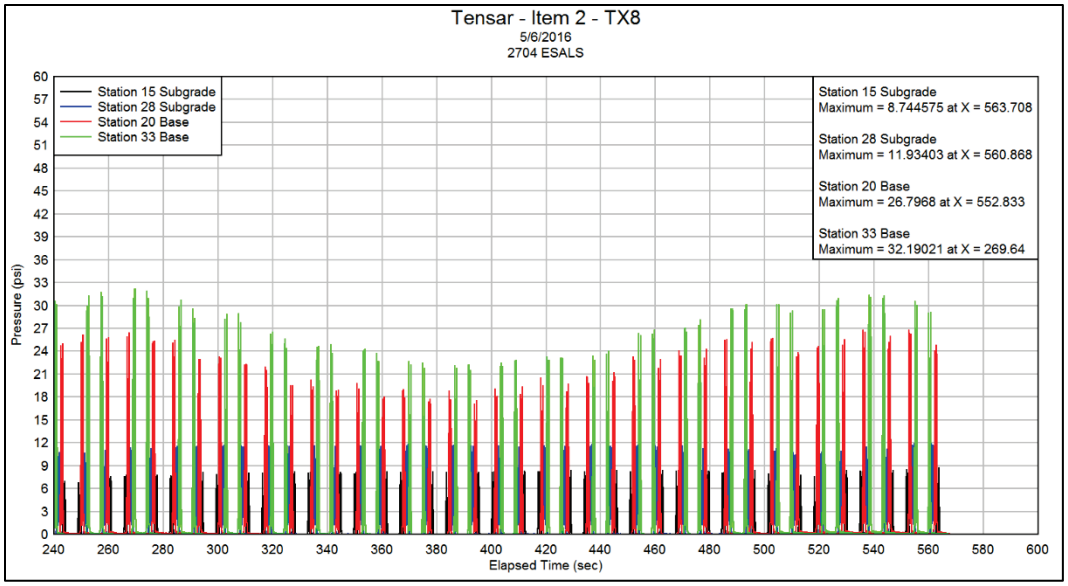

Tensar - Item 2 - TX8
5/2/2016
0 ESALS
Station 15 Subgrade
Station 28 Subgrade
Station 20 Base
Station 33 Base
Station 15 Subgrade
Maximum = 7.298453 at X = 441.788
Station 28 Subgrade
Maximum = 13.0206 at X = 443.862
Station 20 Base
Maximum = 28.10494 at X = 392.138
Station 33 Base
Maximum = 33.14386 at X = 394.23
Pressure (psi)
Elapsed Time (sec)

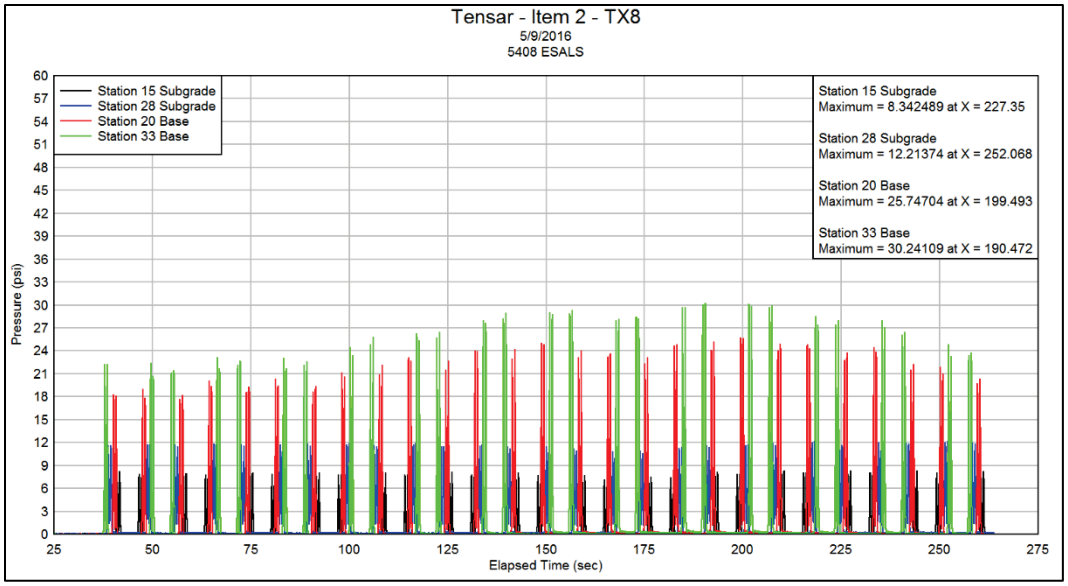

Tensar - Item 2 - TX8
5/3/2016
54 ESALS
Station 15 Subgrade
Station 28 Subgrade
Station 20 Base
Station 33 Base
Station 15 Subgrade
Maximum = 7.887457 at X = 172.021
Station 28 Subgrade
Maximum = 13.22607 at X = 196.59
Station 20 Base
Maximum = 28.9543 at X = 144.083
Station 33 Base
Maximum = 32.9621 at X = 135.1
Pressure (psi)
Elapsed Time (sec)

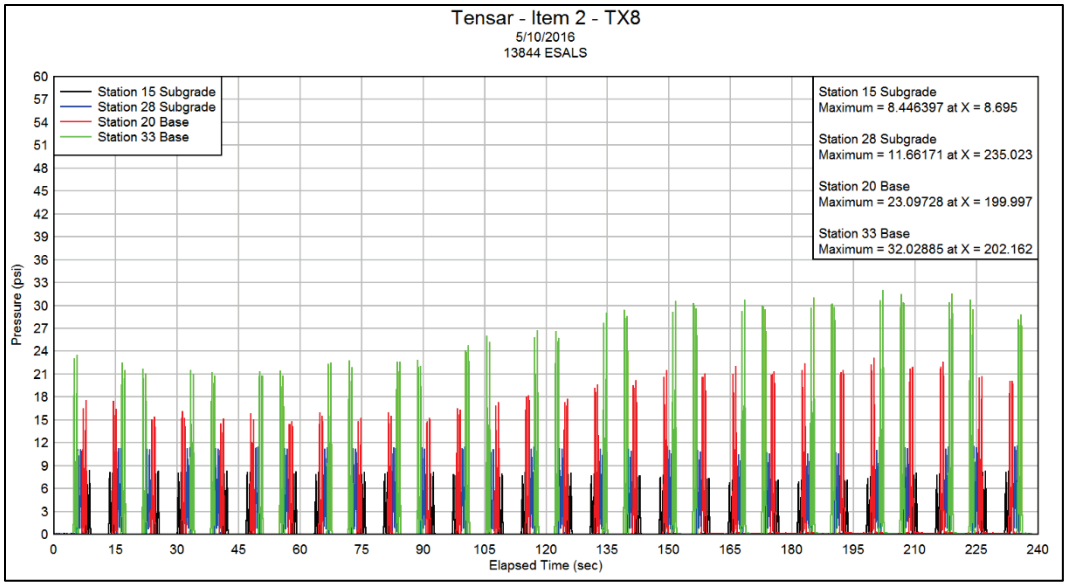

Tensar - Item 2 - TX8
5/4/2016
108 ESALS
Station 15 Subgrade
Station 28 Subgrade
Station 20 Base
Station 33 Base
Station 15 Subgrade
Maximum = 7.839352 at X = 232.766
Station 28 Subgrade
Maximum = 13.15278 at X = 52.905
Station 20 Base
Maximum = 27.71254 at X = 205.2
Station 33 Base
Maximum = 33.27748 at X = 207.288
Pressure (psi)
Elapsed Time (sec)

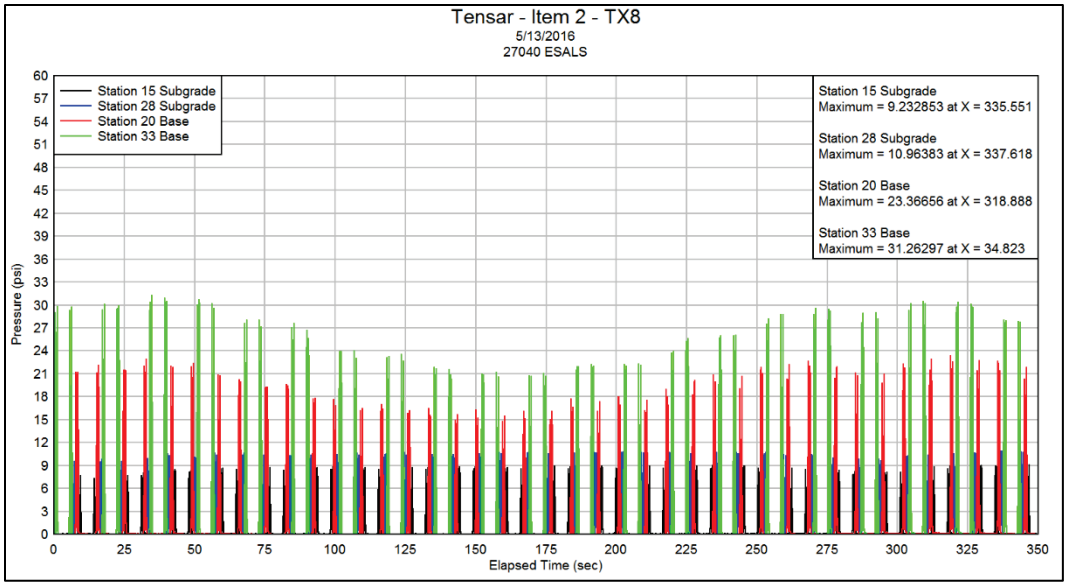

Tensar - Item 2 - TX8
5/4/2016
216 ESALS
Station 15 Subgrade
Station 28 Subgrade
Station 20 Base
Station 33 Base
Station 15 Subgrade
Maximum = 8.294756 at X = 225.496
Station 28 Subgrade
Maximum = 13.13309 at X = 232.5
Station 20 Base
Maximum = 27.88941 at X = 180.765
Station 33 Base
Maximum = 31.42566 at X = 402.474
Pressure (psi)
Elapsed Time (sec)

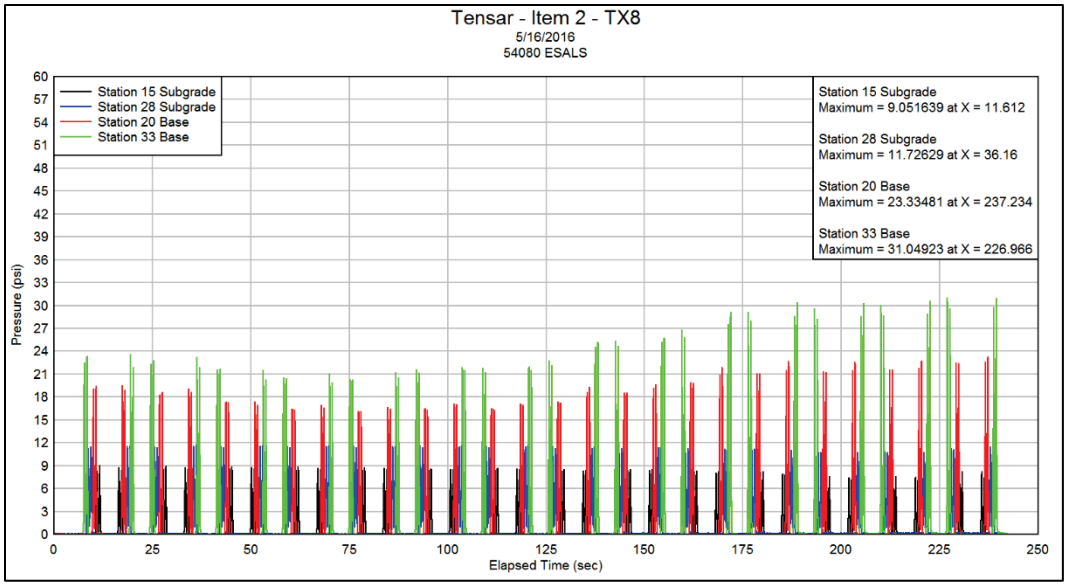

Tensar - Item 2 - TX8
5/5/2016
865 ESALS
Station 15 Subgrade
Station 28 Subgrade
Station 20 Base
Station 33 Base
Station 15 Subgrade
Maximum = 8.705498 at X = 225.405
Station 28 Subgrade
Maximum = 12.97912 at X = 226.853
Station 20 Base
Maximum = 29.60671 at X = 174.958
Station 33 Base
Maximum = 33.45989 at X = 177.666
Pressure (psi)
Elapsed Time (sec)

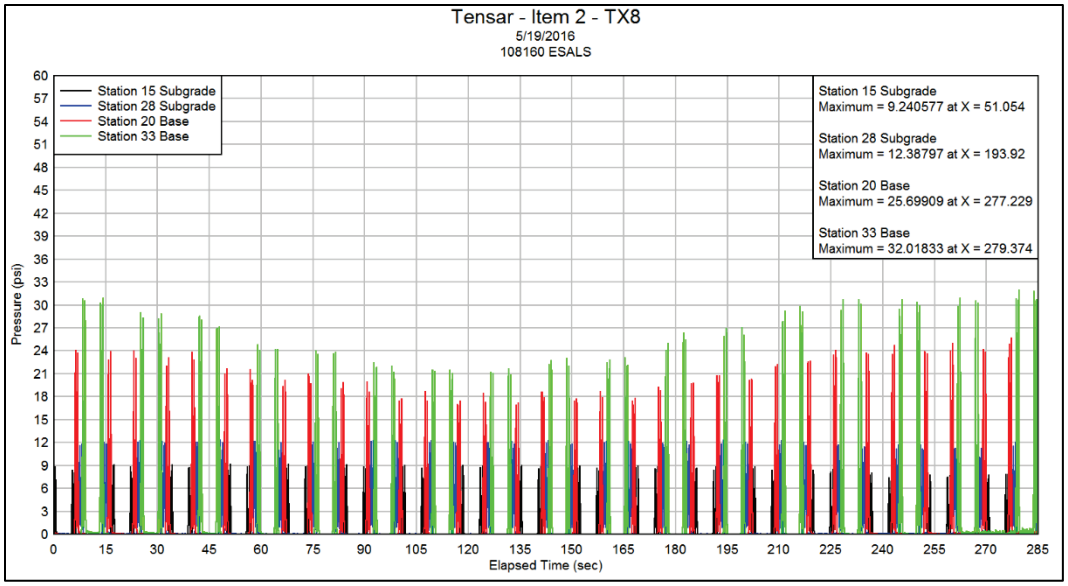

Tensar - Item 2 - TX8
5/6/2016
2704 ESALS
Station 15 Subgrade
Station 28 Subgrade
Station 20 Base
Station 33 Base
Station 15 Subgrade
Maximum = 8.744575 at X = 563.708
Station 28 Subgrade
Maximum = 11.93403 at X = 560.868
Station 20 Base
Maximum = 26.7968 at X = 552.833
Station 33 Base
Maximum = 32.19021 at X = 269.64
Pressure (psi)
Elapsed Time (sec)

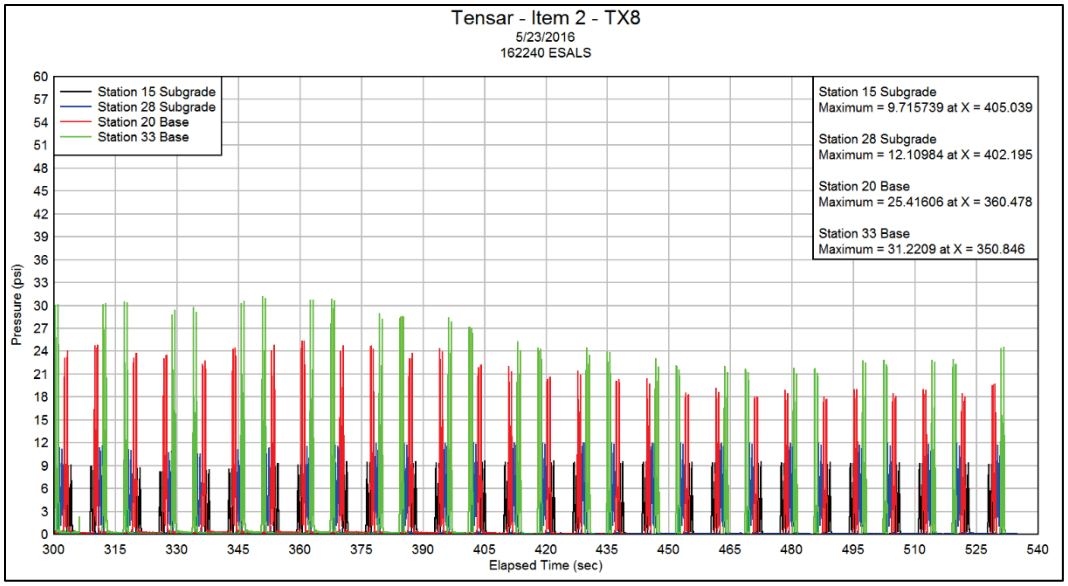

Tensar - Item 2 - TX8
5/9/2016
5408 ESALS
Station 15 Subgrade
Station 28 Subgrade
Station 20 Base
Station 33 Base
Station 15 Subgrade
Maximum = 8.342489 at X = 227.35
Station 28 Subgrade
Maximum = 12.21374 at X = 252.068
Station 20 Base
Maximum = 25.74704 at X = 199.493
Station 33 Base
Maximum = 30.24109 at X = 190.472
Pressure (psi)
Elapsed Time (sec)

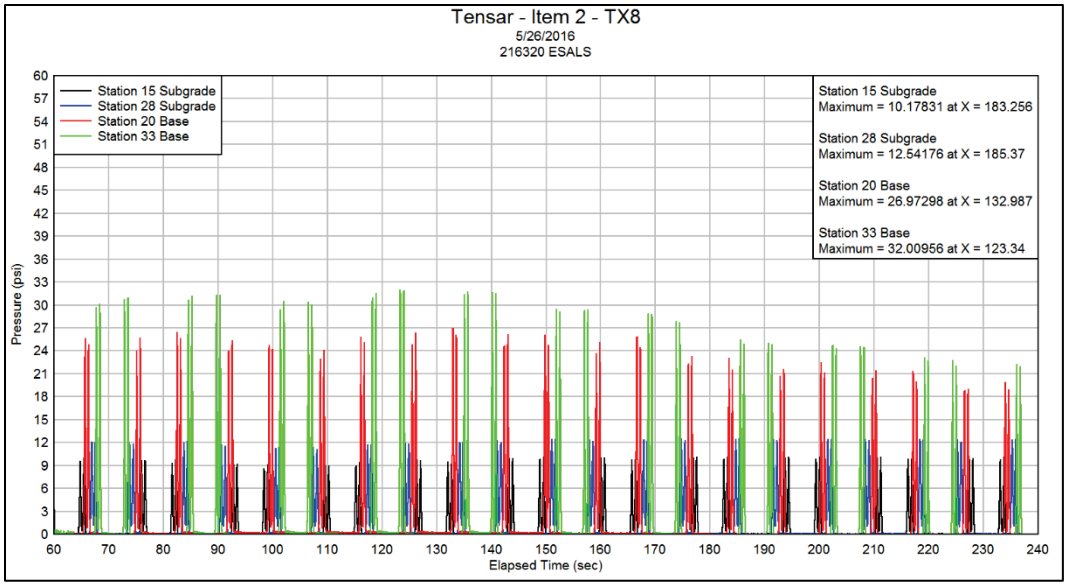

Tensar - Item 2 - TX8
5/10/2016
13844 ESALS
Station 15 Subgrade
Station 28 Subgrade
Station 20 Base
Station 33 Base
Station 15 Subgrade
Maximum = 8.446397 at X = 8.695
Station 28 Subgrade
Maximum = 11.66171 at X = 235.023
Station 20 Base
Maximum = 23.09728 at X = 199.997
Station 33 Base
Maximum = 32.02885 at X = 202.162
Pressure (psi)
Elapsed Time (sec)

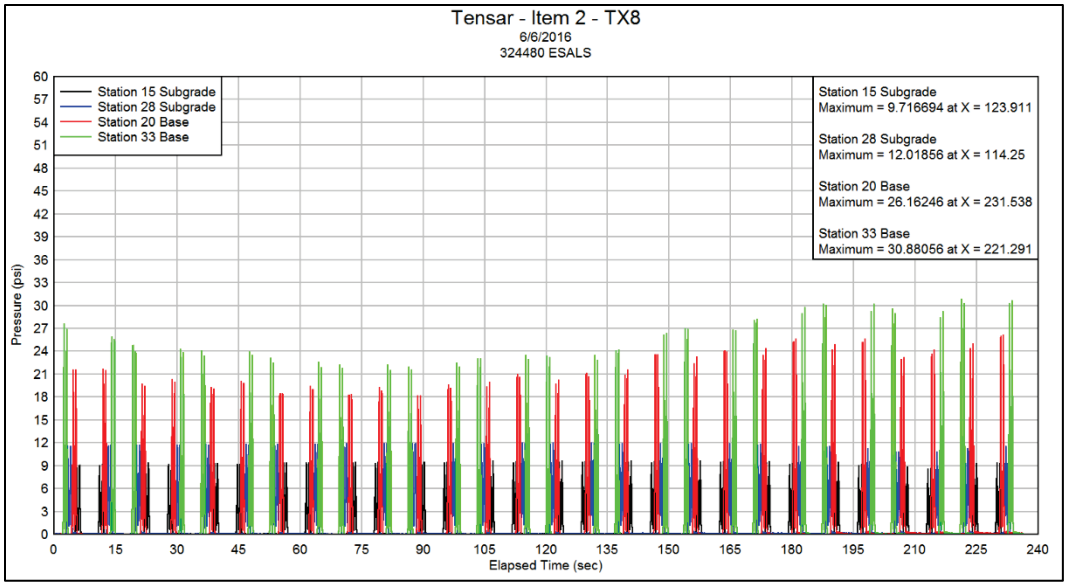

Tensar - Item 2 - TX8
5/13/2016
27040 ESALS
Station 15 Subgrade
Station 28 Subgrade
Station 20 Base
Station 33 Base
Station 15 Subgrade
Maximum = 9.232853 at X = 335.551
Station 28 Subgrade
Maximum = 10.96383 at X = 337.618
Station 20 Base
Maximum = 23.36656 at X = 318.888
Station 33 Base
Maximum = 31.26297 at X = 34.823
Pressure (psi)
Elapsed Time (sec)

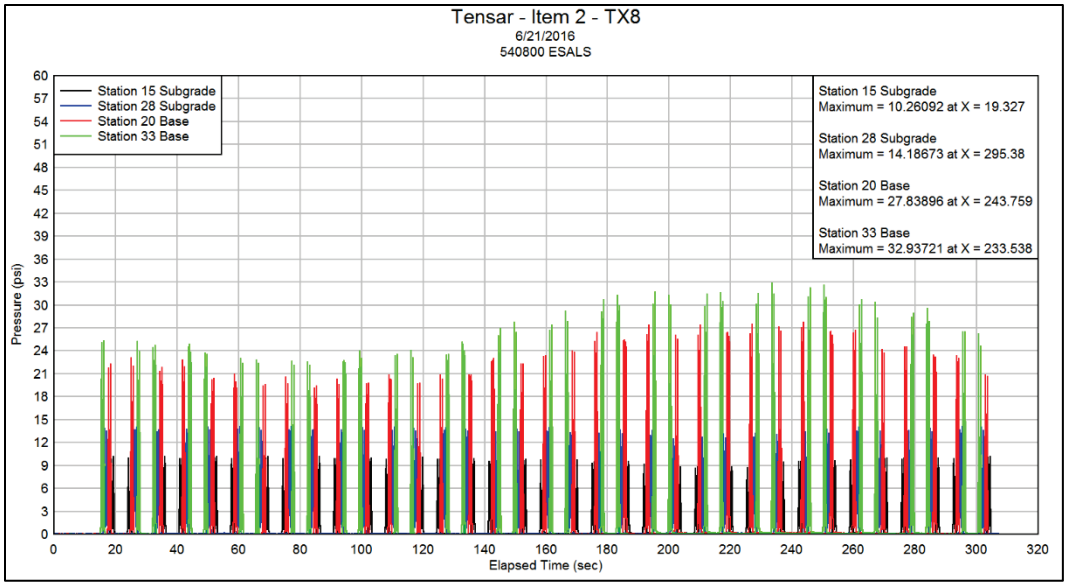

Tensar - Item 2 - TX8
5/16/2016
54080 ESALS
Station 15 Subgrade
Station 28 Subgrade
Station 20 Base
Station 33 Base
Station 15 Subgrade
Maximum = 9.051639 at X = 11.612
Station 28 Subgrade
Maximum = 11.72629 at X = 36.16
Station 20 Base
Maximum = 23.33481 at X = 237.234
Station 33 Base
Maximum = 31.04923 at X = 226.966
Pressure (psi)
Elapsed Time (sec)

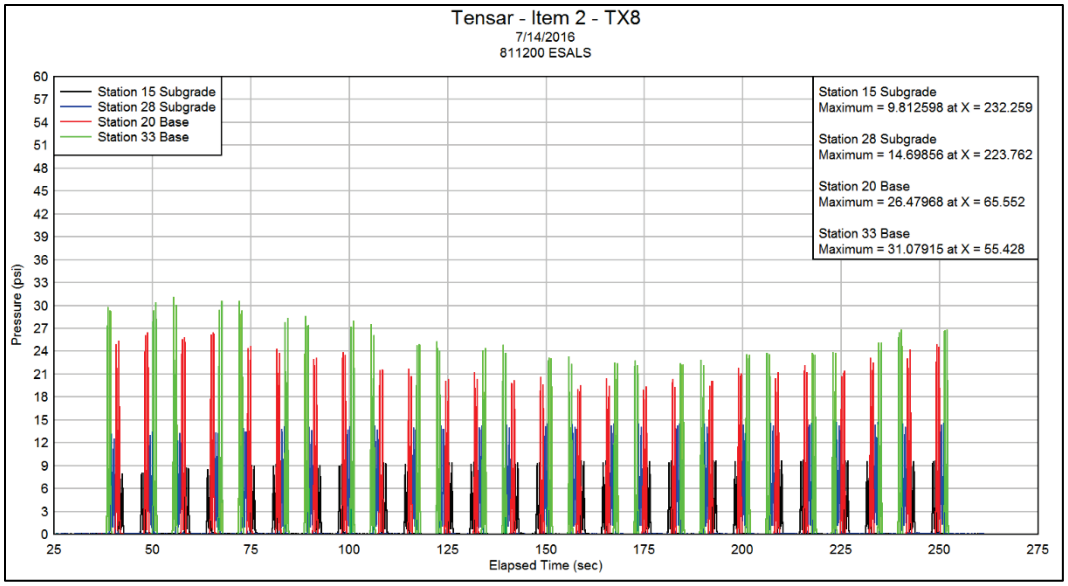

Tensar - Item 2 - TX8
5/19/2016
108160 ESALS
Station 15 Subgrade
Station 28 Subgrade
Station 20 Base
Station 33 Base
Station 15 Subgrade
Maximum = 9.240577 at X = 51.054
Station 28 Subgrade
Maximum = 12.38797 at X = 193.92
Station 20 Base
Maximum = 25.69909 at X = 277.229
Station 33 Base
Maximum = 32.01833 at X = 279.374
Pressure (psi)
Elapsed Time (sec)


Tensar - Item 2 - TX8
5/23/2016
162240 ESALS
Station 15 Subgrade
Station 28 Subgrade
Station 20 Base
Station 33 Base
Station 15 Subgrade
Maximum = 9.715739 at X = 405.039
Station 28 Subgrade
Maximum = 12.10984 at X = 402.195
Station 20 Base
Maximum = 25.41606 at X = 360.478
Station 33 Base
Maximum = 31.2209 at X = 350.846
Pressure (psi)
Elapsed Time (sec)

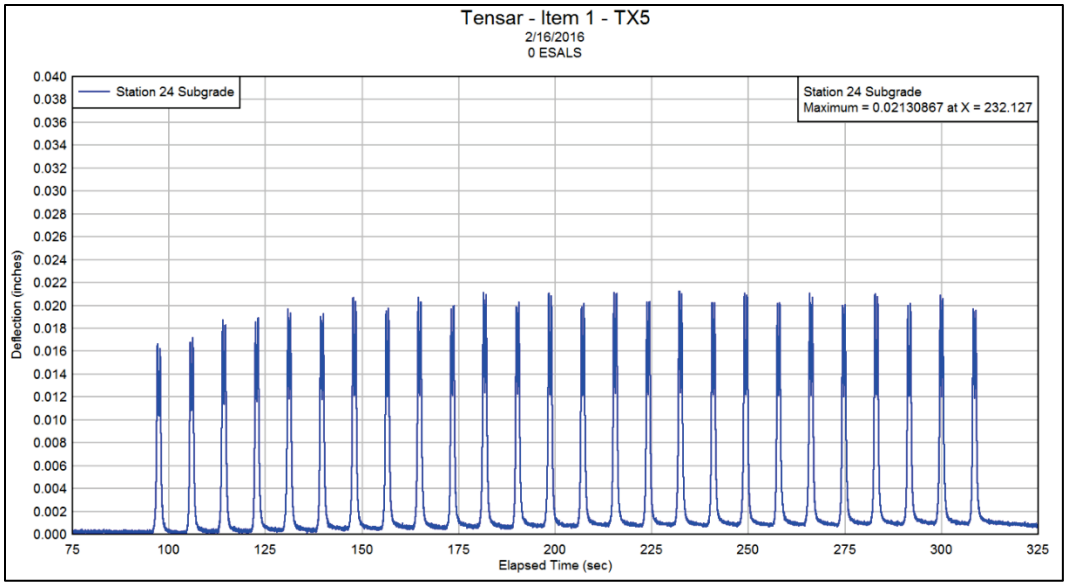

Tensar - Item 2 - TX8
5/26/2016
216320 ESALS
Station 15 Subgrade
Station 28 Subgrade
Station 20 Base
Station 33 Base
Station 15 Subgrade
Maximum = 10.17831 at X = 183.256
Station 28 Subgrade
Maximum = 12.54176 at X = 185.37
Station 20 Base
Maximum = 26.97298 at X = 132.987
Station 33 Base
Maximum = 32.00956 at X = 123.34
Pressure (psi)
Elapsed Time (sec)

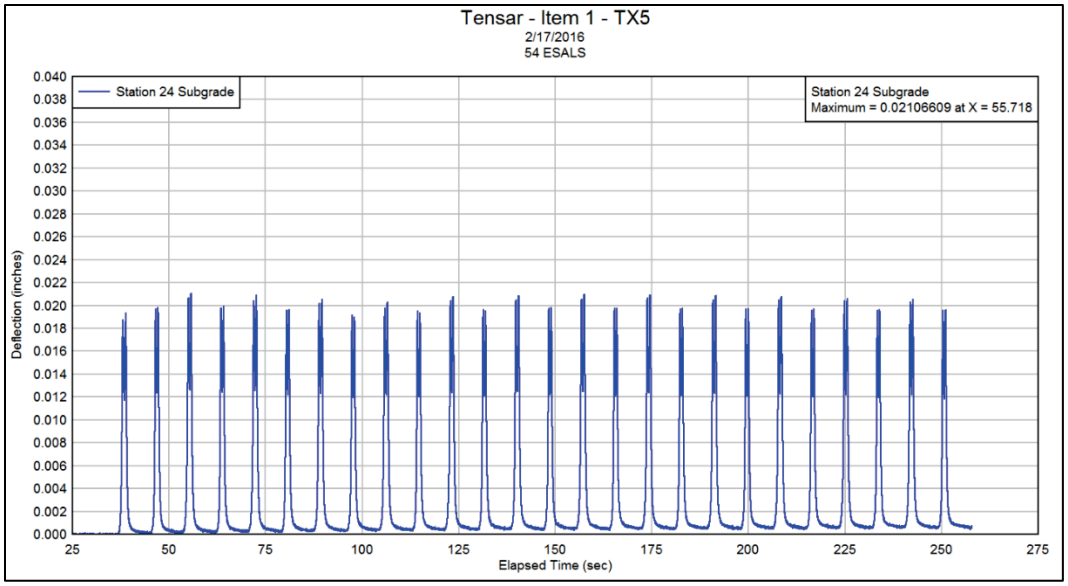

Tensar - Item 2 - TX8
6/6/2016
324480 ESALS
Station 15 Subgrade
Station 28 Subgrade
Station 20 Base
Station 33 Base
Station 15 Subgrade
Maximum = 9.716694 at X = 123.911
Station 28 Subgrade
Maximum = 12.01856 at X = 114.25
Station 20 Base
Maximum = 26.16246 at X = 231.538
Station 33 Base
Maximum = 30.88056 at X = 221.291
Pressure (psi)
Elapsed Time (sec)

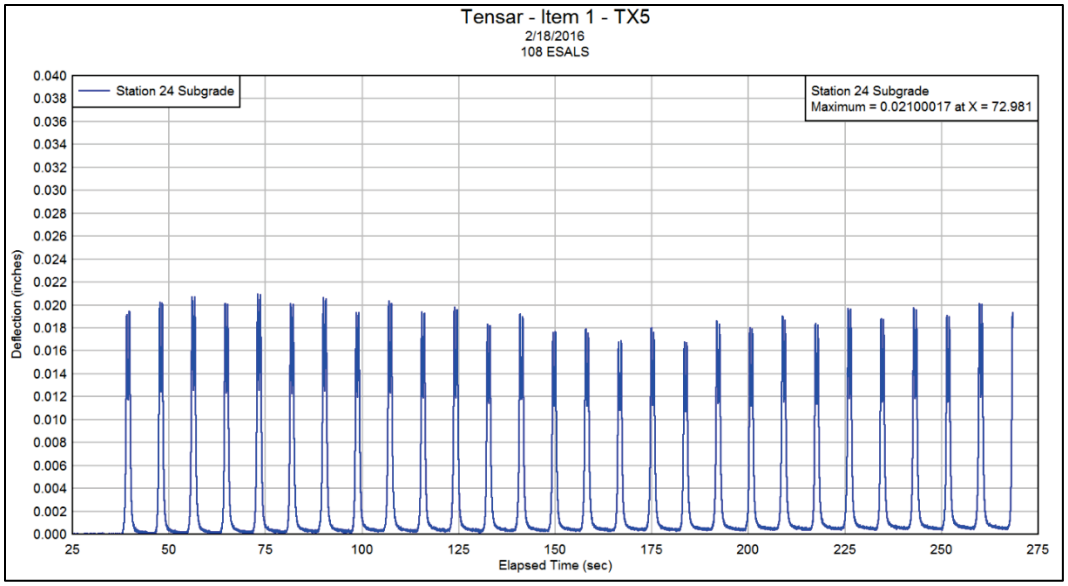

Tensar - Item 2 - TX8
6/21/2016
540800 ESALS
Station 15 Subgrade
Station 28 Subgrade
Station 20 Base
Station 33 Base
Station 15 Subgrade
Maximum = 10.26092 at X = 19.327
Station 28 Subgrade
Maximum = 14.18673 at X = 295.38
Station 20 Base
Maximum = 27.83896 at X = 243.759
Station 33 Base
Maximum = 32.93721 at X = 233.538
Pressure (psi)
Elapsed Time (sec)

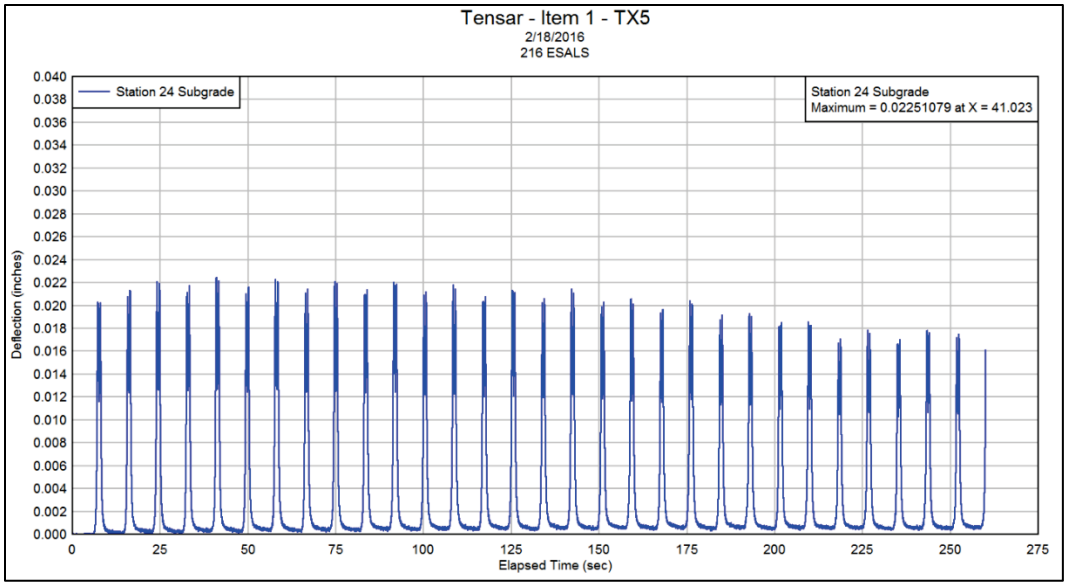

Tensar - Item 2 - TX8
7/14/2016
811200 ESALS
Station 15 Subgrade
Station 28 Subgrade
Station 20 Base
Station 33 Base
Station 15 Subgrade
Maximum = 9.812598 at X = 232.259
Station 28 Subgrade
Maximum = 14.69856 at X = 223.762
Station 20 Base
Maximum = 26.47968 at X = 65.552
Station 33 Base
Maximum = 31.07915 at X = 55.428
Pressure (psi)
Elapsed Time (sec)

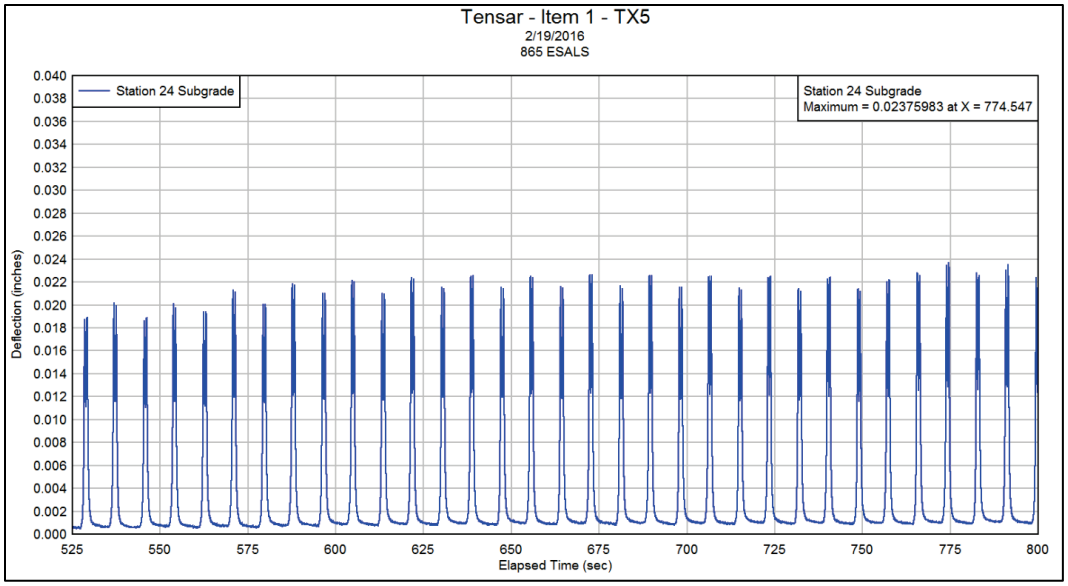
# Appendix B: Single-Depth Deflectometer Responses

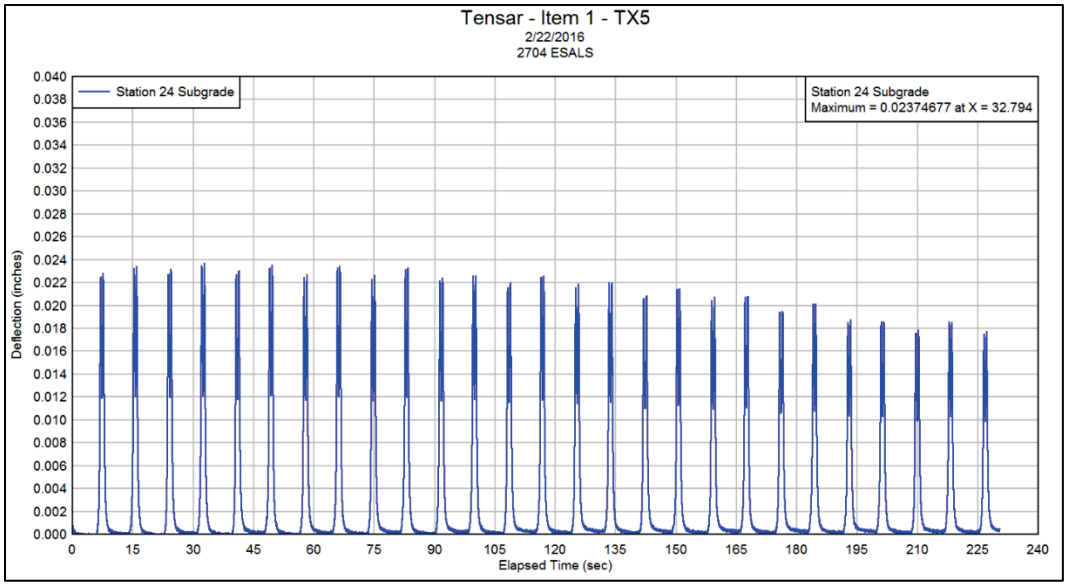


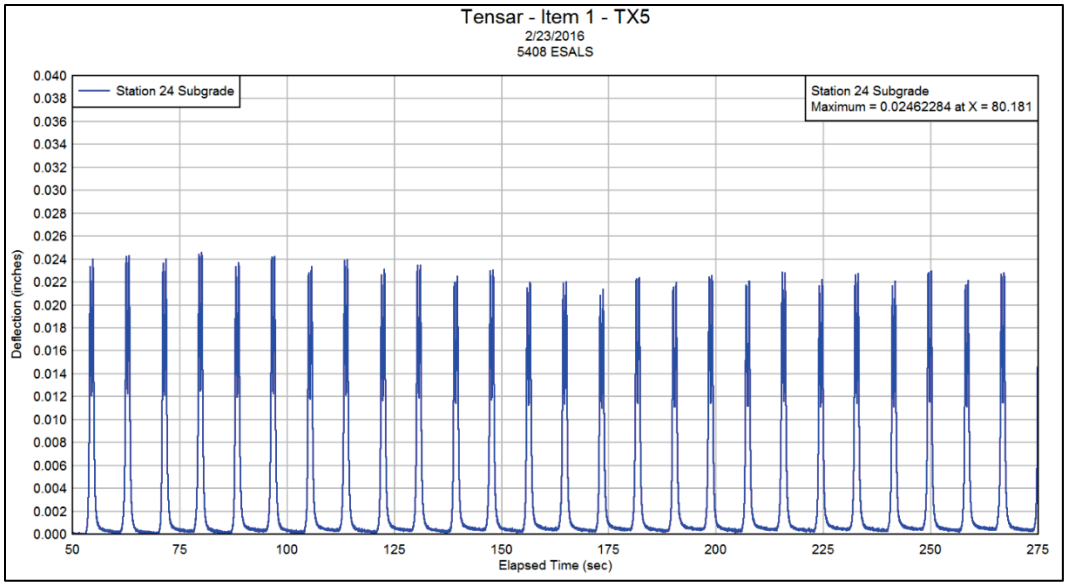



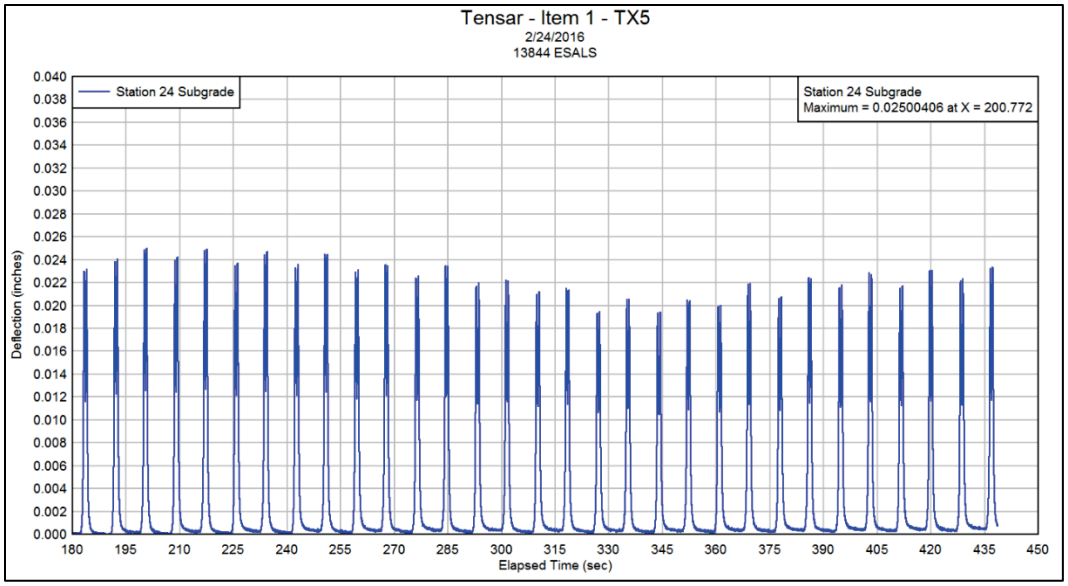

Tensar - Item 1 - TX5
2/18/2016
108 ESALS
Station 24 Subgrade
Station 24 Subgrade
Maximum = 0.02100017 at X = 72.981
Deflection (inches)
Elapsed Time (sec)

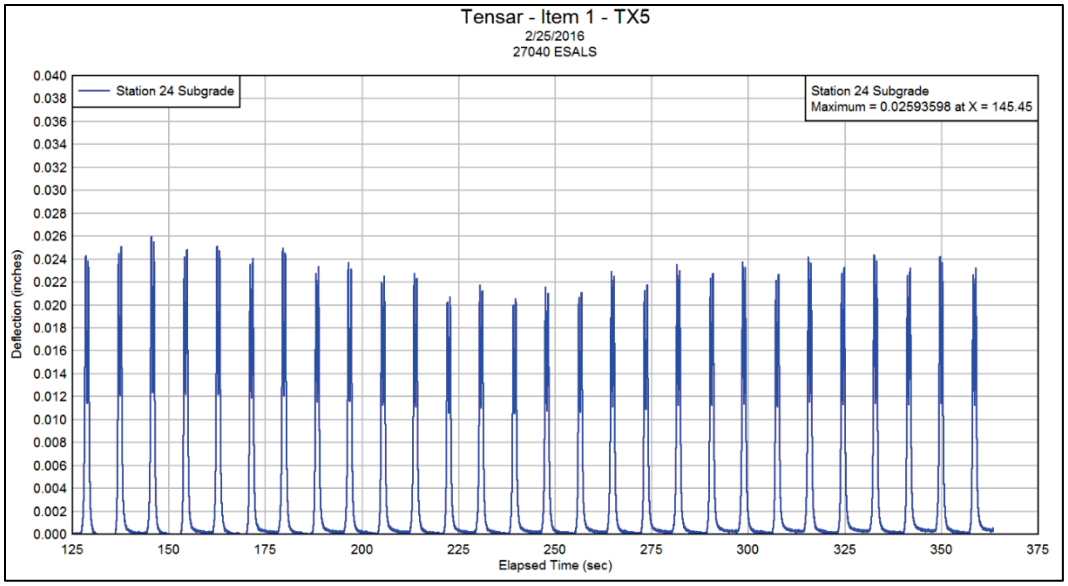

Tensar - Item 1 - TX5
2/18/2016
216 ESALS
Station 24 Subgrade
Station 24 Subgrade
Maximum = 0.02251079 at X = 41.023
Deflection (inches)
Elapsed Time (sec)

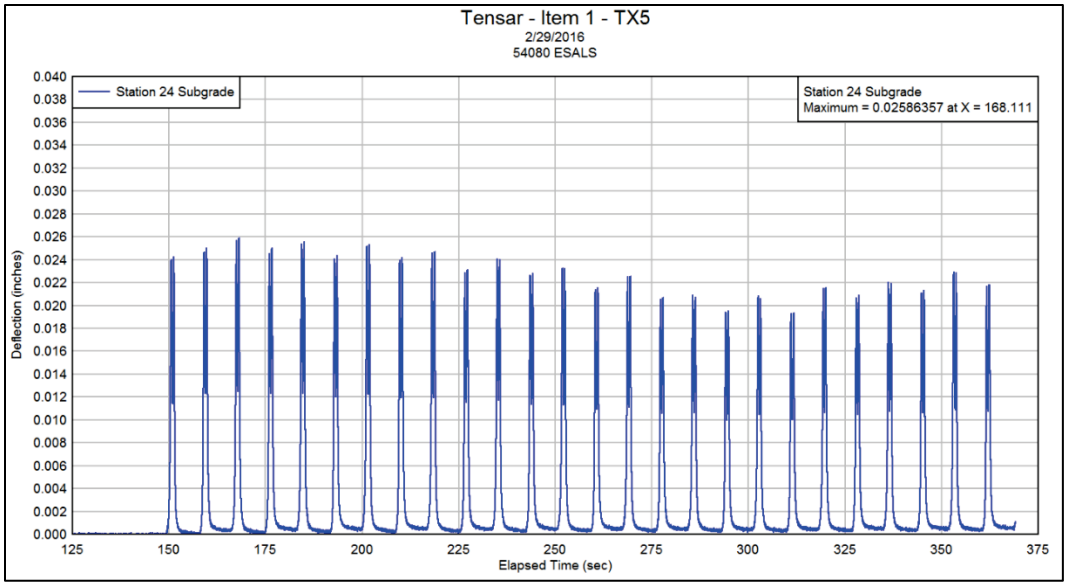

Tensar - Item 1 - TX5
2/19/2016
865 ESALS
Station 24 Subgrade
Station 24 Subgrade
Maximum = 0.02375983 at X = 774.547
Deflection (inches)
0.040
0.038
0.036
0.034
0.032
0.030
0.028
0.026
0.024
0.022
0.020
0.018
0.016
0.014
0.012
0.010
0.008
0.006
0.004
0.002
0.000
525
550
575
600
625
650
675
700
725
750
775
800
Elapsed Time (sec)

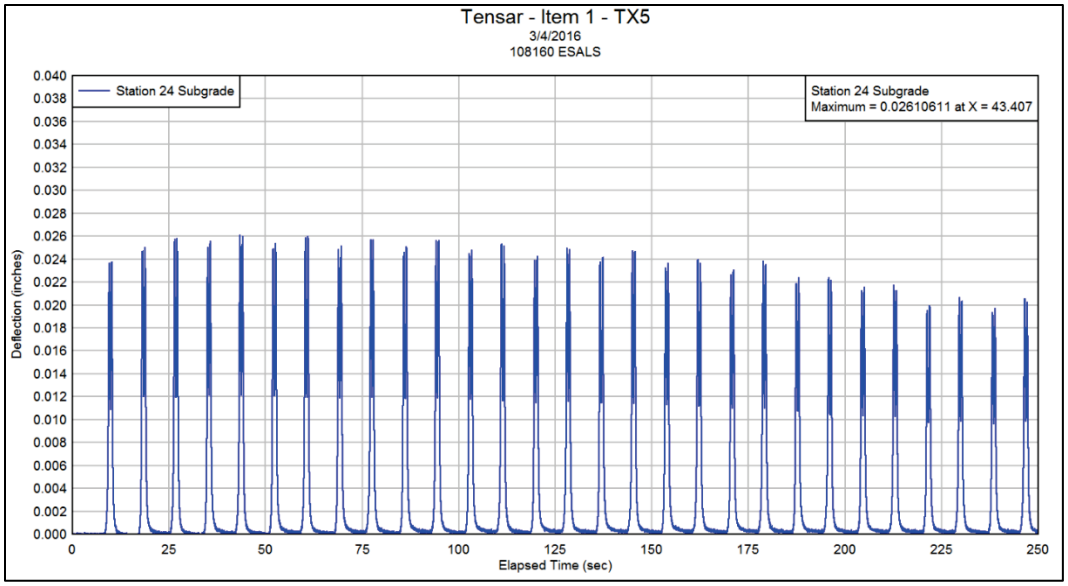

Tensar - Item 1 - TX5
2/22/2016
2704 ESALS
Station 24 Subgrade
Station 24 Subgrade
Maximum = 0.02374677 at X = 32.794
Deflection (inches)
0.040
0.038
0.036
0.034
0.032
0.030
0.028
0.026
0.024
0.022
0.020
0.018
0.016
0.014
0.012
0.010
0.008
0.006
0.004
0.002
0.000
0
15
30
45
60
75
90
105
120
135
150
165
180
195
210
225
240
Elapsed Time (sec)

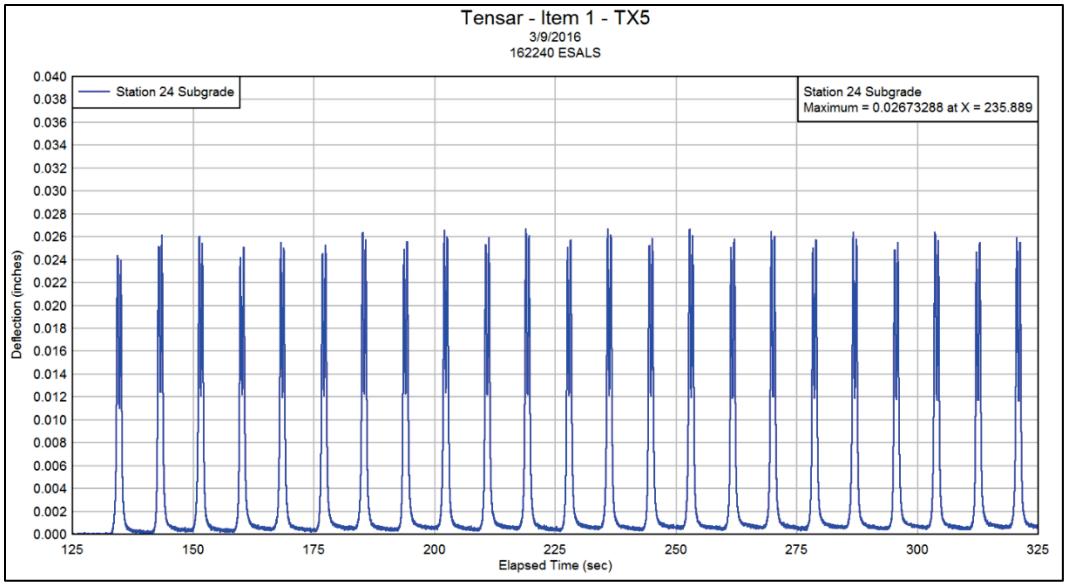

Tensar - Item 1 - TX5
2/23/2016
5408 ESALS
Station 24 Subgrade
Station 24 Subgrade
Maximum = 0.02462284 at X = 80.181
Deflection (inches)
0.040
0.038
0.036
0.034
0.032
0.030
0.028
0.026
0.024
0.022
0.020
0.018
0.016
0.014
0.012
0.010
0.008
0.006
0.004
0.002
0.000
50
75
100
125
150
175
200
225
250
275
Elapsed Time (sec)

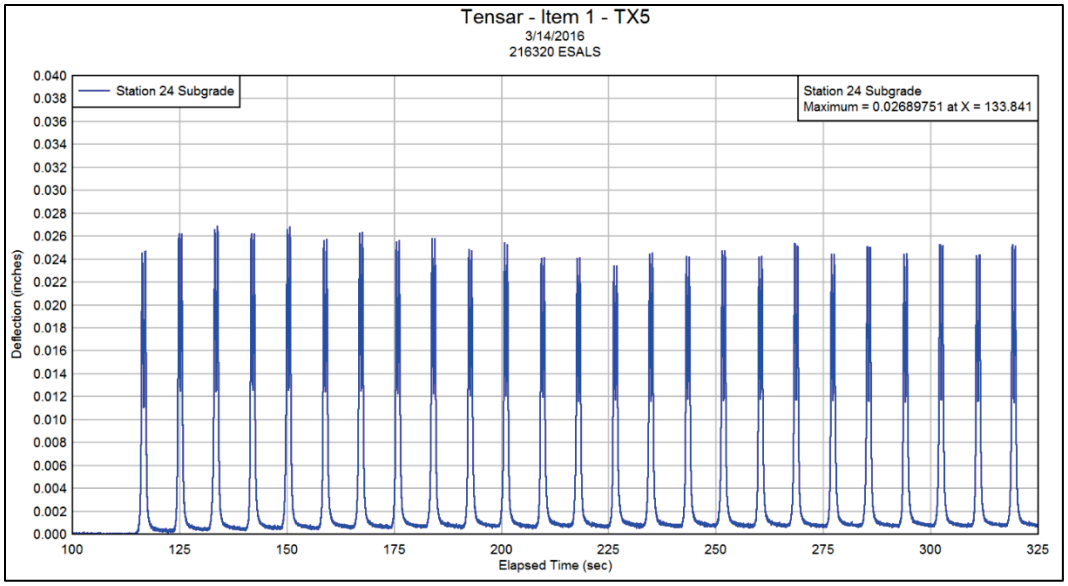

Tensar - Item 1 - TX5
2/24/2016
13844 ESALS
Station 24 Subgrade
Station 24 Subgrade
Maximum = 0.02500406 at X = 200.772
Deflection (inches)
0.040
0.038
0.036
0.034
0.032
0.030
0.028
0.026
0.024
0.022
0.020
0.018
0.016
0.014
0.012
0.010
0.008
0.006
0.004
0.002
0.000
180
195
210
225
240
255
270
285
300
315
330
345
360
375
390
405
420
435
450
Elapsed Time (sec)

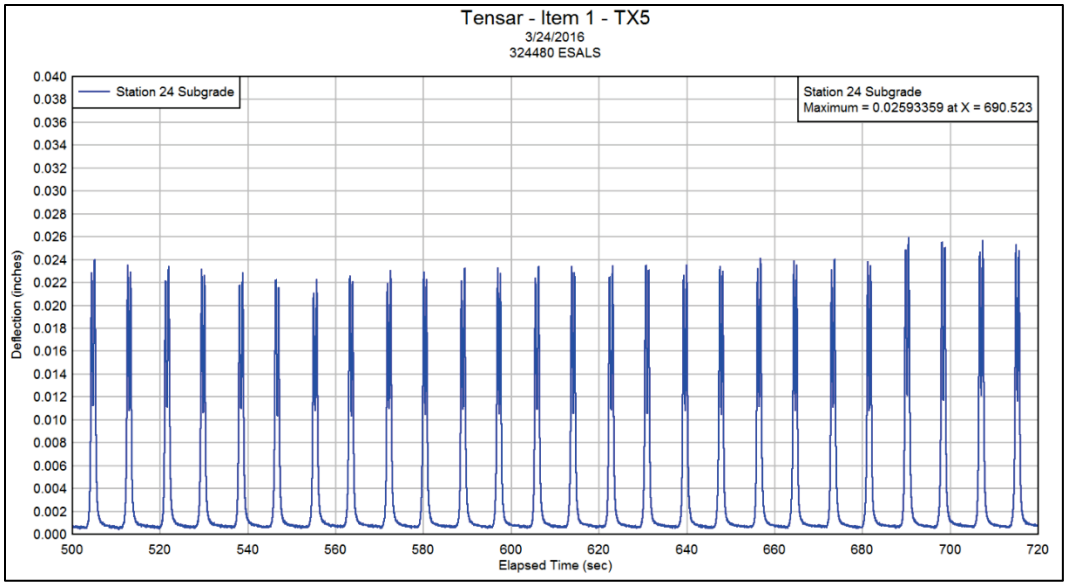

Tensar - Item 1 - TX5
2/25/2016
27040 ESALS
Station 24 Subgrade
Station 24 Subgrade
Maximum = 0.02593598 at X = 145.45
Deflection (inches)
Elapsed Time (sec)

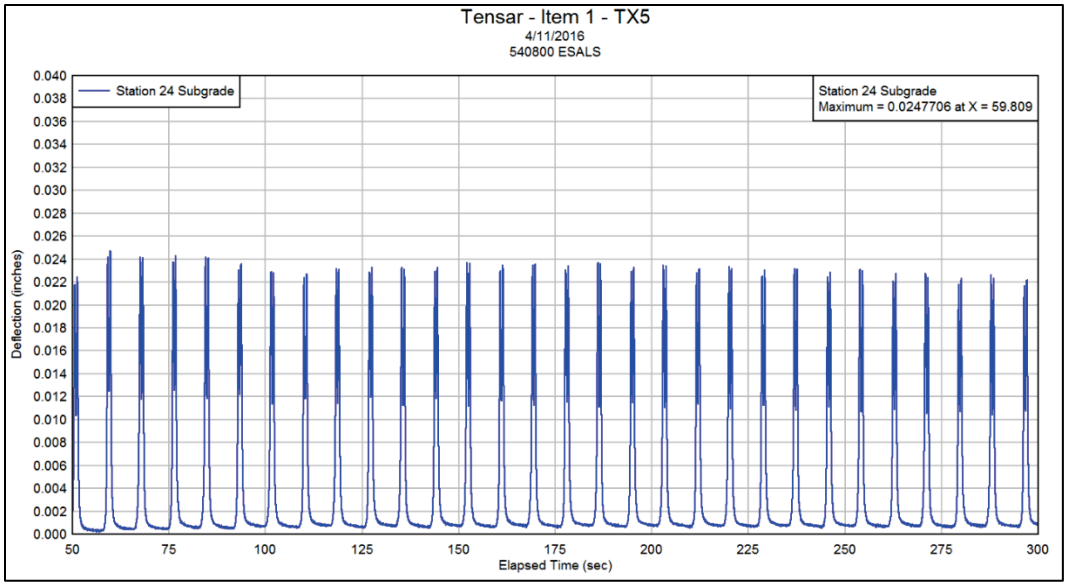

Tensar - Item 1 - TX5
2/29/2016
54080 ESALS
Station 24 Subgrade
Station 24 Subgrade
Maximum = 0.02586357 at X = 168.111
Deflection (inches)
Elapsed Time (sec)

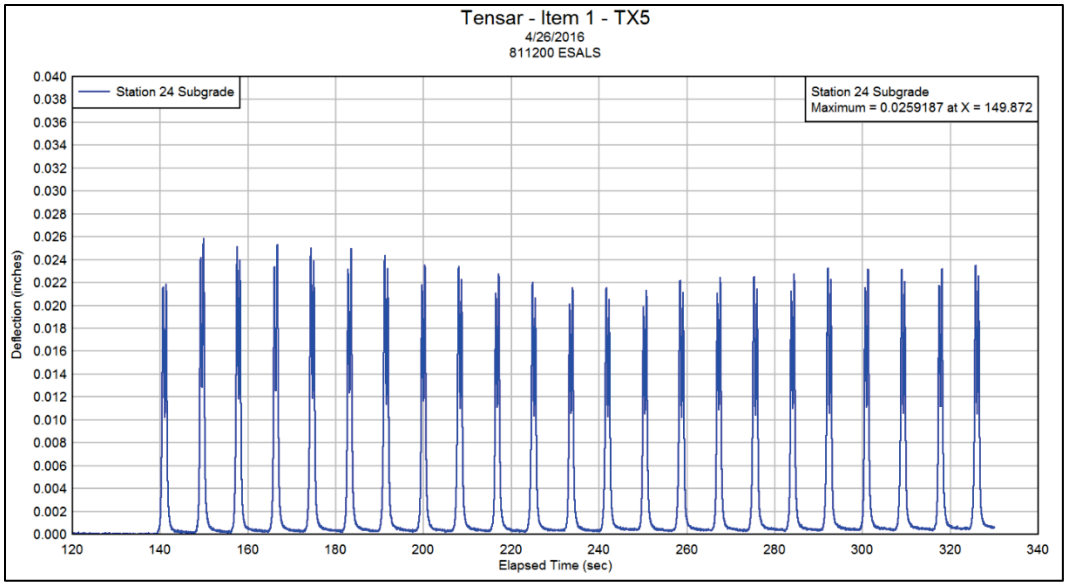

Tensar - Item 1 - TX5
3/4/2016
108160 ESALS
Station 24 Subgrade
Station 24 Subgrade
Maximum = 0.02610611 at X = 43.407
Deflection (inches)
Elapsed Time (sec)

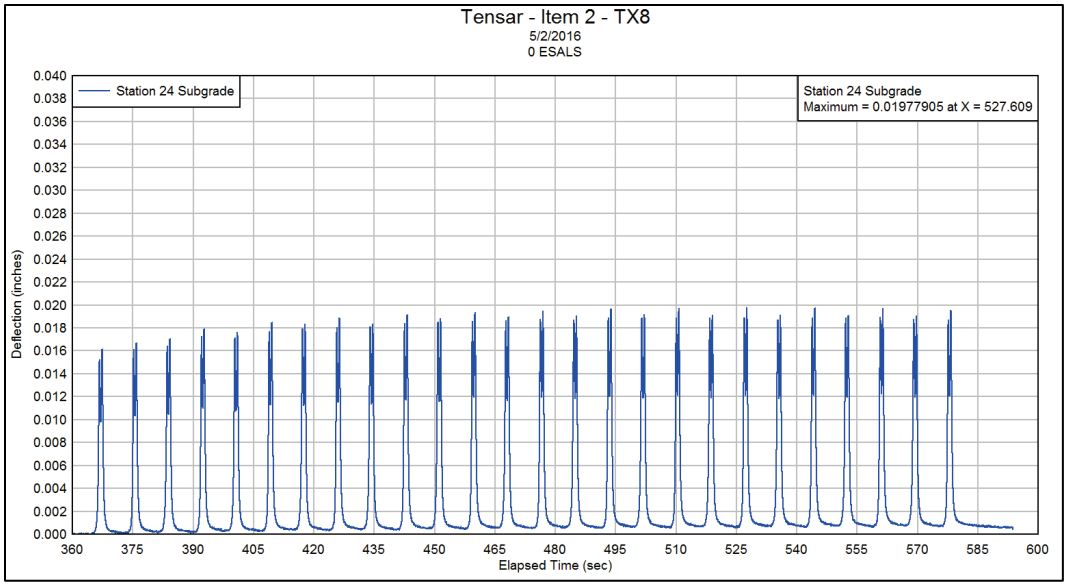

Tensar - Item 1 - TX5
3/9/2016
162240 ESALS
Station 24 Subgrade
Station 24 Subgrade
Maximum = 0.02673288 at X = 235.889
Deflection (inches)
Elapsed Time (sec)

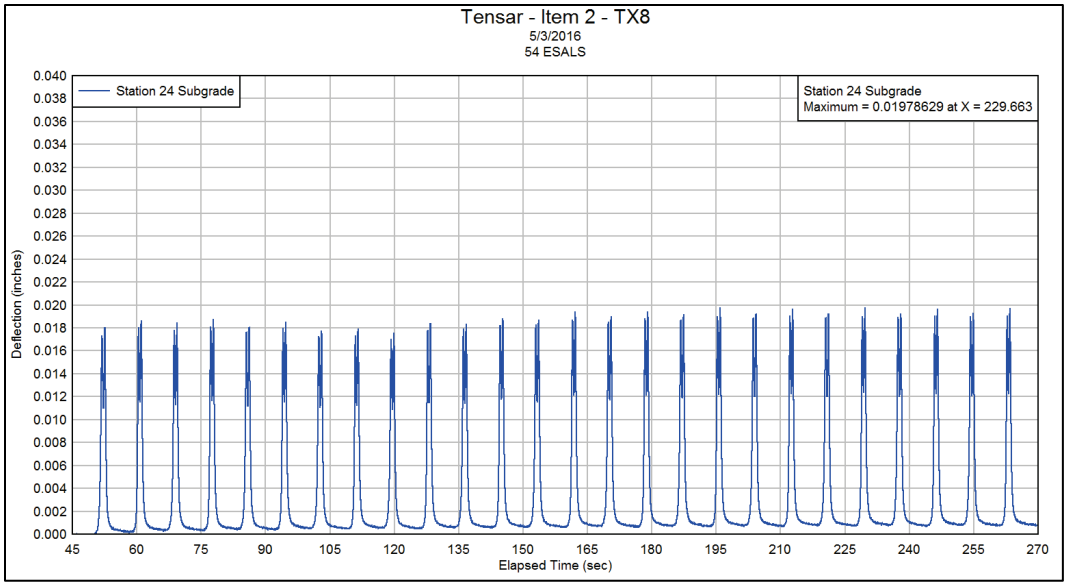

Tensar - Item 1 - TX5
3/14/2016
216320 ESALS
Station 24 Subgrade
Station 24 Subgrade
Maximum = 0.02689751 at X = 133.841
Deflection (inches)
Elapsed Time (sec)

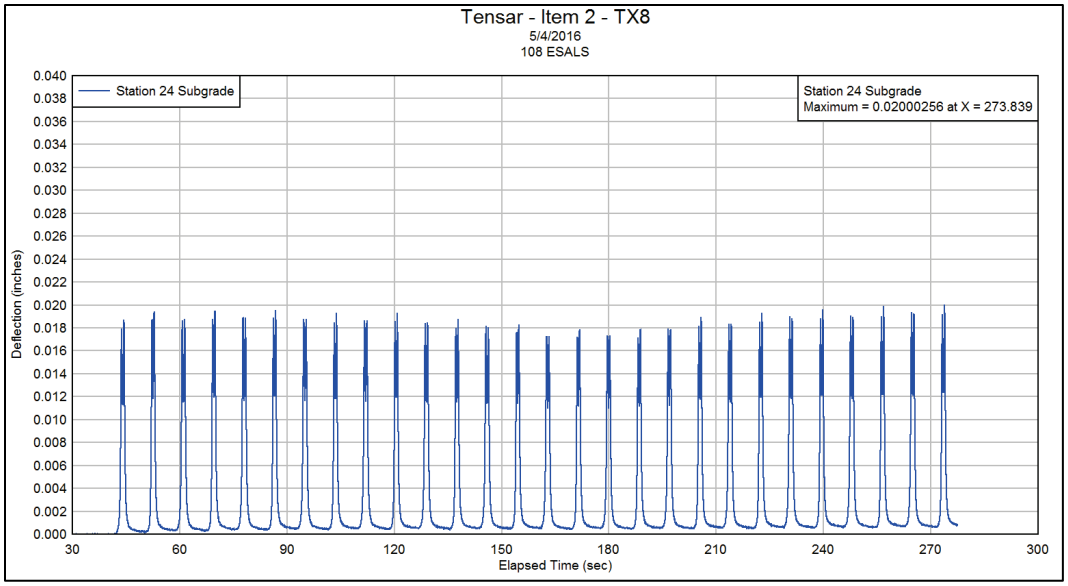

Tensar - Item 1 - TX5
3/24/2016
324480 ESALS
Station 24 Subgrade
Station 24 Subgrade
Maximum = 0.02593359 at X = 690.523
Deflection (inches)
Elapsed Time (sec)

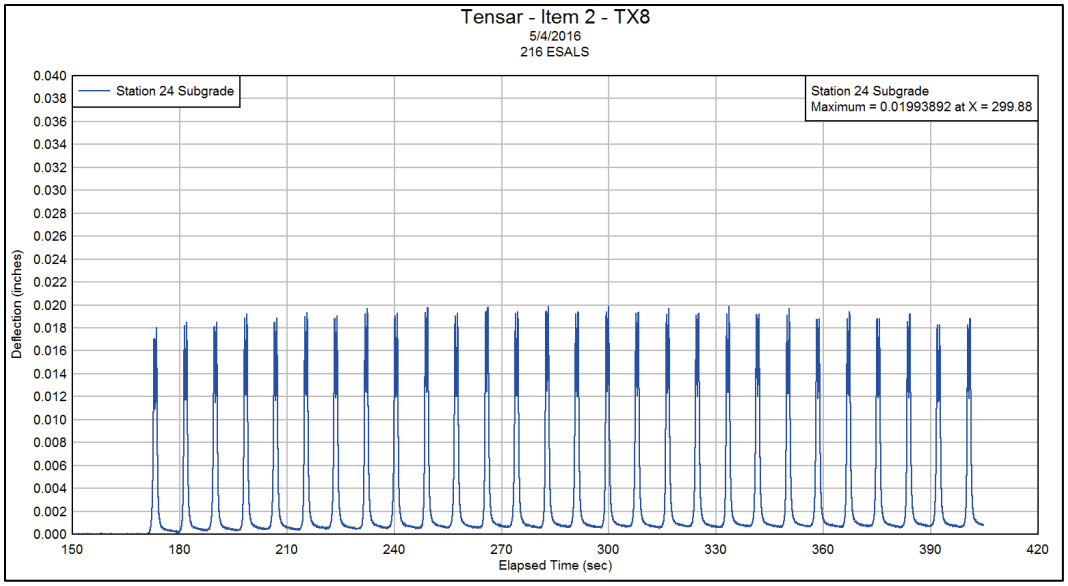

Tensar - Item 1 - TX5
4/11/2016
540800 ESALS
Station 24 Subgrade
Station 24 Subgrade
Maximum = 0.0247706 at X = 59.809
Deflection (inches)
Elapsed Time (sec)

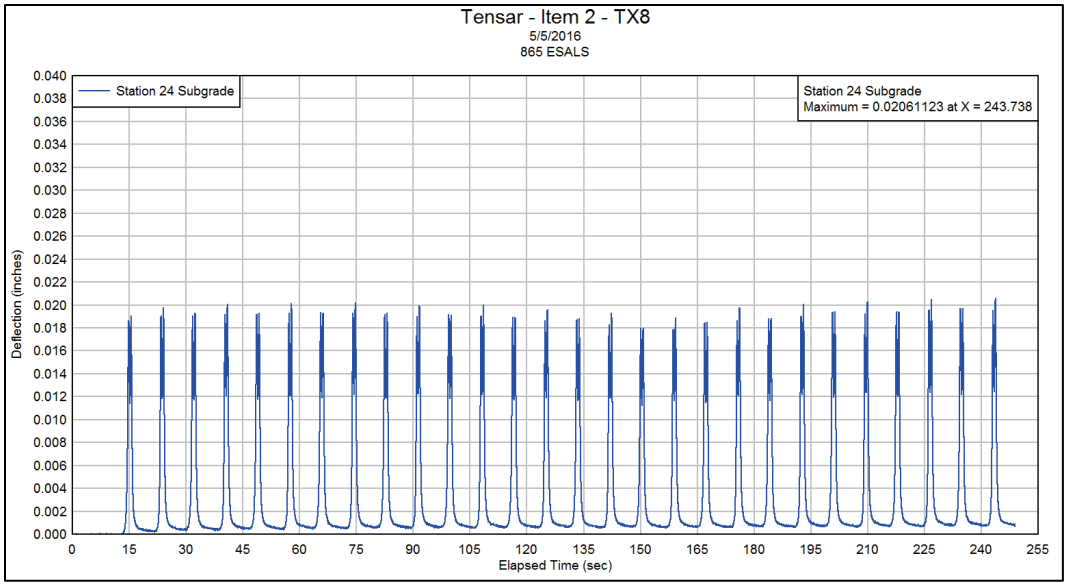

Tensar - Item 1 - TX5
4/26/2016
811200 ESALS
Station 24 Subgrade
Station 24 Subgrade
Maximum = 0.0259187 at X = 149.872
Deflection (inches)
Elapsed Time (sec)

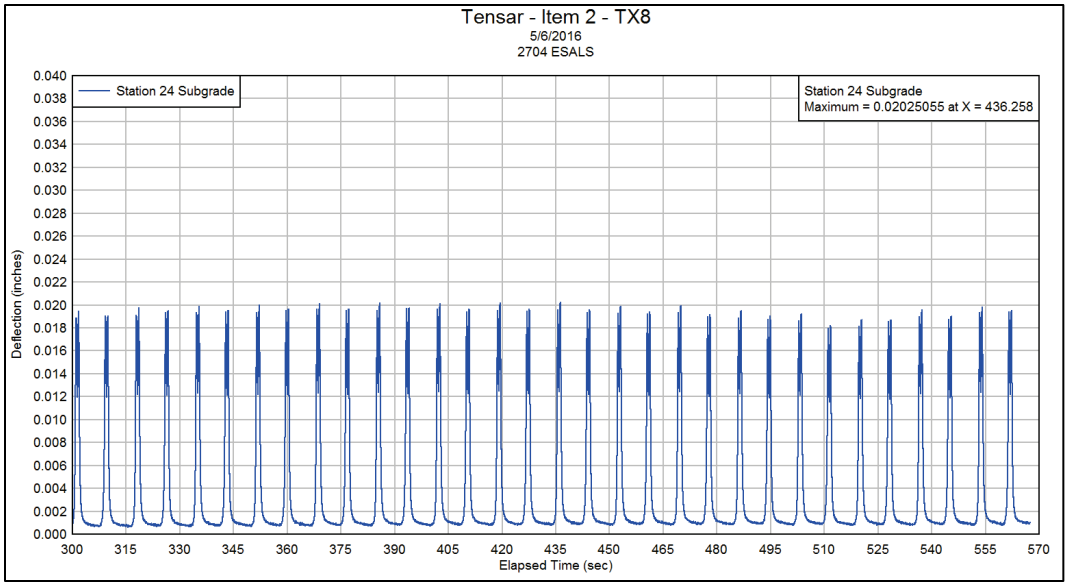

Tensar - Item 2 - TX8
5/2/2016
0 ESALS
Station 24 Subgrade
Station 24 Subgrade
Maximum = 0.01977905 at X = 527.609
Deflection (inches)
0.040
0.038
0.036
0.034
0.032
0.030
0.028
0.026
0.024
0.022
0.020
0.018
0.016
0.014
0.012
0.010
0.008
0.006
0.004
0.002
0.000
360 375 390 405 420 435 450 465 480 495 510 525 540 555 570 585 600
Elapsed Time (sec)

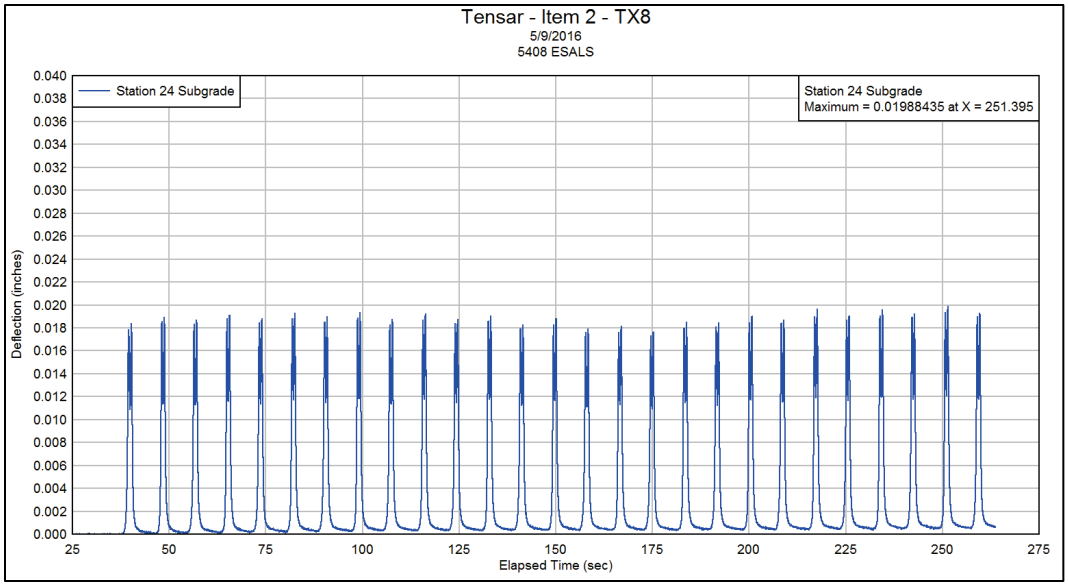

Tensar - Item 2 - TX8
5/3/2016
54 ESALS
Station 24 Subgrade
Station 24 Subgrade
Maximum = 0.01978629 at X = 229.663
Deflection (inches)
0.040
0.038
0.036
0.034
0.032
0.030
0.028
0.026
0.024
0.022
0.020
0.018
0.016
0.014
0.012
0.010
0.008
0.006
0.004
0.002
0.000
45 60 75 90 105 120 135 150 165 180 195 210 225 240 255 270
Elapsed Time (sec)

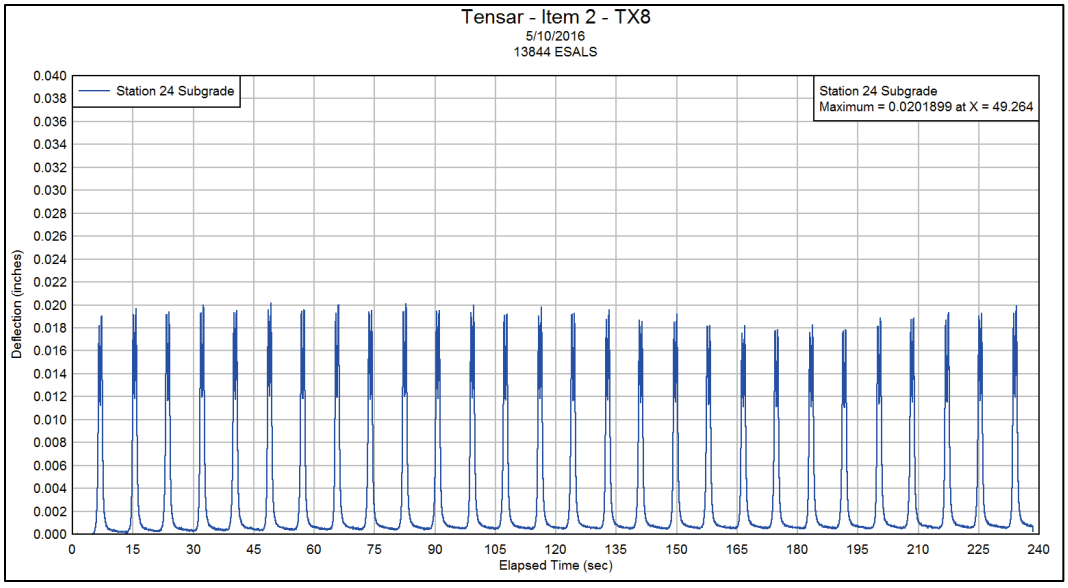

Tensar - Item 2 - TX8
5/4/2016
108 ESALS
Station 24 Subgrade
Station 24 Subgrade
Maximum = 0.02000256 at X = 273.839
Deflection (inches)
0.040
0.038
0.036
0.034
0.032
0.030
0.028
0.026
0.024
0.022
0.020
0.018
0.016
0.014
0.012
0.010
0.008
0.006
0.004
0.002
0.000
30
60
90
120
150
180
210
240
270
300
Elapsed Time (sec)

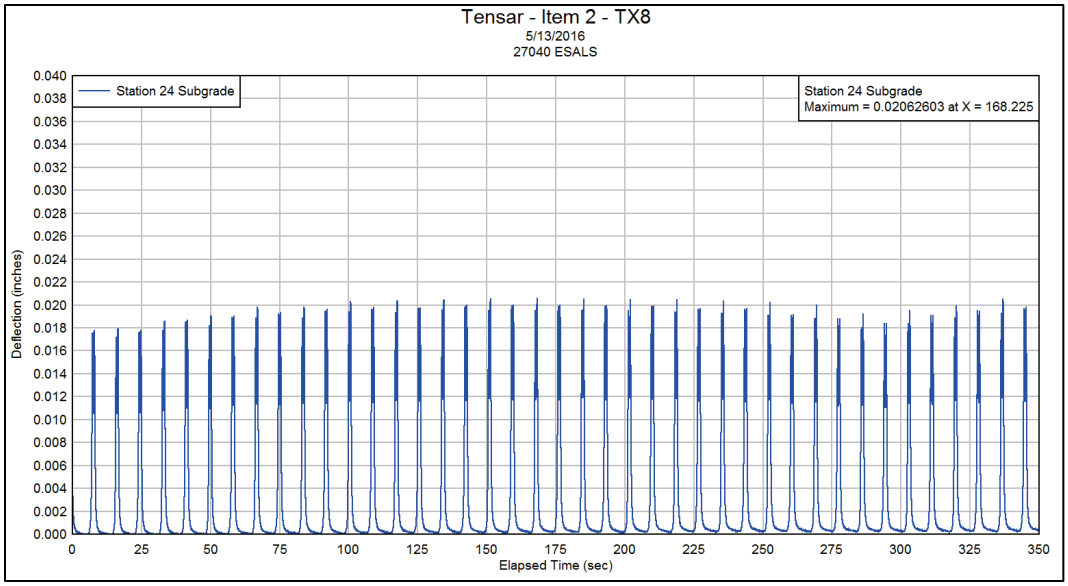

Tensar - Item 2 - TX8
5/4/2016
216 ESALS
Station 24 Subgrade
Station 24 Subgrade
Maximum = 0.01993892 at X = 299.88
Deflection (inches)
0.040
0.038
0.036
0.034
0.032
0.030
0.028
0.026
0.024
0.022
0.020
0.018
0.016
0.014
0.012
0.010
0.008
0.006
0.004
0.002
0.000
150
180
210
240
270
300
330
360
390
420
Elapsed Time (sec)

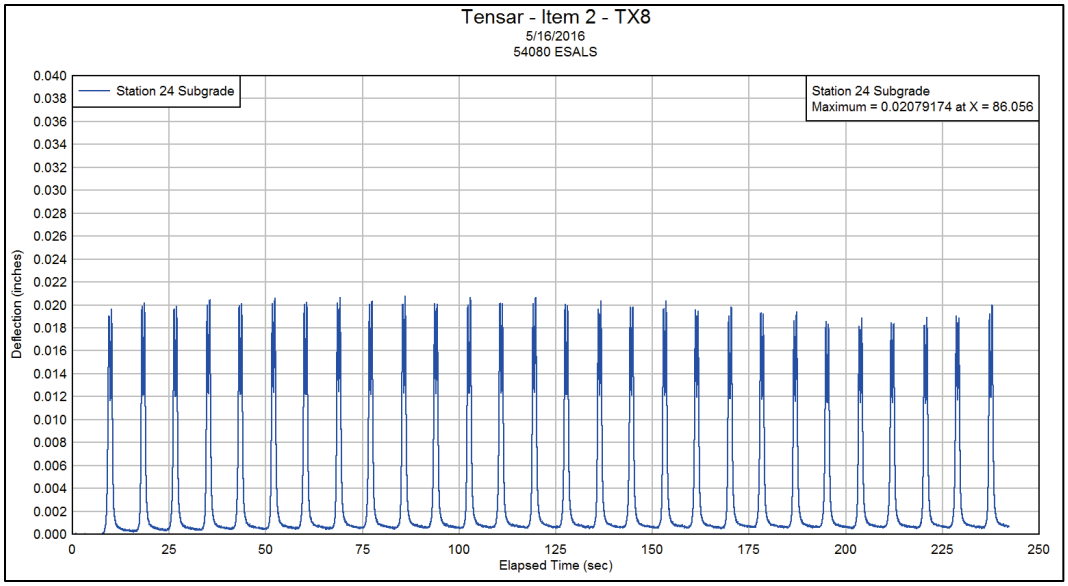

Tensar - Item 2 - TX8
5/5/2016
865 ESALS
Station 24 Subgrade
Station 24 Subgrade
Maximum = 0.02061123 at X = 243.738
Deflection (inches)
0.040
0.038
0.036
0.034
0.032
0.030
0.028
0.026
0.024
0.022
0.020
0.018
0.016
0.014
0.012
0.010
0.008
0.006
0.004
0.002
0.000
0 15 30 45 60 75 90 105 120 135 150 165 180 195 210 225 240 255
Elapsed Time (sec)

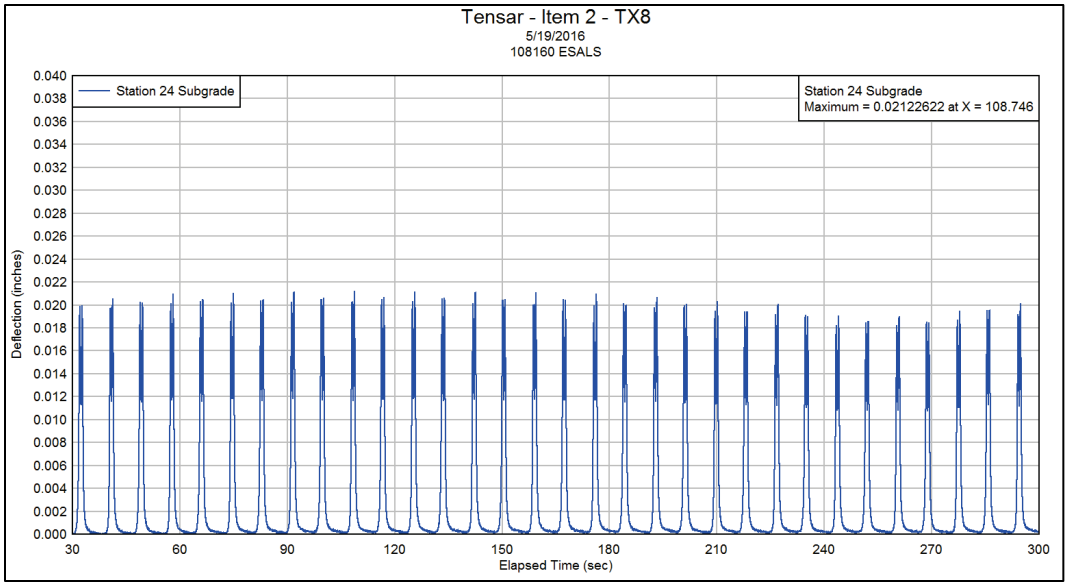

Tensar - Item 2 - TX8
5/6/2016
2704 ESALS
Station 24 Subgrade
Station 24 Subgrade
Maximum = 0.02025055 at X = 436.258
Deflection (inches)
0.040
0.038
0.036
0.034
0.032
0.030
0.028
0.026
0.024
0.022
0.020
0.018
0.016
0.014
0.012
0.010
0.008
0.006
0.004
0.002
0.000
300 315 330 345 360 375 390 405 420 435 450 465 480 495 510 525 540 555 570
Elapsed Time (sec)

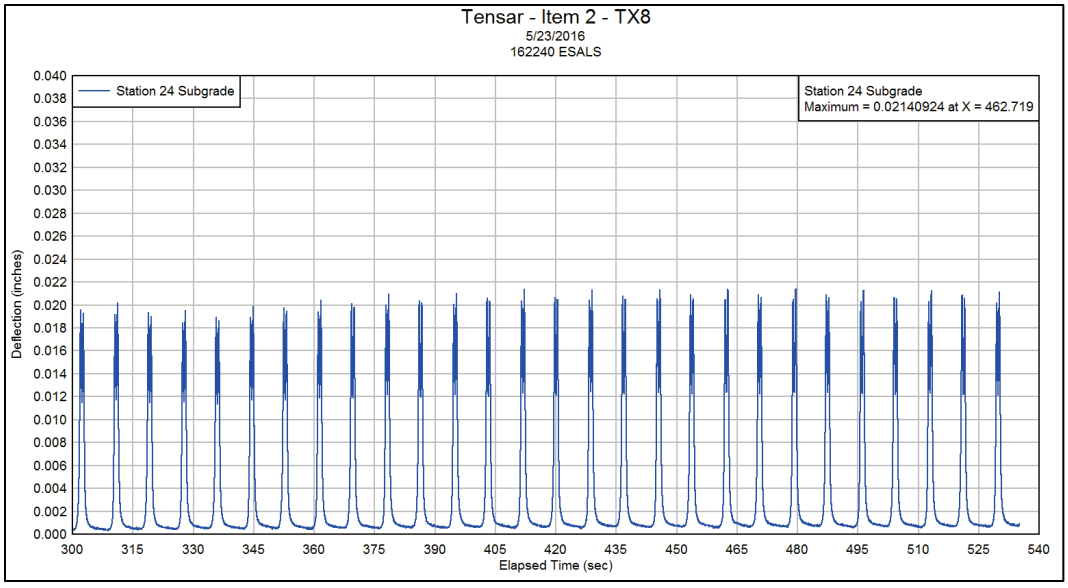

Tensar - Item 2 - TX8
5/9/2016
5408 ESALS
Station 24 Subgrade
Station 24 Subgrade
Maximum = 0.01988435 at X = 251.395
Deflection (inches)
Elapsed Time (sec)

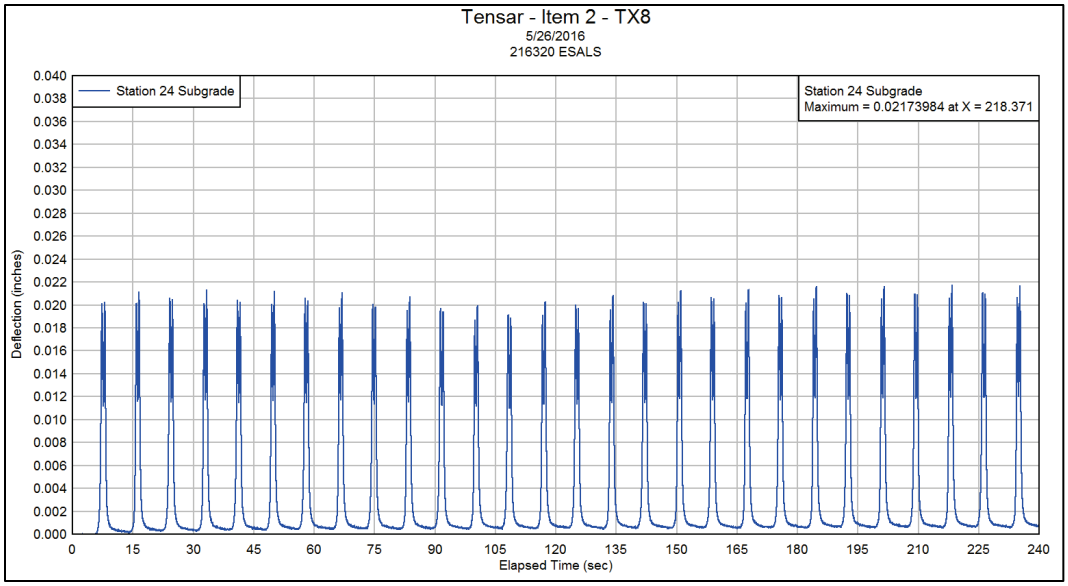

Tensar - Item 2 - TX8
5/10/2016
13844 ESALS
Station 24 Subgrade
Station 24 Subgrade
Maximum = 0.0201899 at X = 49.264
Deflection (inches)
Elapsed Time (sec)

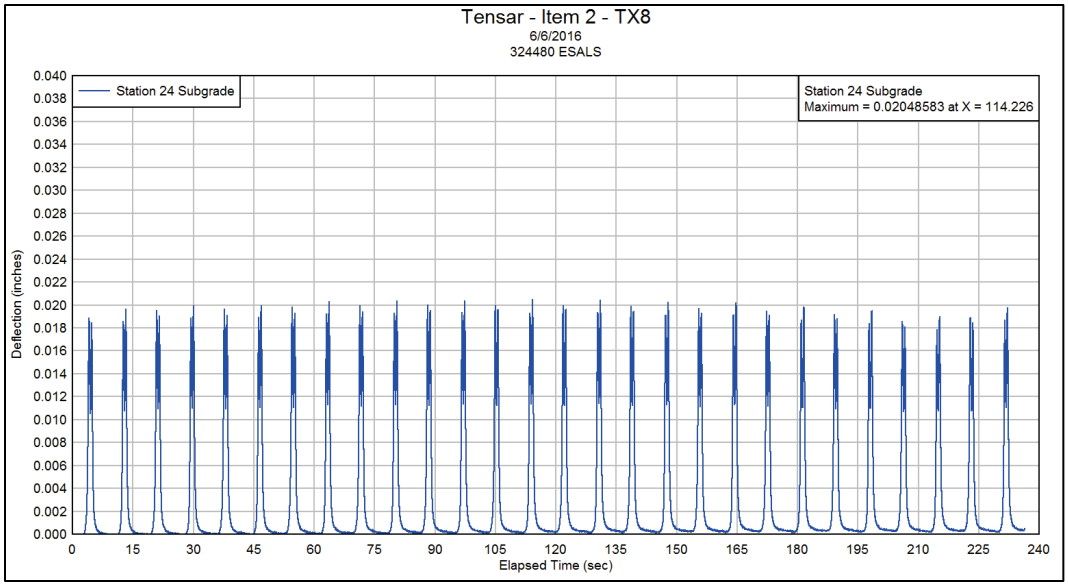

Tensar - Item 2 - TX8
5/13/2016
27040 ESALS
Station 24 Subgrade
Station 24 Subgrade
Maximum = 0.02062603 at X = 168.225
Deflection (inches)
Elapsed Time (sec)

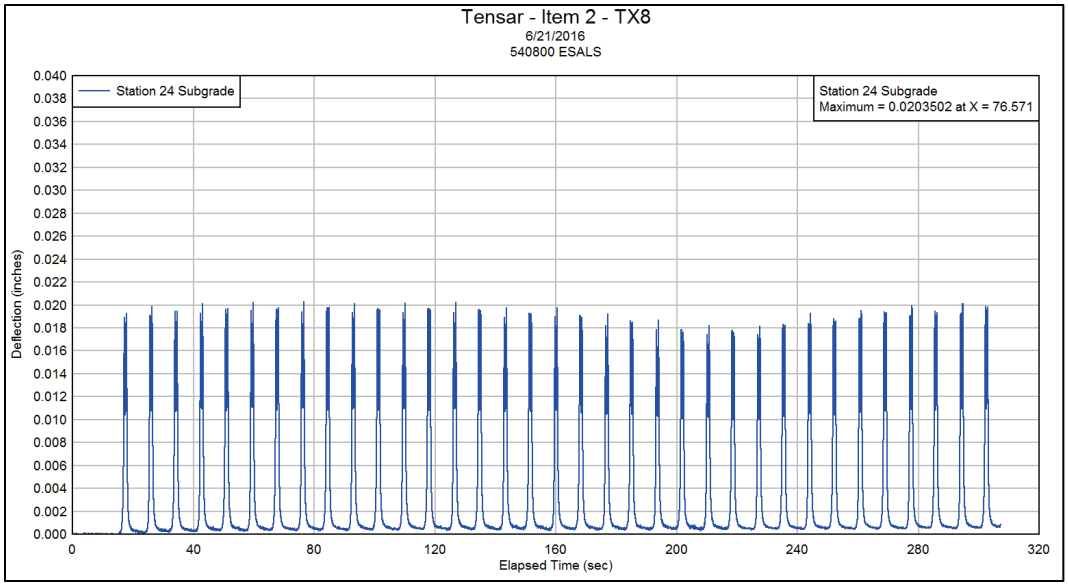

Tensar - Item 2 - TX8
5/16/2016
54080 ESALS
Station 24 Subgrade
Station 24 Subgrade
Maximum = 0.02079174 at X = 86.056
Deflection (inches)
Elapsed Time (sec)

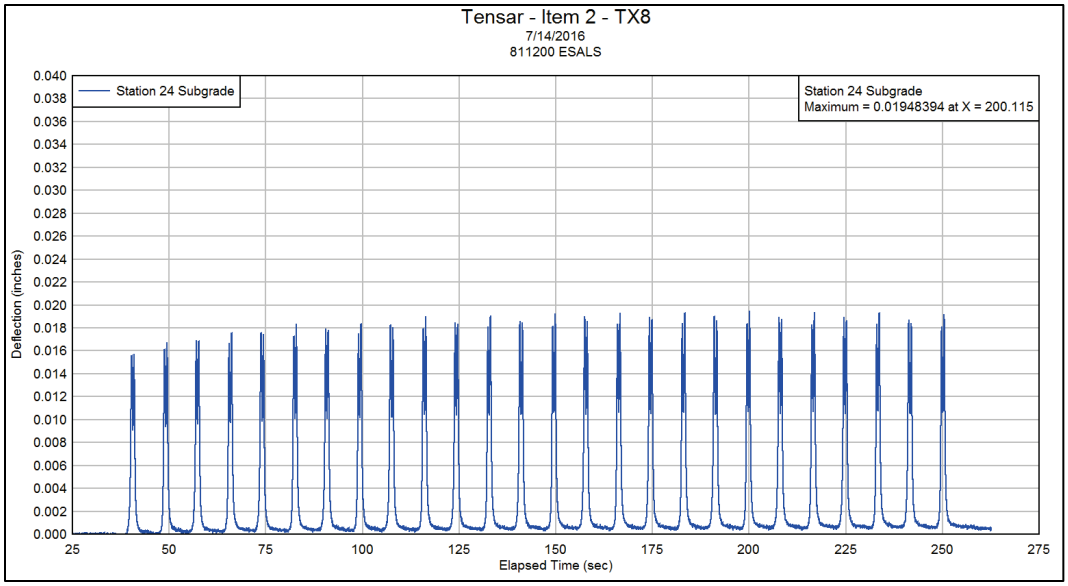

Tensar - Item 2 - TX8
5/19/2016
108160 ESALS
Station 24 Subgrade
Station 24 Subgrade
Maximum = 0.02122622 at X = 108.746
Deflection (inches)
0.040
0.038
0.036
0.034
0.032
0.030
0.028
0.026
0.024
0.022
0.020
0.018
0.016
0.014
0.012
0.010
0.008
0.006
0.004
0.002
0.000
30
60
90
120
150
180
210
240
270
300
Elapsed Time (sec)


Tensar - Item 2 - TX8
5/23/2016
162240 ESALS
Station 24 Subgrade
Station 24 Subgrade
Maximum = 0.02140924 at X = 462.719
Deflection (inches)
0.040
0.038
0.036
0.034
0.032
0.030
0.028
0.026
0.024
0.022
0.020
0.018
0.016
0.014
0.012
0.010
0.008
0.006
0.004
0.002
0.000
300
315
330
345
360
375
390
405
420
435
450
465
480
495
510
525
540
Elapsed Time (sec)

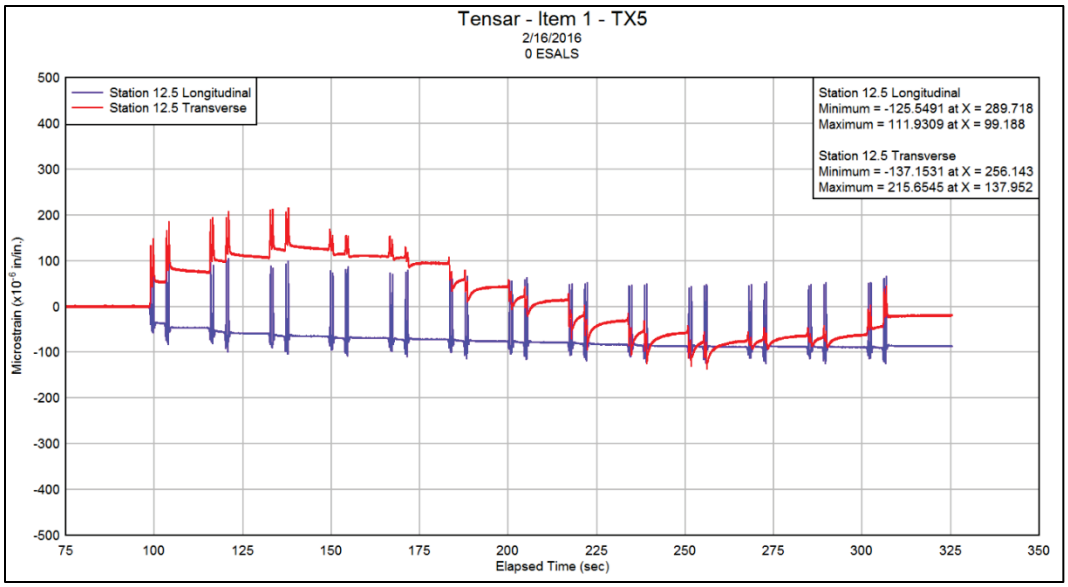

Tensar - Item 2 - TX8
5/26/2016
216320 ESALS
Station 24 Subgrade
Station 24 Subgrade
Maximum = 0.02173984 at X = 218.371
Deflection (inches)
Elapsed Time (sec)

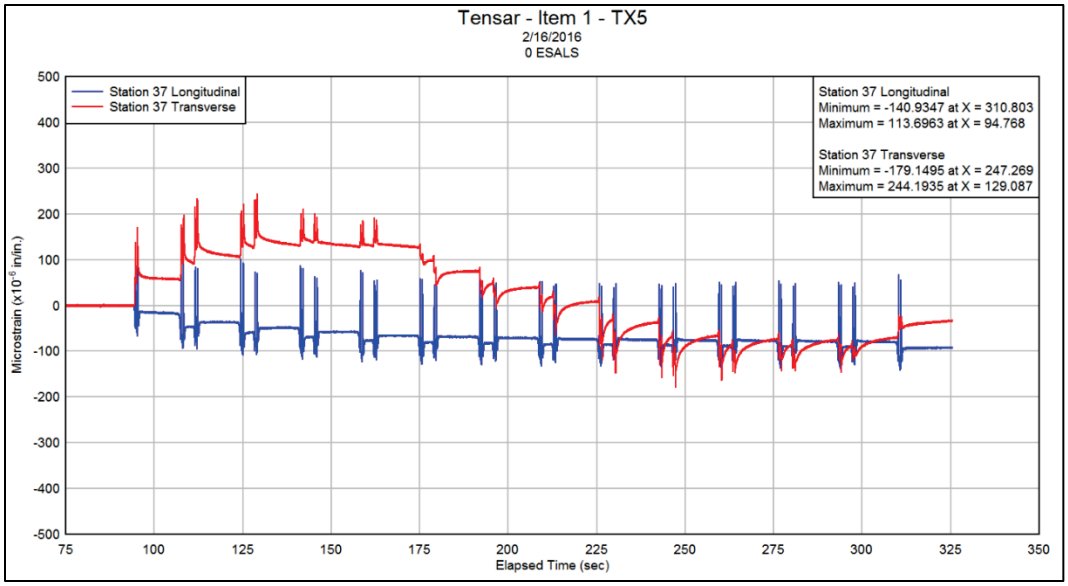

Tensar - Item 2 - TX8
6/6/2016
324480 ESALS
Station 24 Subgrade
Station 24 Subgrade
Maximum = 0.02048583 at X = 114.226
Deflection (inches)
Elapsed Time (sec)

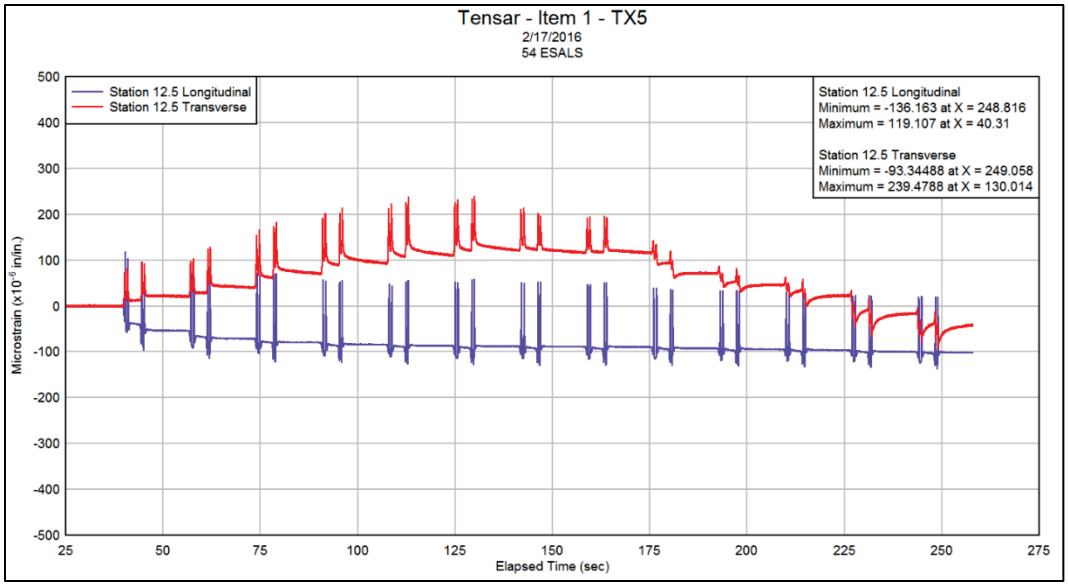

Tensar - Item 2 - TX8
6/21/2016
540800 ESALS
Station 24 Subgrade
Station 24 Subgrade
Maximum = 0.0203502 at X = 76.571
Deflection (inches)
0.040
0.038
0.036
0.034
0.032
0.030
0.028
0.026
0.024
0.022
0.020
0.018
0.016
0.014
0.012
0.010
0.008
0.006
0.004
0.002
0.000
0
40
80
120
160
200
240
280
320
Elapsed Time (sec)

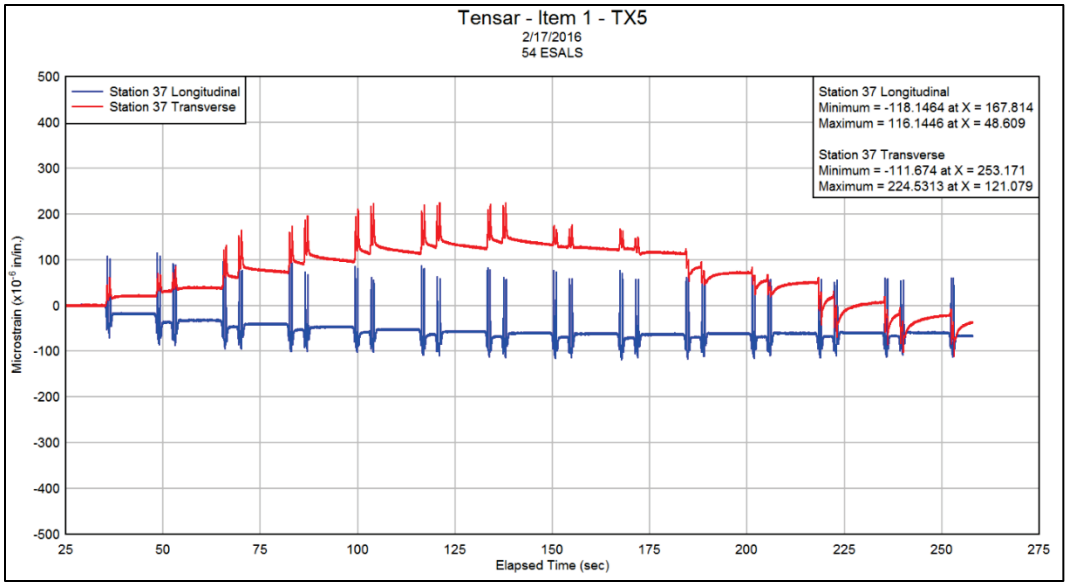

Tensar - Item 2 - TX8
7/14/2016
811200 ESALS
Station 24 Subgrade
Station 24 Subgrade
Maximum = 0.01948394 at X = 200.115
Deflection (inches)
0.040
0.038
0.036
0.034
0.032
0.030
0.028
0.026
0.024
0.022
0.020
0.018
0.016
0.014
0.012
0.010
0.008
0.006
0.004
0.002
0.000
25
50
75
100
125
150
175
200
225
250
275
Elapsed Time (sec)

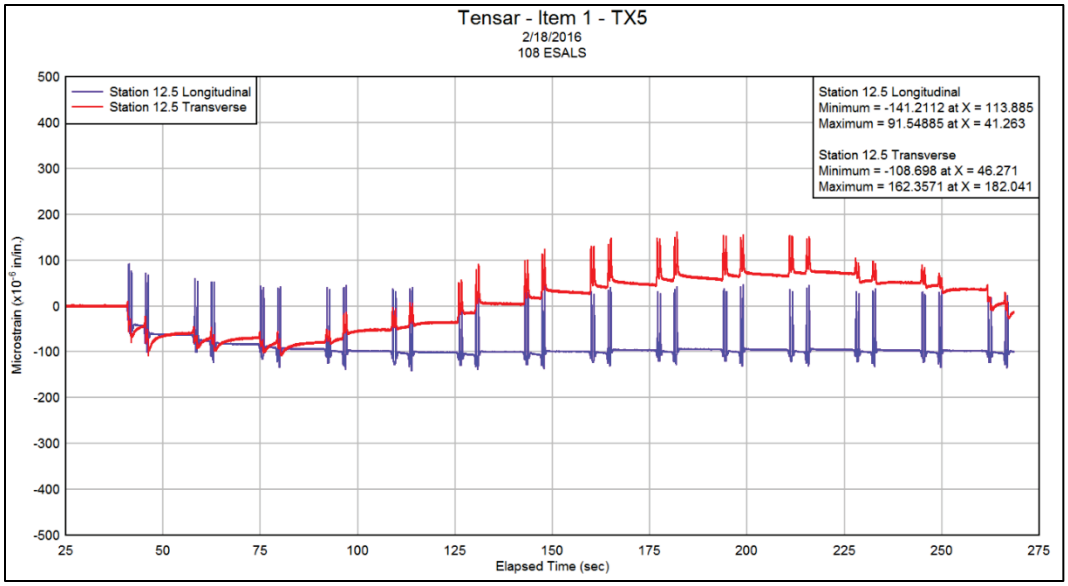
# Appendix C: Asphalt Strain Gauge Responses

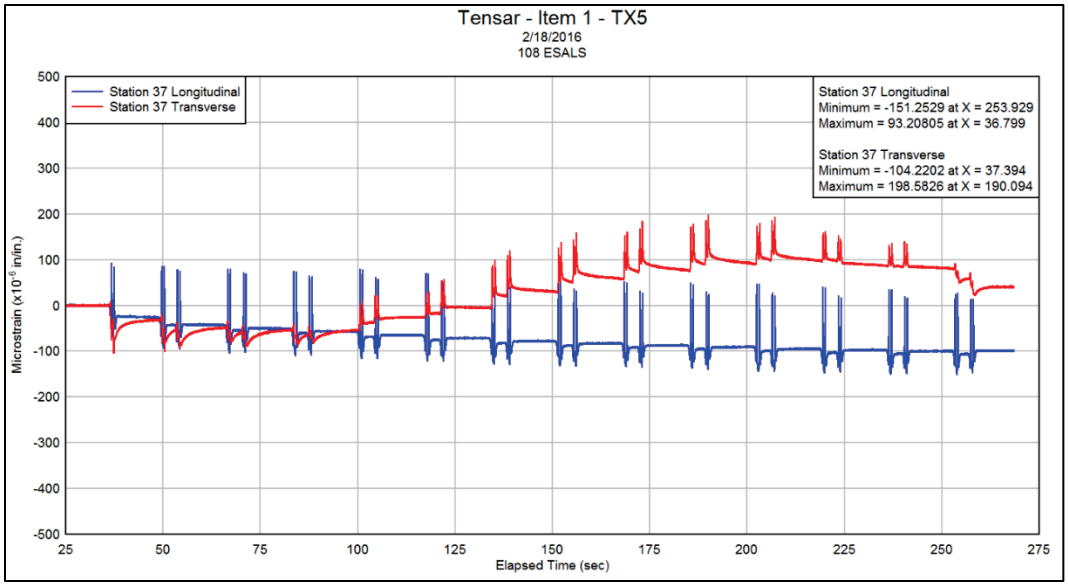


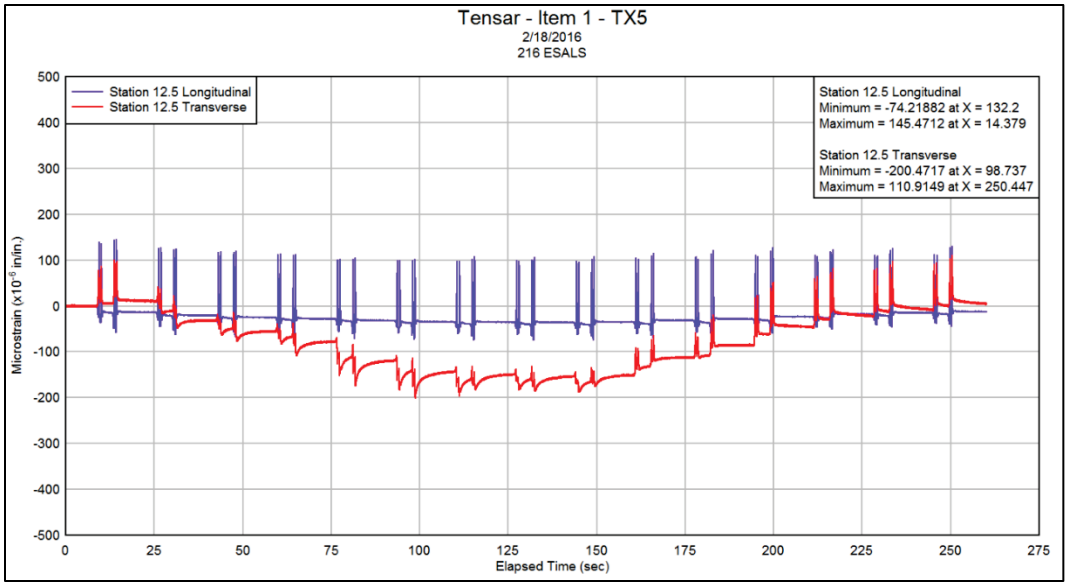



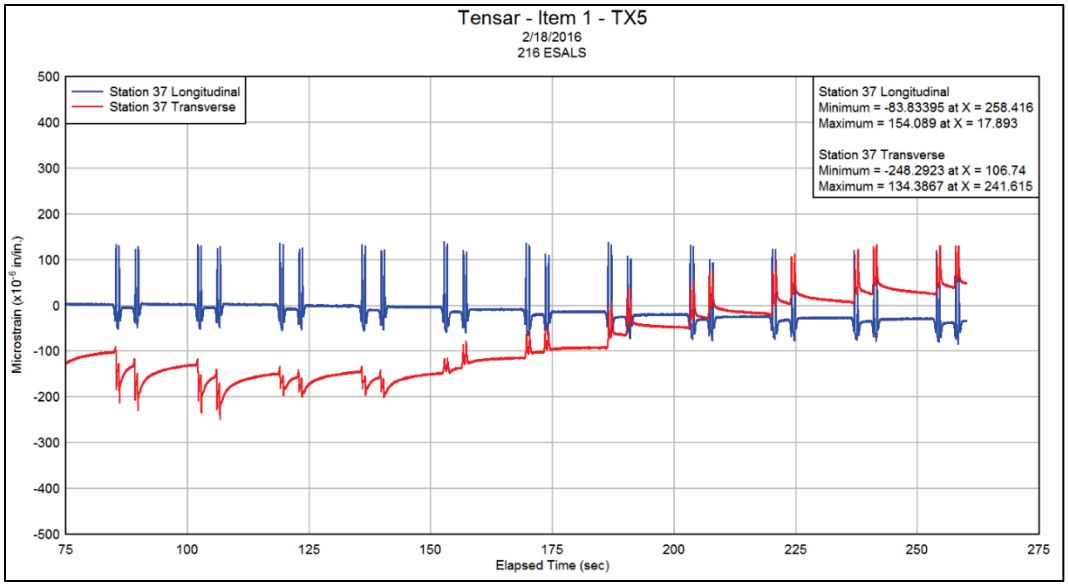

Tensar - Item 1 - TX5
2/17/2016
54 ESALS
Station 12.5 Longitudinal
Station 12.5 Transverse
Station 12.5 Longitudinal
Minimum = -136.163 at X = 248.816
Maximum = 119.107 at X = 40.31
Station 12.5 Transverse
Minimum = -93.34488 at X = 249.058
Maximum = 239.4788 at X = 130.014
Microstrain (x10-6 in/in.)
Elapsed Time (sec)

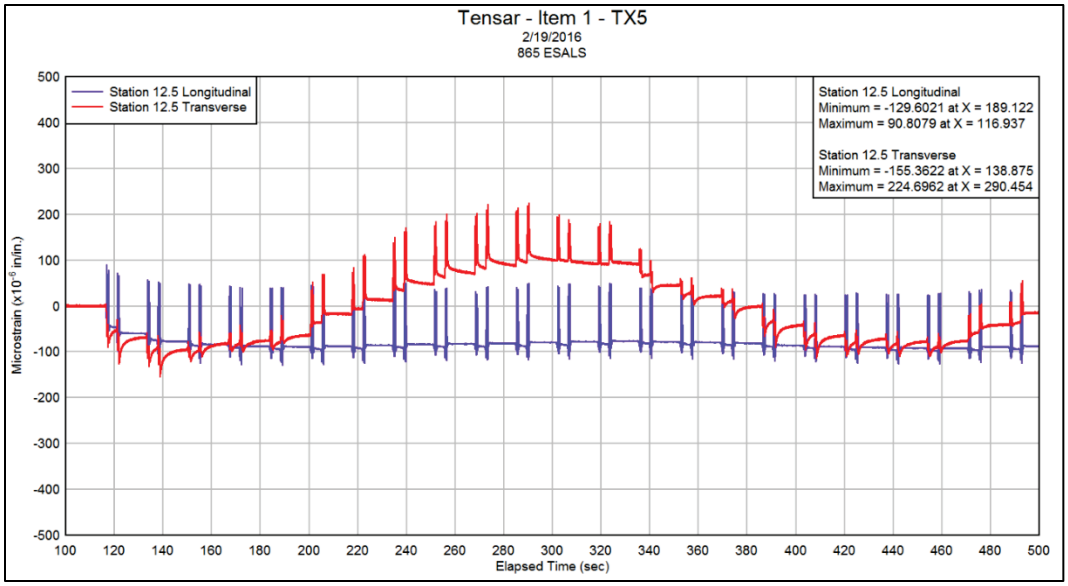

Tensar - Item 1 - TX5
2/17/2016
54 ESALS
Station 37 Longitudinal
Station 37 Transverse
Station 37 Longitudinal
Minimum = -118.1464 at X = 167.814
Maximum = 116.1446 at X = 48.609
Station 37 Transverse
Minimum = -111.674 at X = 253.171
Maximum = 224.5313 at X = 121.079
Microstrain (x10-6 in/in.)
Elapsed Time (sec)

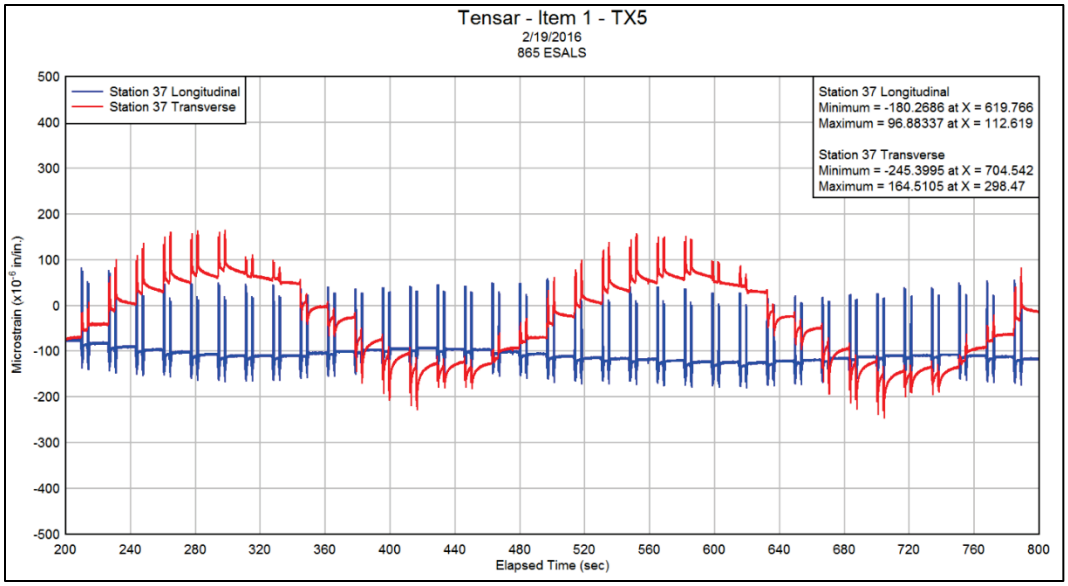

Tensar - Item 1 - TX5
2/18/2016
108 ESALS
Station 12.5 Longitudinal
Station 12.5 Transverse
Station 12.5 Longitudinal
Minimum = -141.2112 at X = 113.885
Maximum = 91.54885 at X = 41.263
Station 12.5 Transverse
Minimum = -108.698 at X = 46.271
Maximum = 162.3571 at X = 182.041
Microstrain (x10-6 in/in.)
Elapsed Time (sec)

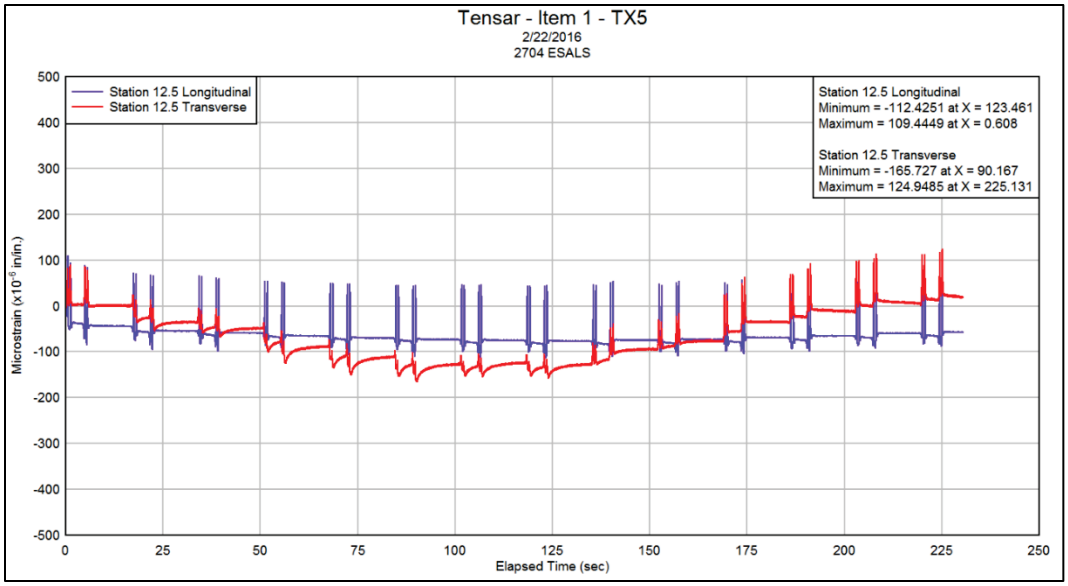

Tensar - Item 1 - TX5
2/18/2016
108 ESALS
Station 37 Longitudinal
Station 37 Transverse
Station 37 Longitudinal
Minimum = -151.2529 at X = 253.929
Maximum = 93.20805 at X = 36.799
Station 37 Transverse
Minimum = -104.2202 at X = 37.394
Maximum = 198.5826 at X = 190.094
Microstrain (x10-6 in/in.)
Elapsed Time (sec)

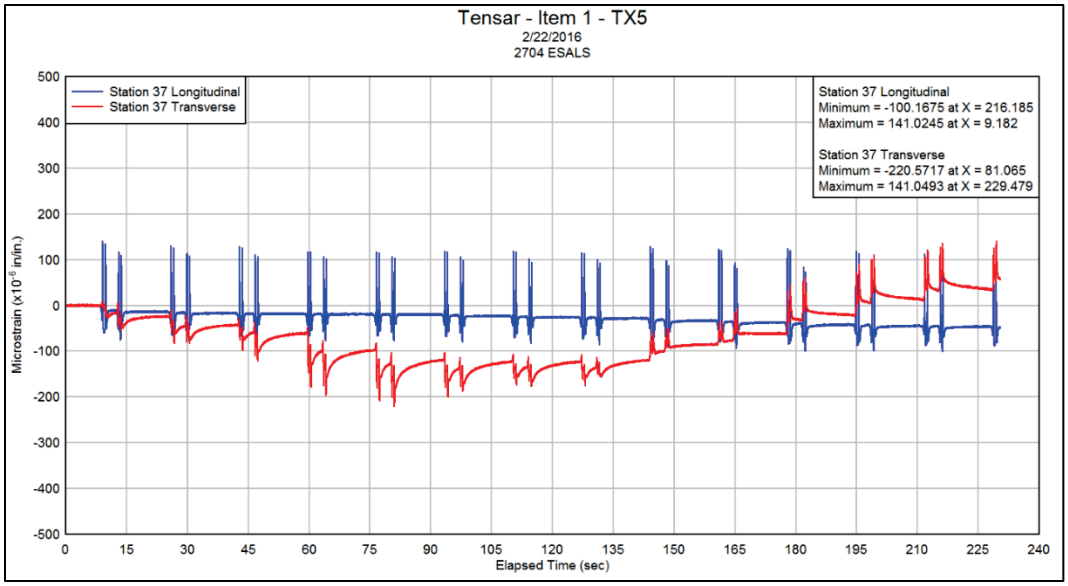

Tensar - Item 1 - TX5
2/18/2016
216 ESALS
Station 12.5 Longitudinal
Station 12.5 Transverse
Station 12.5 Longitudinal
Minimum = -74.21882 at X = 132.2
Maximum = 145.4712 at X = 14.379
Station 12.5 Transverse
Minimum = -200.4717 at X = 98.737
Maximum = 110.9149 at X = 250.447
Microstrain (x10-6 in/in.)
Elapsed Time (sec)

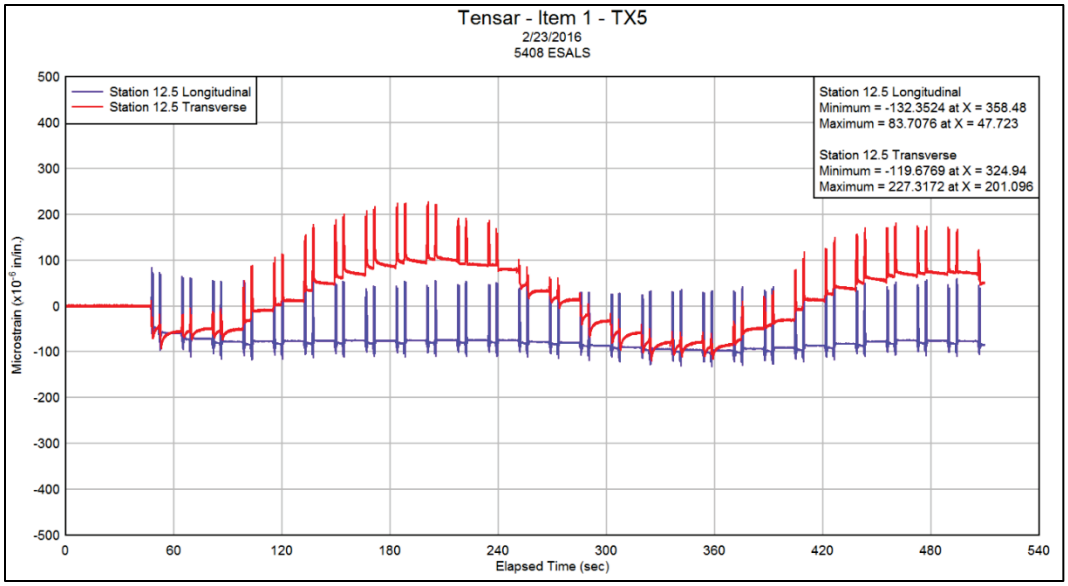

Tensar - Item 1 - TX5
2/18/2016
216 ESALS
Station 37 Longitudinal
Station 37 Transverse
Station 37 Longitudinal
Minimum = -83.83395 at X = 258.416
Maximum = 154.089 at X = 17.893
Station 37 Transverse
Minimum = -248.2923 at X = 106.74
Maximum = 134.3867 at X = 241.615
Microstrain (x10-6 in/in.)
Elapsed Time (sec)

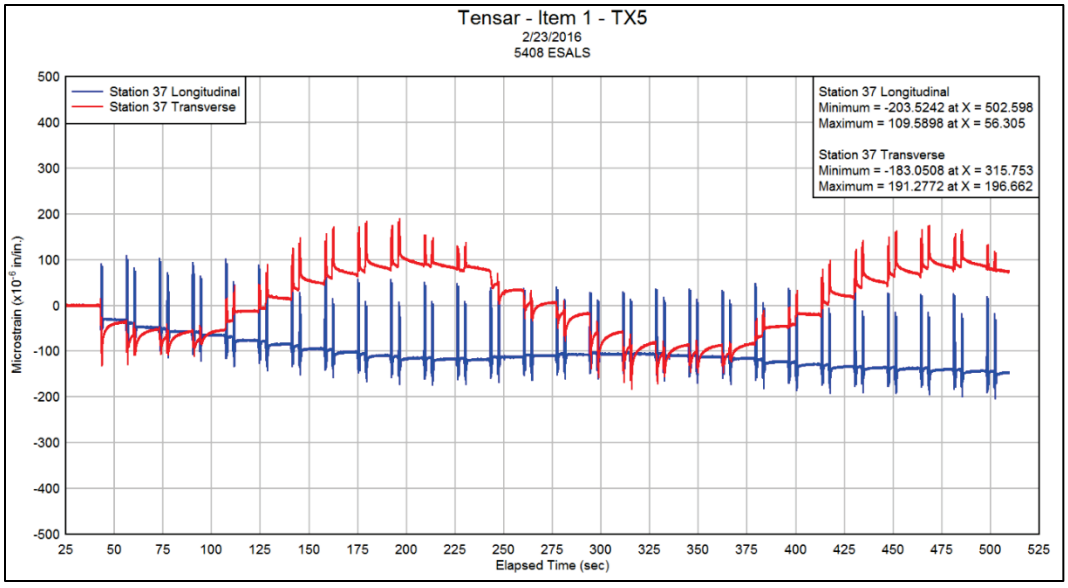

Tensar - Item 1 - TX5
2/19/2016
865 ESALS
Station 12.5 Longitudinal
Station 12.5 Transverse
Station 12.5 Longitudinal
Minimum = -129.6021 at X = 189.122
Maximum = 90.8079 at X = 116.937
Station 12.5 Transverse
Minimum = -155.3622 at X = 138.875
Maximum = 224.6962 at X = 290.454
Microstrain (x10⁻⁶ in/in.)
Elapsed Time (sec)

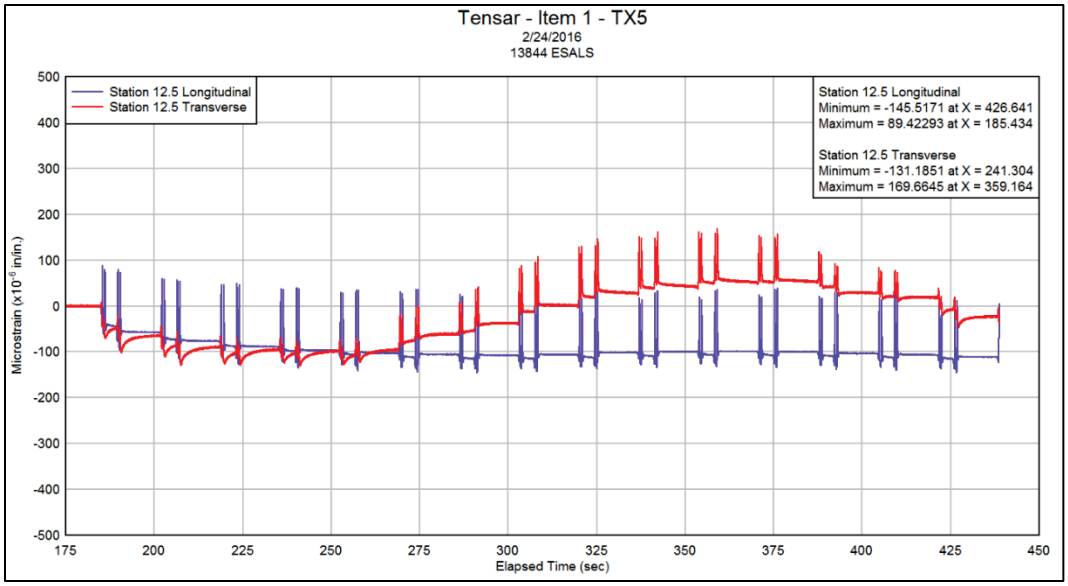

Tensar - Item 1 - TX5
2/19/2016
865 ESALS
Station 37 Longitudinal
Station 37 Transverse
Station 37 Longitudinal
Minimum = -180.2686 at X = 619.766
Maximum = 96.88337 at X = 112.619
Station 37 Transverse
Minimum = -245.3995 at X = 704.542
Maximum = 164.5105 at X = 298.47
Microstrain (x10⁻⁶ in/in.)
Elapsed Time (sec)

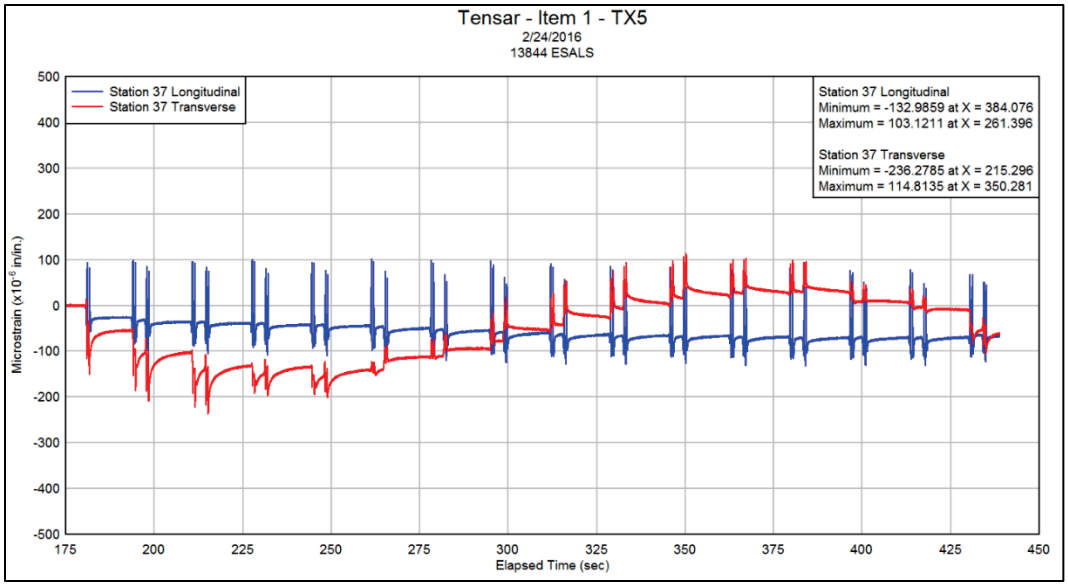

Tensar - Item 1 - TX5
2/22/2016
2704 ESALS
Station 12.5 Longitudinal
Station 12.5 Transverse
Station 12.5 Longitudinal
Minimum = -112.4251 at X = 123.461
Maximum = 109.4449 at X = 0.608
Station 12.5 Transverse
Minimum = -165.727 at X = 90.167
Maximum = 124.9485 at X = 225.131
Microstrain (x10^-6 in/in.)
Elapsed Time (sec)

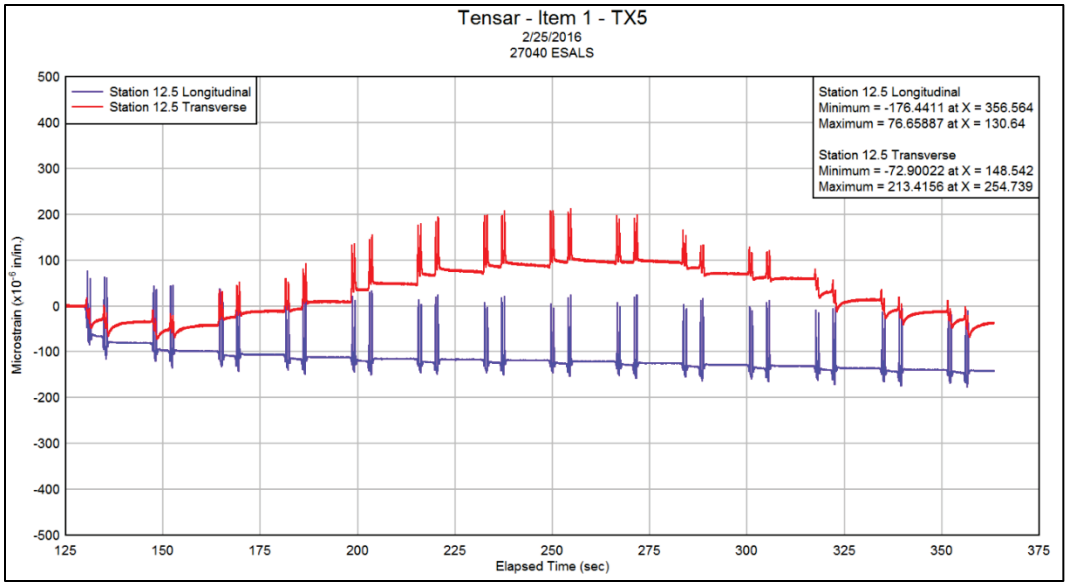

Tensar - Item 1 - TX5
2/22/2016
2704 ESALS
Station 37 Longitudinal
Station 37 Transverse
Station 37 Longitudinal
Minimum = -100.1675 at X = 216.185
Maximum = 141.0245 at X = 9.182
Station 37 Transverse
Minimum = -220.5717 at X = 81.065
Maximum = 141.0493 at X = 229.479
Microstrain (x10^-6 in/in.)
Elapsed Time (sec)

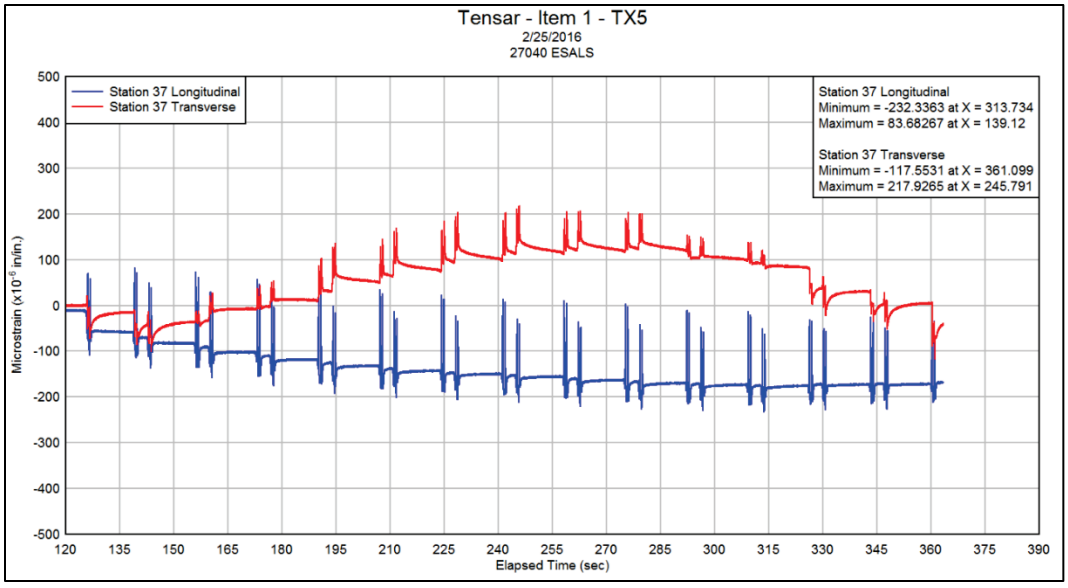

Tensar - Item 1 - TX5
2/23/2016
5408 ESALS
Station 12.5 Longitudinal
Station 12.5 Transverse
Station 12.5 Longitudinal
Minimum = -132.3524 at X = 358.48
Maximum = 83.7076 at X = 47.723
Station 12.5 Transverse
Minimum = -119.6769 at X = 324.94
Maximum = 227.3172 at X = 201.096
Microstrain (x10-6 in/in.)
Elapsed Time (sec)

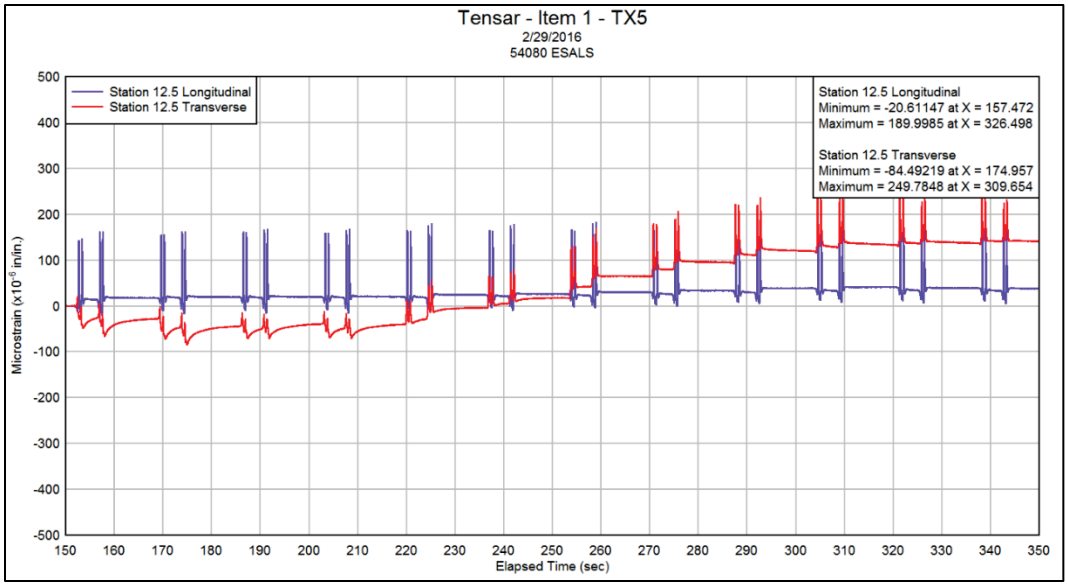

Tensar - Item 1 - TX5
2/23/2016
5408 ESALS
Station 37 Longitudinal
Station 37 Transverse
Station 37 Longitudinal
Minimum = -203.5242 at X = 502.598
Maximum = 109.5898 at X = 56.305
Station 37 Transverse
Minimum = -183.0508 at X = 315.753
Maximum = 191.2772 at X = 196.662
Microstrain (x10-6 in/in.)
Elapsed Time (sec)

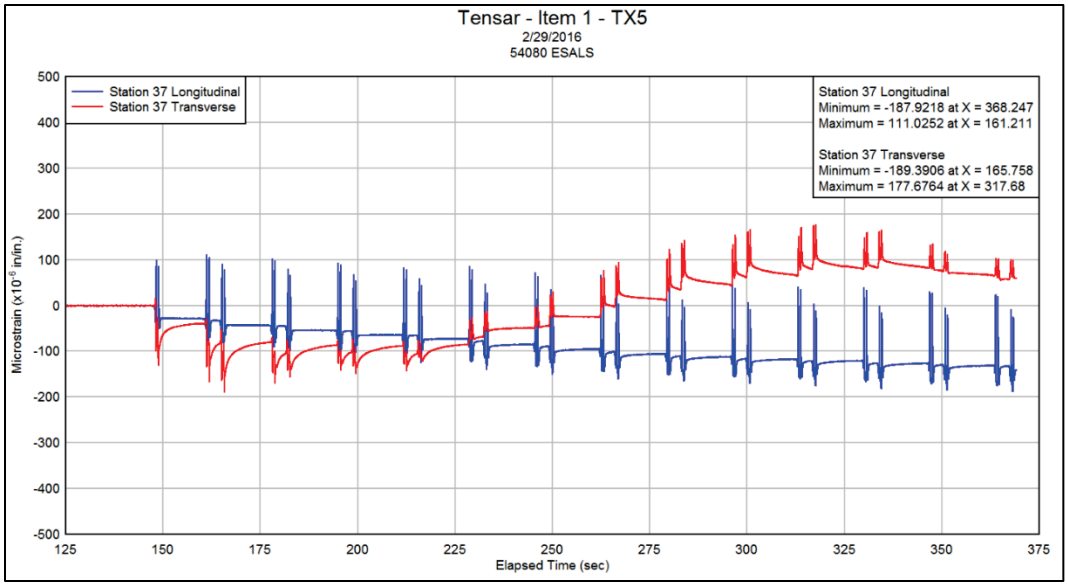

Tensar - Item 1 - TX5
2/24/2016
13844 ESALS
Station 12.5 Longitudinal
Station 12.5 Transverse
Station 12.5 Longitudinal
Minimum = -145.5171 at X = 426.641
Maximum = 89.42293 at X = 185.434
Station 12.5 Transverse
Minimum = -131.1851 at X = 241.304
Maximum = 169.6645 at X = 359.164
Microstrain (x10-6 in/in.)
Elapsed Time (sec)

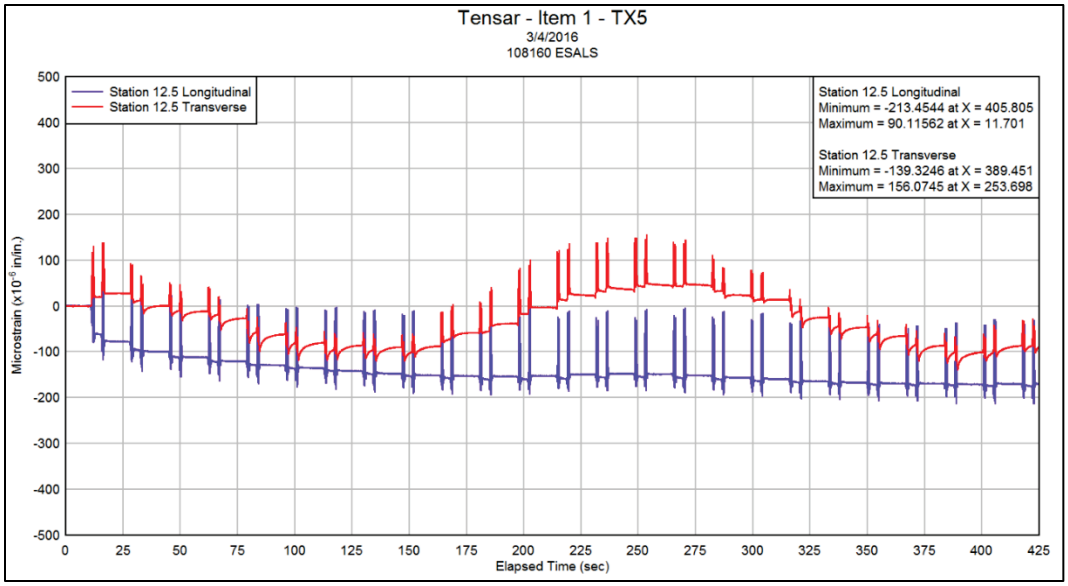

Tensar - Item 1 - TX5
2/24/2016
13844 ESALS
Station 37 Longitudinal
Station 37 Transverse
Station 37 Longitudinal
Minimum = -132.9859 at X = 384.076
Maximum = 103.1211 at X = 261.396
Station 37 Transverse
Minimum = -236.2785 at X = 215.296
Maximum = 114.8135 at X = 350.281
Microstrain (x10-6 in/in.)
Elapsed Time (sec)

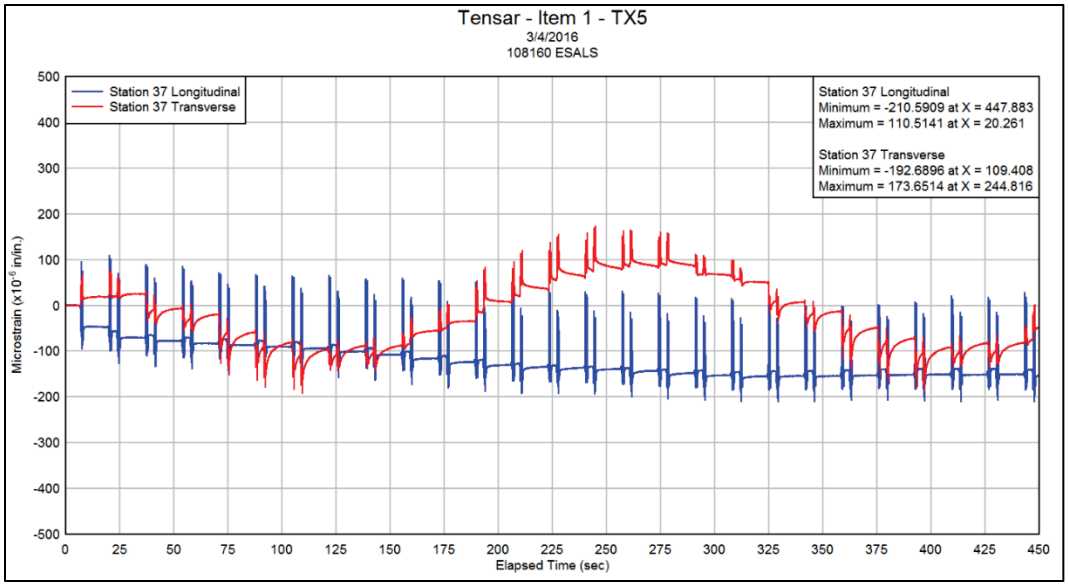

Tensar - Item 1 - TX5
2/25/2016
27040 ESALS
Station 12.5 Longitudinal
Station 12.5 Transverse
Station 12.5 Longitudinal
Minimum = -176.4411 at X = 356.564
Maximum = 76.65887 at X = 130.64
Station 12.5 Transverse
Minimum = -72.90022 at X = 148.542
Maximum = 213.4156 at X = 254.739
Microstrain (x10^-6 in/in.)
Elapsed Time (sec)

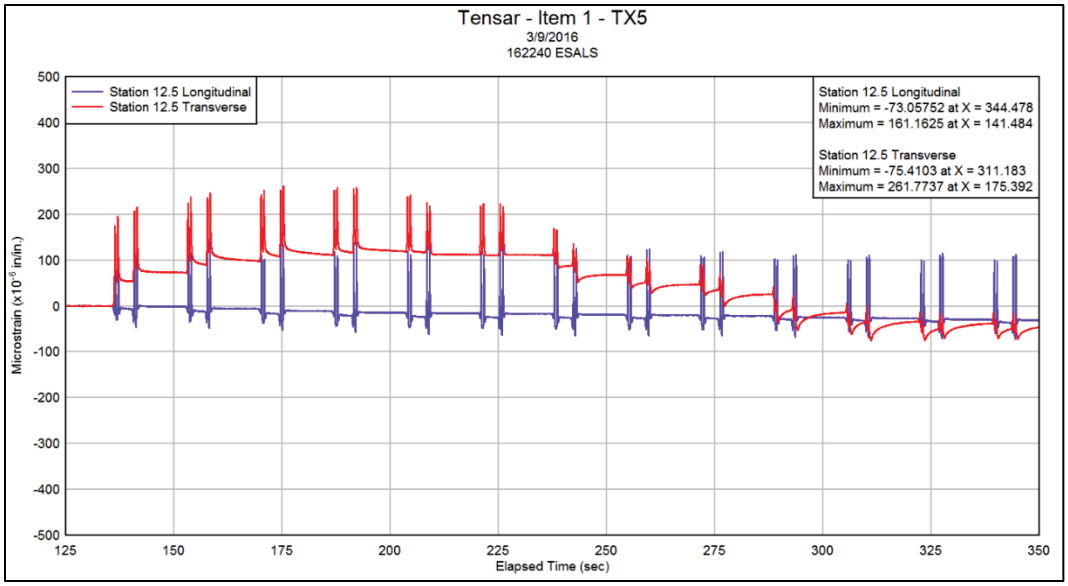

Tensar - Item 1 - TX5
2/25/2016
27040 ESALS
Station 37 Longitudinal
Station 37 Transverse
Station 37 Longitudinal
Minimum = -232.3363 at X = 313.734
Maximum = 83.68267 at X = 139.12
Station 37 Transverse
Minimum = -117.5531 at X = 361.099
Maximum = 217.9265 at X = 245.791
Microstrain (x10^-6 in/in.)
Elapsed Time (sec)

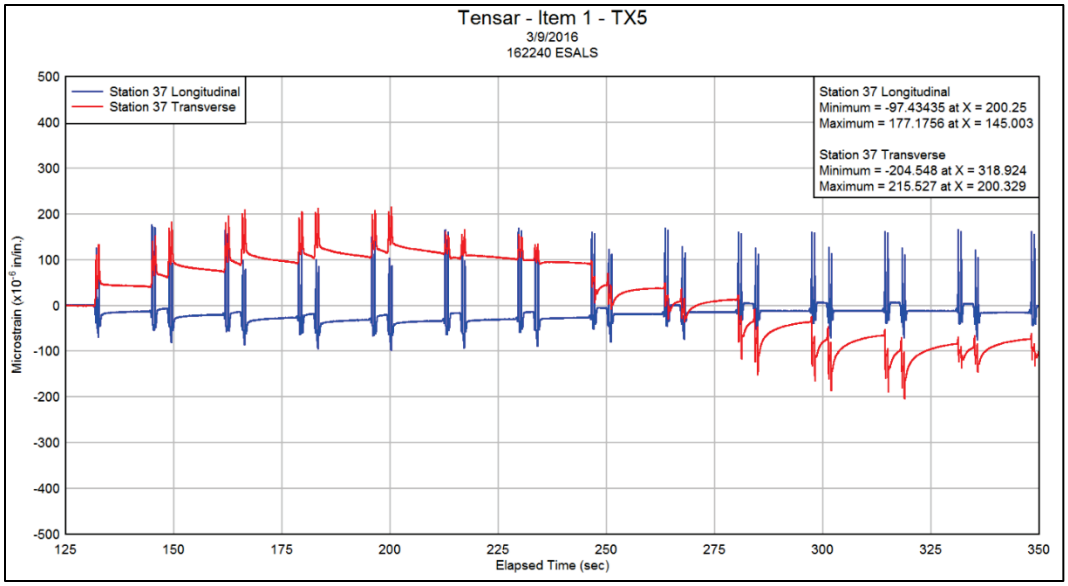

Tensar - Item 1 - TX5
2/29/2016
54080 ESALS
Station 12.5 Longitudinal
Station 12.5 Transverse
Station 12.5 Longitudinal
Minimum = -20.61147 at X = 157.472
Maximum = 189.9985 at X = 326.498
Station 12.5 Transverse
Minimum = -84.49219 at X = 174.957
Maximum = 249.7848 at X = 309.654
Microstrain (x10^-6 in/in.)
Elapsed Time (sec)

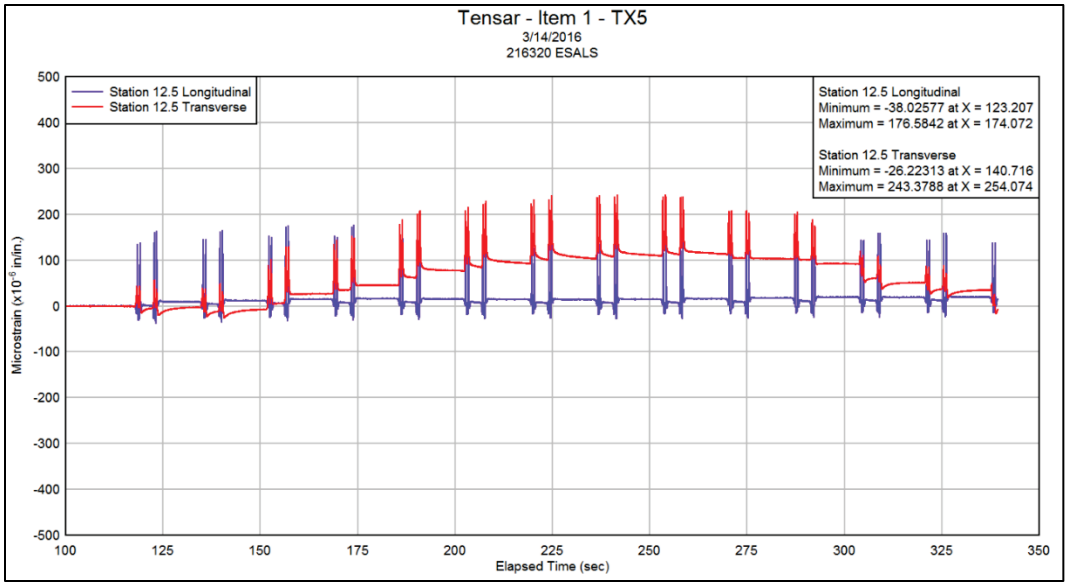

Tensar - Item 1 - TX5
2/29/2016
54080 ESALS
Station 37 Longitudinal
Station 37 Transverse
Station 37 Longitudinal
Minimum = -187.9218 at X = 368.247
Maximum = 111.0252 at X = 161.211
Station 37 Transverse
Minimum = -189.3906 at X = 165.758
Maximum = 177.6764 at X = 317.68
Microstrain (x10^-6 in/in.)
Elapsed Time (sec)

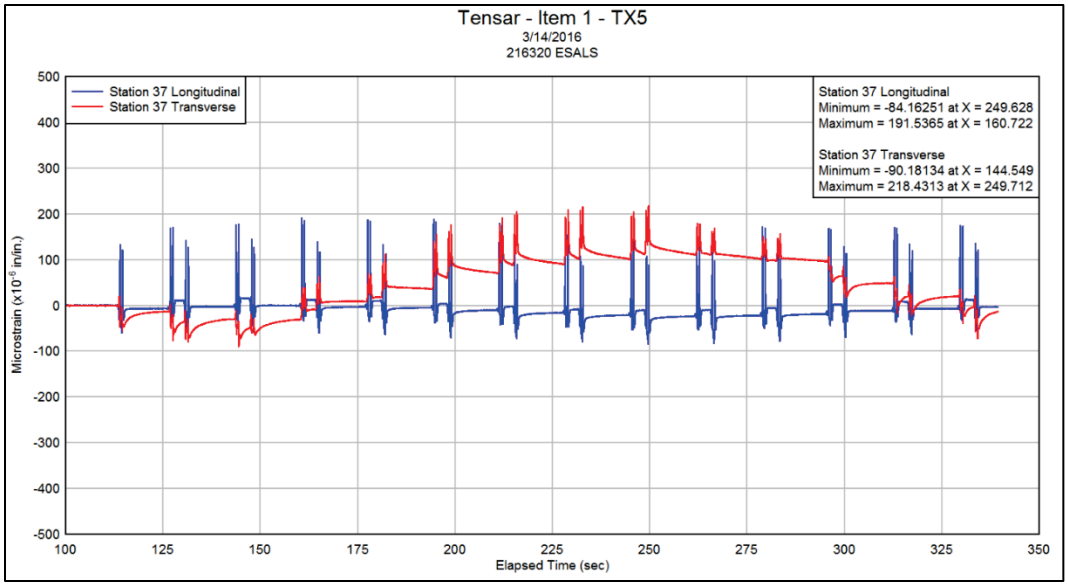

Tensar - Item 1 - TX5
3/4/2016
108160 ESALS
Station 12.5 Longitudinal
Station 12.5 Transverse
Station 12.5 Longitudinal
Minimum = -213.4544 at X = 405.805
Maximum = 90.11562 at X = 11.701
Station 12.5 Transverse
Minimum = -139.3246 at X = 389.451
Maximum = 156.0745 at X = 253.698
Microstrain (x10-6 in/in.)
Elapsed Time (sec)

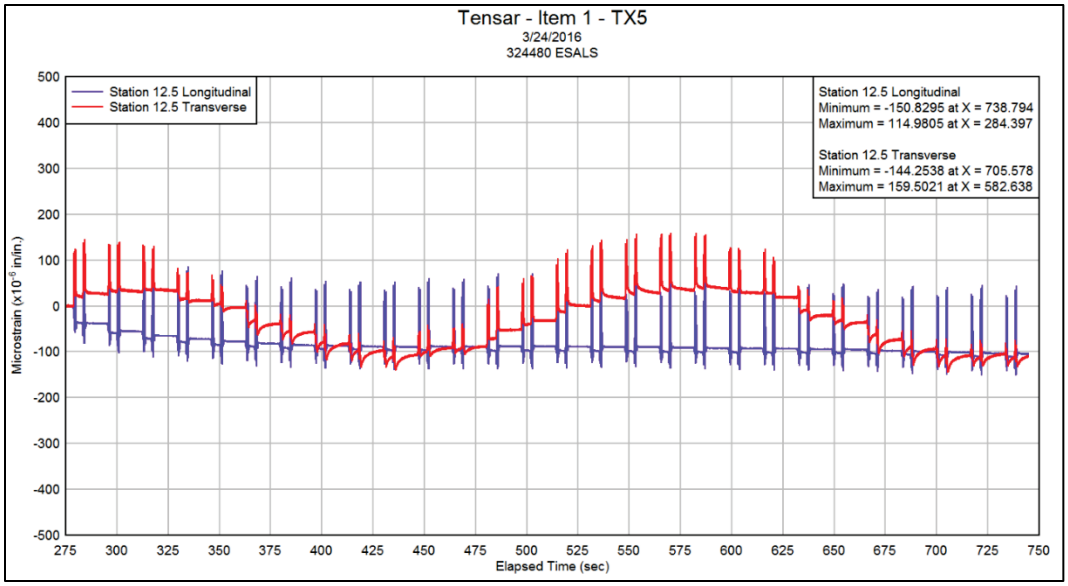

Tensar - Item 1 - TX5
3/4/2016
108160 ESALS
Station 37 Longitudinal
Station 37 Transverse
Station 37 Longitudinal
Minimum = -210.5909 at X = 447.883
Maximum = 110.5141 at X = 20.261
Station 37 Transverse
Minimum = -192.6896 at X = 109.408
Maximum = 173.6514 at X = 244.816
Microstrain (x10-6 in/in.)
Elapsed Time (sec)

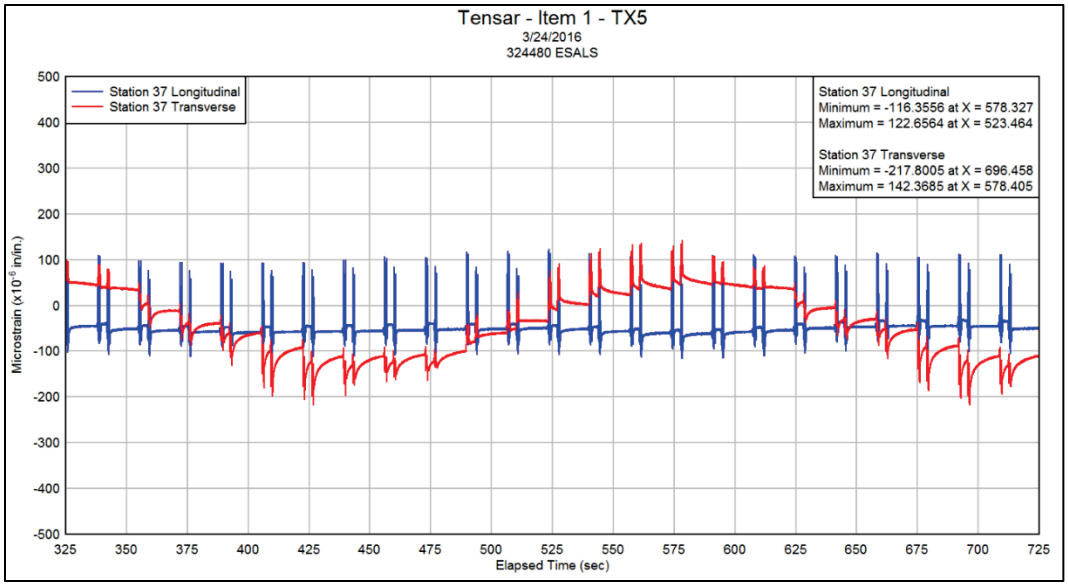

Tensar - Item 1 - TX5
3/9/2016
162240 ESALS
Station 12.5 Longitudinal
Station 12.5 Transverse
Station 12.5 Longitudinal
Minimum = -73.05752 at X = 344.478
Maximum = 161.1625 at X = 141.484
Station 12.5 Transverse
Minimum = -75.4103 at X = 311.183
Maximum = 261.7737 at X = 175.392
Microstrain (x10-6 in/in.)
Elapsed Time (sec)

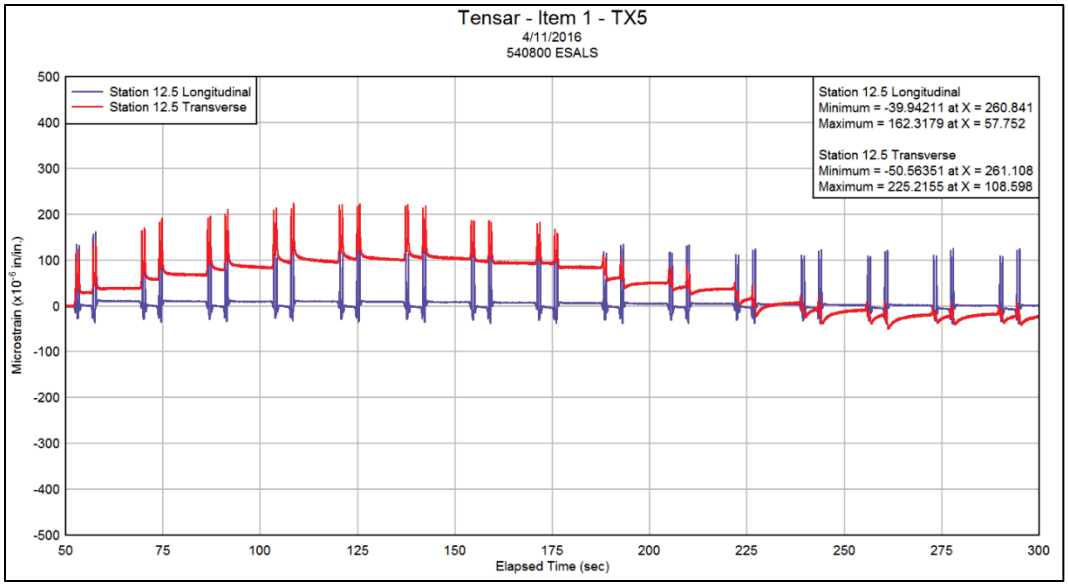

Tensar - Item 1 - TX5
3/9/2016
162240 ESALS
Station 37 Longitudinal
Station 37 Transverse
Station 37 Longitudinal
Minimum = -97.43435 at X = 200.25
Maximum = 177.1756 at X = 145.003
Station 37 Transverse
Minimum = -204.548 at X = 318.924
Maximum = 215.527 at X = 200.329
Microstrain (x10-6 in/in.)
Elapsed Time (sec)

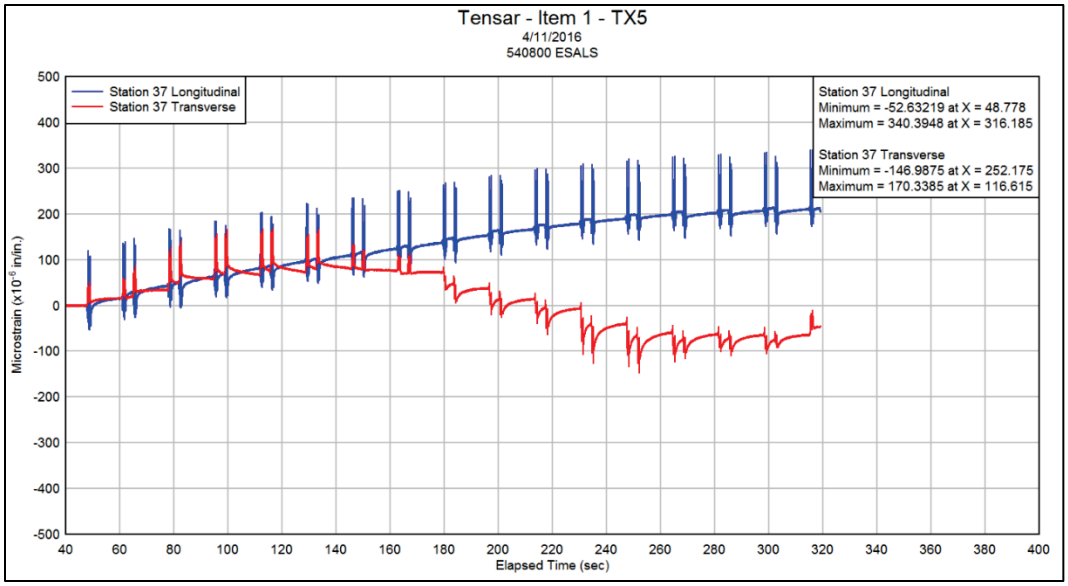

Tensar - Item 1 - TX5
3/14/2016
216320 ESALS
Station 12.5 Longitudinal
Station 12.5 Transverse
Station 12.5 Longitudinal
Minimum = -38.02577 at X = 123.207
Maximum = 176.5842 at X = 174.072
Station 12.5 Transverse
Minimum = -26.22313 at X = 140.716
Maximum = 243.3788 at X = 254.074
Microstrain (x10-6 in/in.)
Elapsed Time (sec)

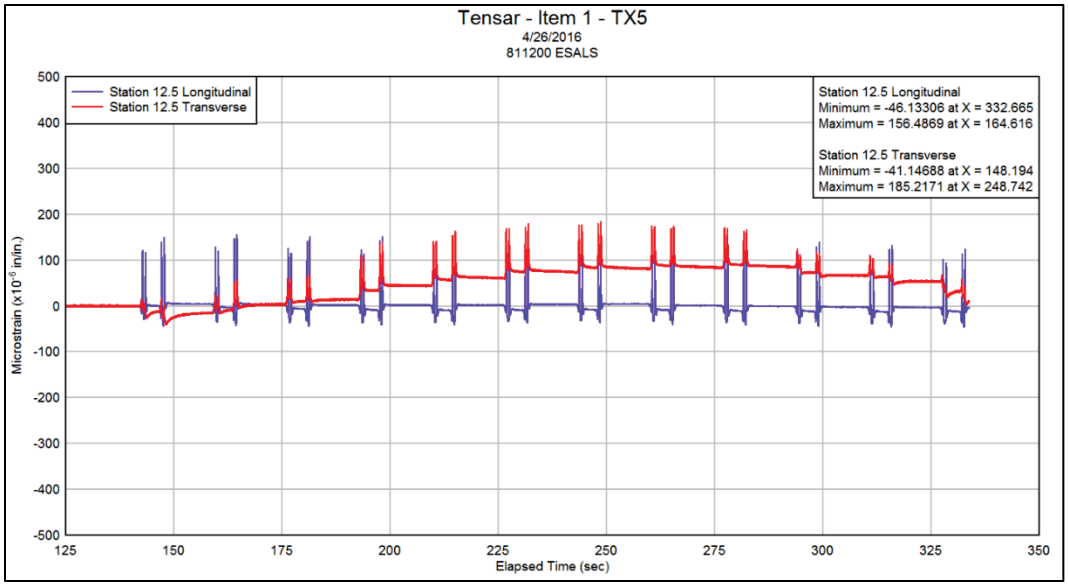

Tensar - Item 1 - TX5
3/14/2016
216320 ESALS
Station 37 Longitudinal
Station 37 Transverse
Station 37 Longitudinal
Minimum = -84.16251 at X = 249.628
Maximum = 191.5365 at X = 160.722
Station 37 Transverse
Minimum = -90.18134 at X = 144.549
Maximum = 218.4313 at X = 249.712
Microstrain (x10-6 in/in.)
Elapsed Time (sec)

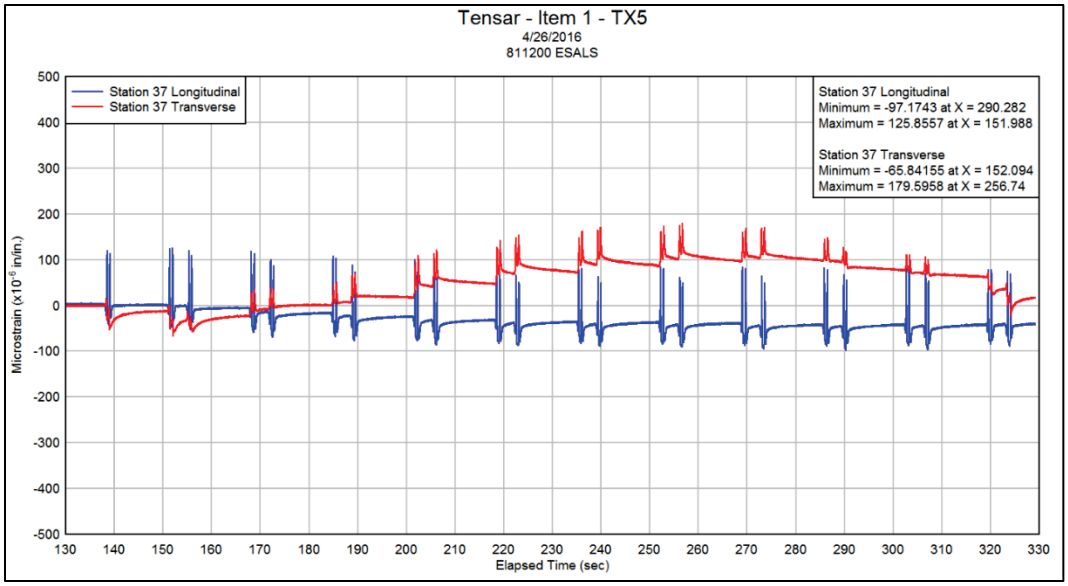

Tensar - Item 1 - TX5
3/24/2016
324480 ESALS
Station 12.5 Longitudinal
Station 12.5 Transverse
Station 12.5 Longitudinal
Minimum = -150.8295 at X = 738.794
Maximum = 114.9805 at X = 284.397
Station 12.5 Transverse
Minimum = -144.2538 at X = 705.578
Maximum = 159.5021 at X = 582.638
Microstrain (x10⁻⁶ in/in.)
Elapsed Time (sec)

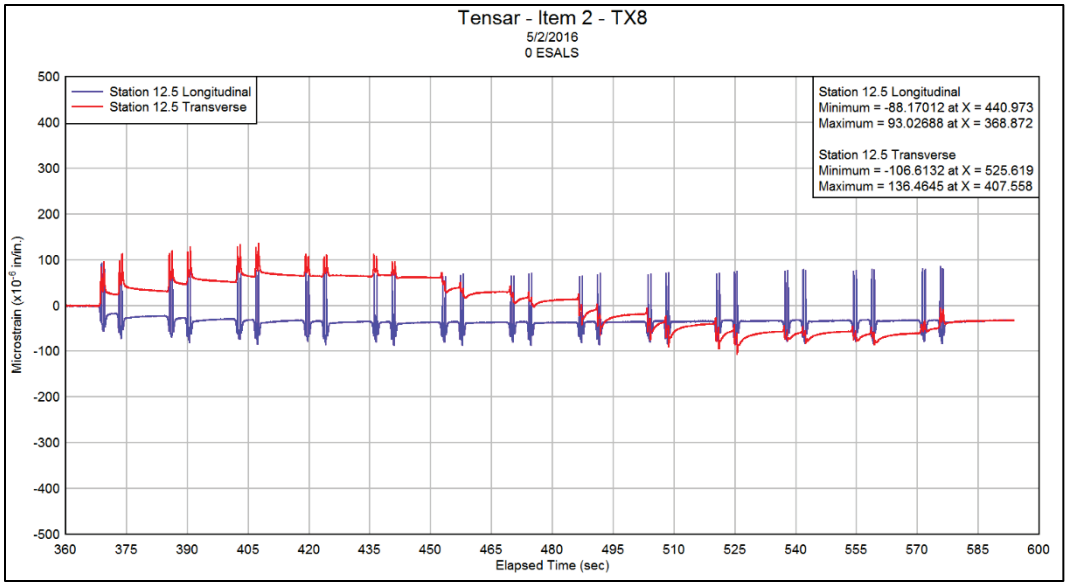

Tensar - Item 1 - TX5
3/24/2016
324480 ESALS
Station 37 Longitudinal
Station 37 Transverse
Station 37 Longitudinal
Minimum = -116.3556 at X = 578.327
Maximum = 122.6564 at X = 523.464
Station 37 Transverse
Minimum = -217.8005 at X = 696.458
Maximum = 142.3685 at X = 578.405
Microstrain (x10⁻⁶ in/in.)
Elapsed Time (sec)

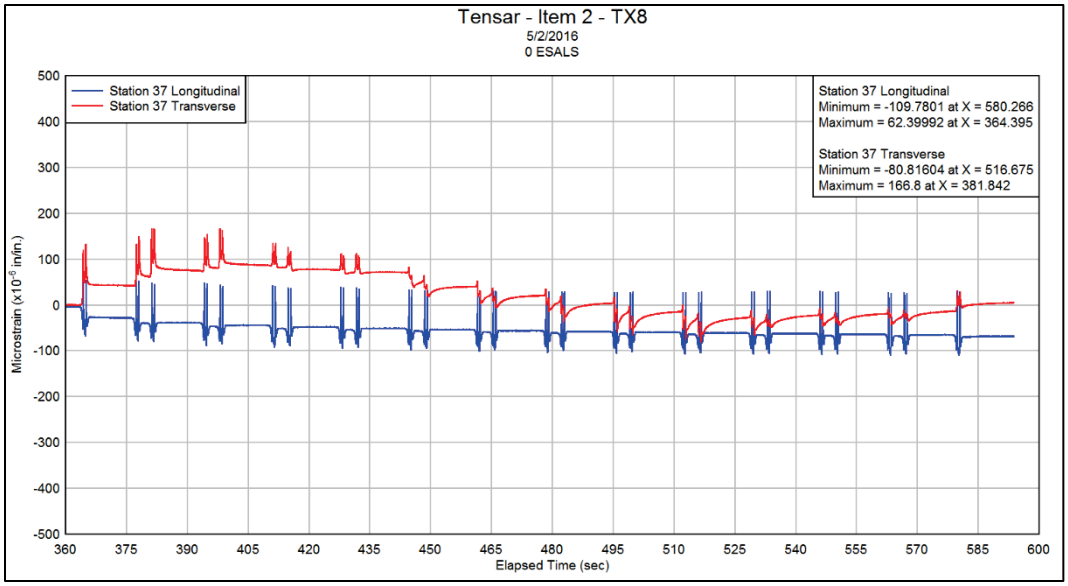

Tensar - Item 1 - TX5
4/11/2016
540800 ESALS
Station 12.5 Longitudinal
Station 12.5 Transverse
Station 12.5 Longitudinal
Minimum = -39.94211 at X = 260.841
Maximum = 162.3179 at X = 57.752
Station 12.5 Transverse
Minimum = -50.56351 at X = 261.108
Maximum = 225.2155 at X = 108.598
Microstrain (x10⁻⁶ in/in.)
Elapsed Time (sec)

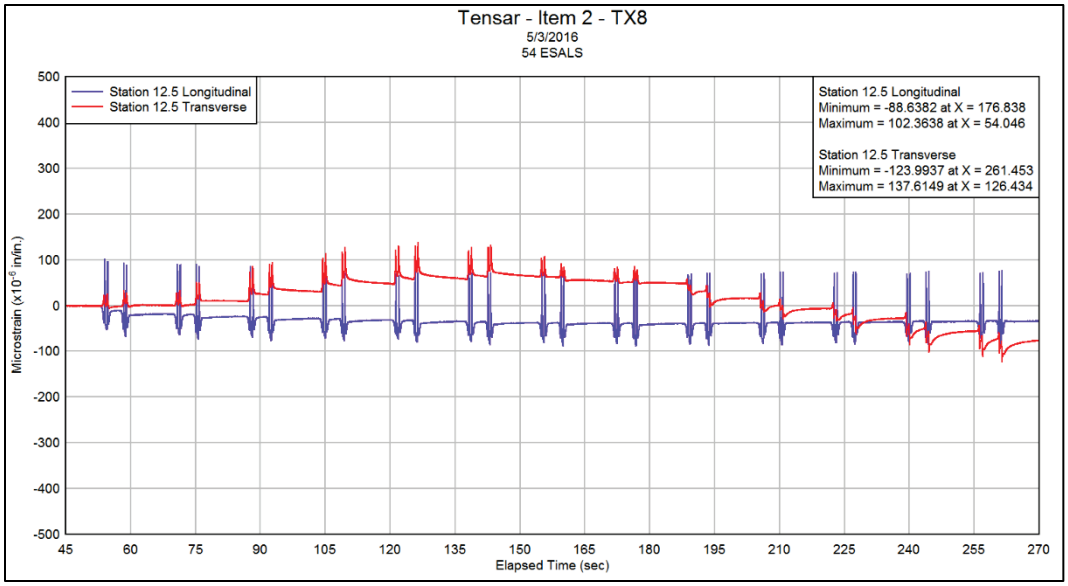

Tensar - Item 1 - TX5
4/11/2016
540800 ESALS
Station 37 Longitudinal
Station 37 Transverse
Station 37 Longitudinal
Minimum = -52.63219 at X = 48.778
Maximum = 340.3948 at X = 316.185
Station 37 Transverse
Minimum = -146.9875 at X = 252.175
Maximum = 170.3385 at X = 116.615
Microstrain (x10⁻⁶ in/in.)
Elapsed Time (sec)

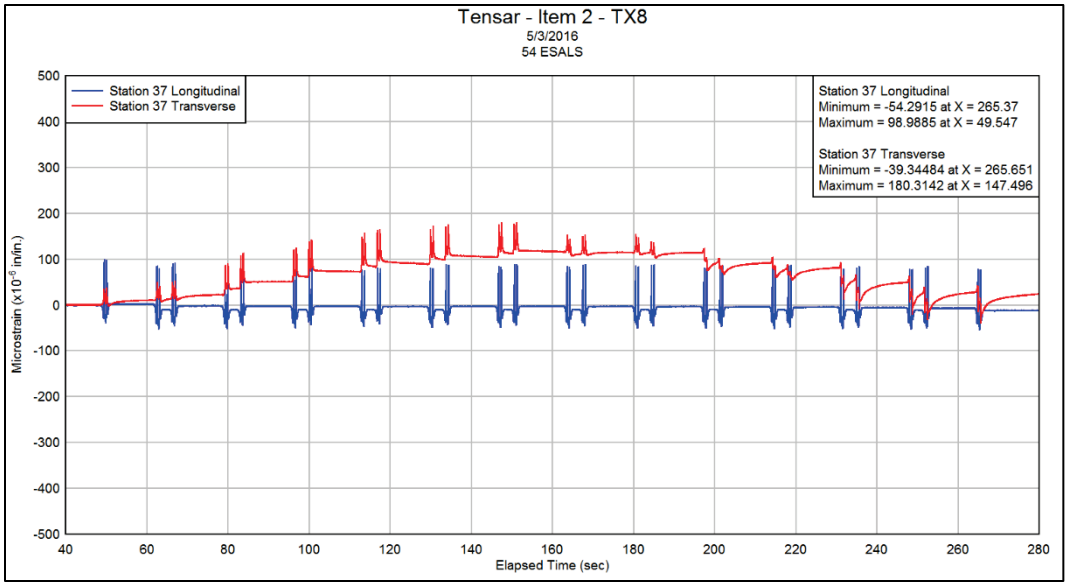

Tensar - Item 1 - TX5
4/26/2016
811200 ESALS
Station 12.5 Longitudinal
Station 12.5 Transverse
Station 12.5 Longitudinal
Minimum = -46.13306 at X = 332.665
Maximum = 156.4869 at X = 164.616
Station 12.5 Transverse
Minimum = -41.14688 at X = 148.194
Maximum = 185.2171 at X = 248.742
Microstrain (x10^-6 in/in.)
Elapsed Time (sec)

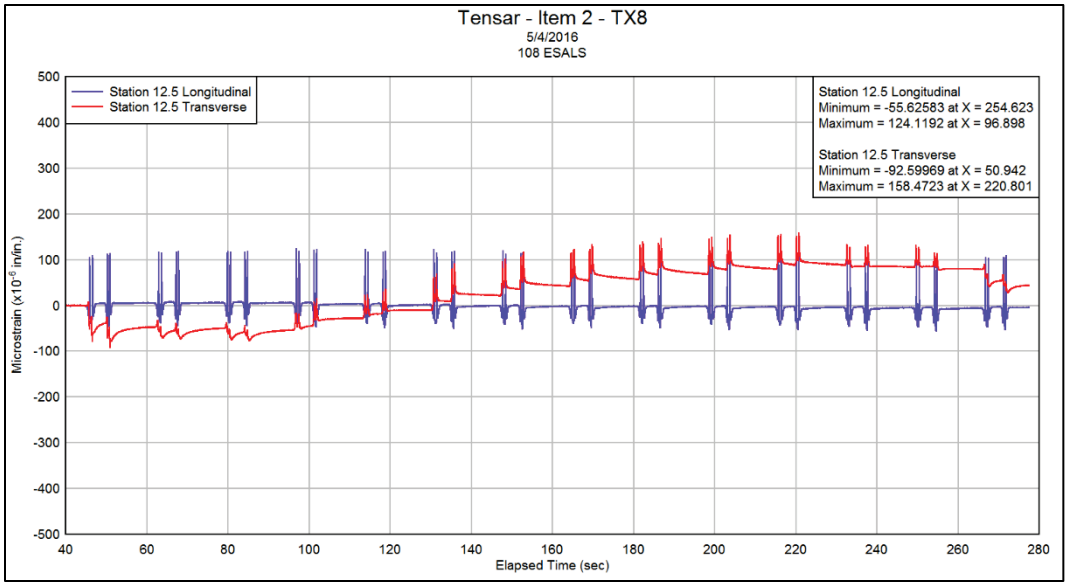

Tensar - Item 1 - TX5
4/26/2016
811200 ESALS
Station 37 Longitudinal
Station 37 Transverse
Station 37 Longitudinal
Minimum = -97.1743 at X = 290.282
Maximum = 125.8557 at X = 151.988
Station 37 Transverse
Minimum = -65.84155 at X = 152.094
Maximum = 179.5958 at X = 256.74
Microstrain (x10^-6 in/in.)
Elapsed Time (sec)

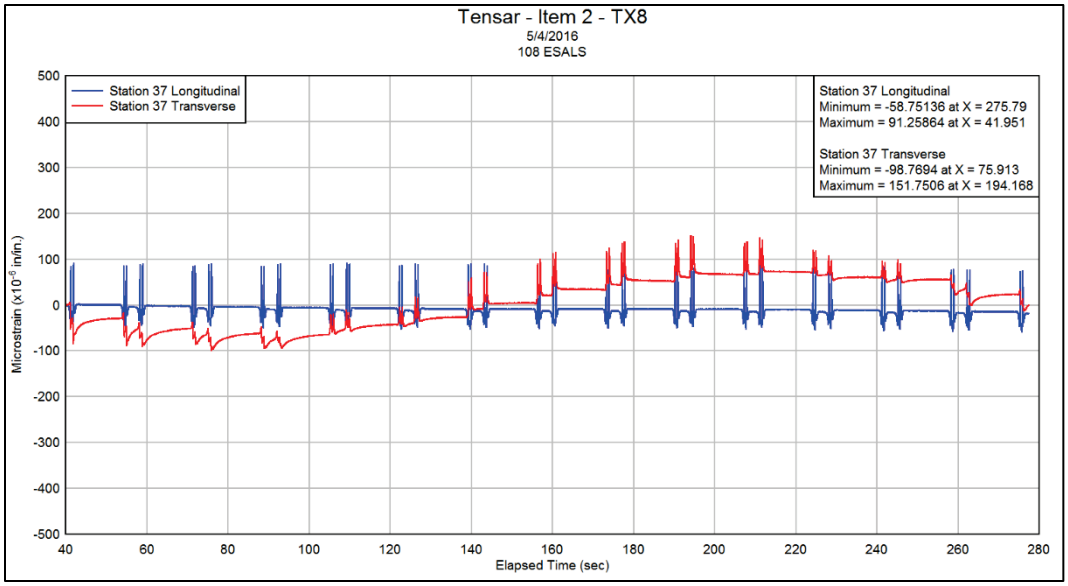

Tensar - Item 2 - TX8
5/2/2016
0 ESALS
Station 12.5 Longitudinal
Station 12.5 Transverse
Station 12.5 Longitudinal
Minimum = -88.17012 at X = 440.973
Maximum = 93.02688 at X = 368.872
Station 12.5 Transverse
Minimum = -106.6132 at X = 525.619
Maximum = 136.4645 at X = 407.558
Microstrain (x10^-6 in/in.)
Elapsed Time (sec)

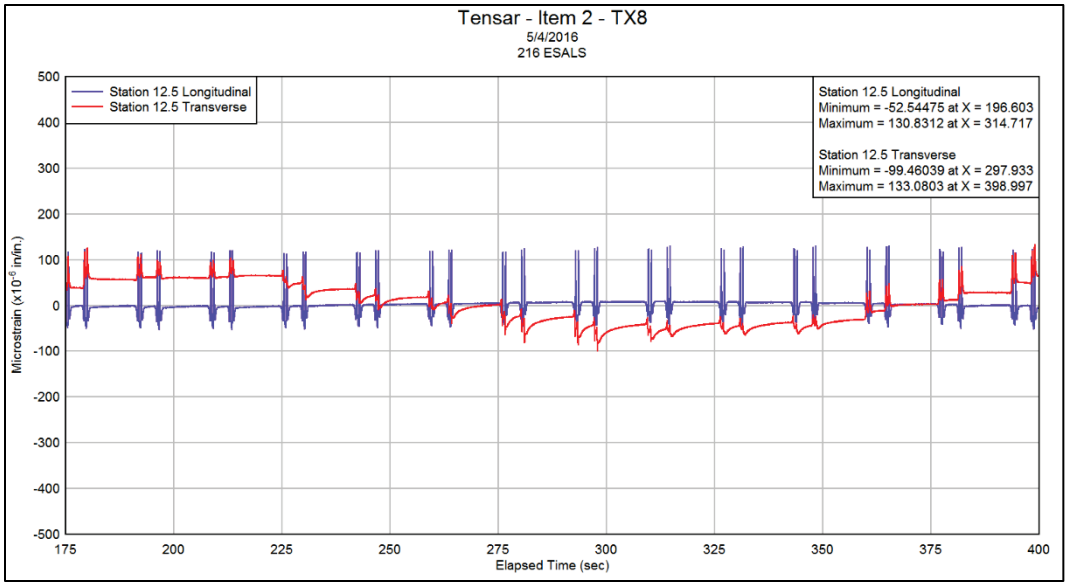

Tensar - Item 2 - TX8
5/2/2016
0 ESALS
Station 37 Longitudinal
Station 37 Transverse
Station 37 Longitudinal
Minimum = -109.7801 at X = 580.266
Maximum = 62.39992 at X = 364.395
Station 37 Transverse
Minimum = -80.81604 at X = 516.675
Maximum = 166.8 at X = 381.842
Microstrain (x10^-6 in/in.)
Elapsed Time (sec)

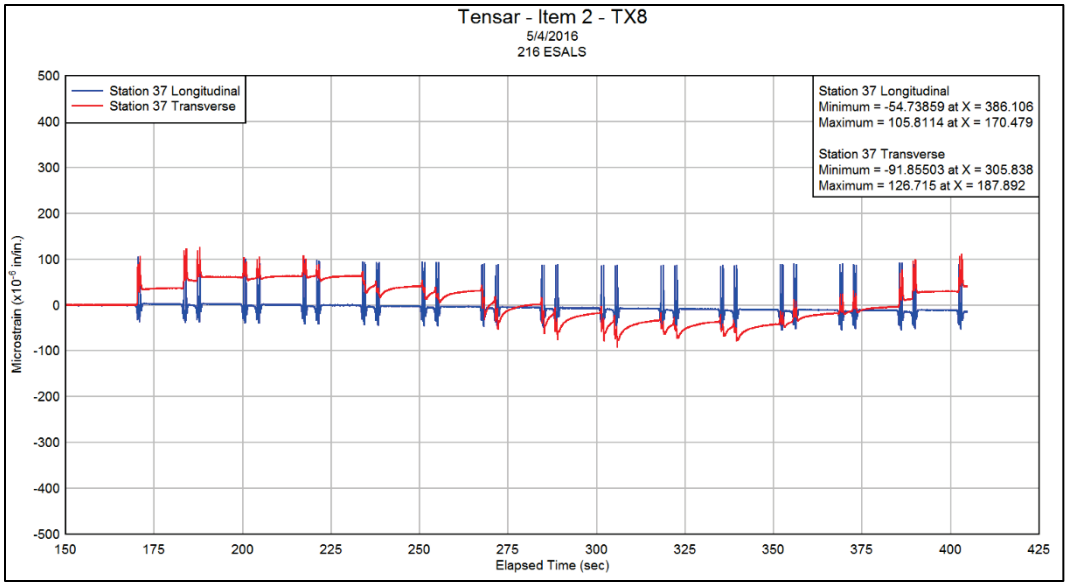

Tensar - Item 2 - TX8
5/3/2016
54 ESALS
Station 12.5 Longitudinal
Station 12.5 Transverse
Station 12.5 Longitudinal
Minimum = -88.6382 at X = 176.838
Maximum = 102.3638 at X = 54.046
Station 12.5 Transverse
Minimum = -123.9937 at X = 261.453
Maximum = 137.6149 at X = 126.434
Microstrain (x10-6 in/in.)
Elapsed Time (sec)

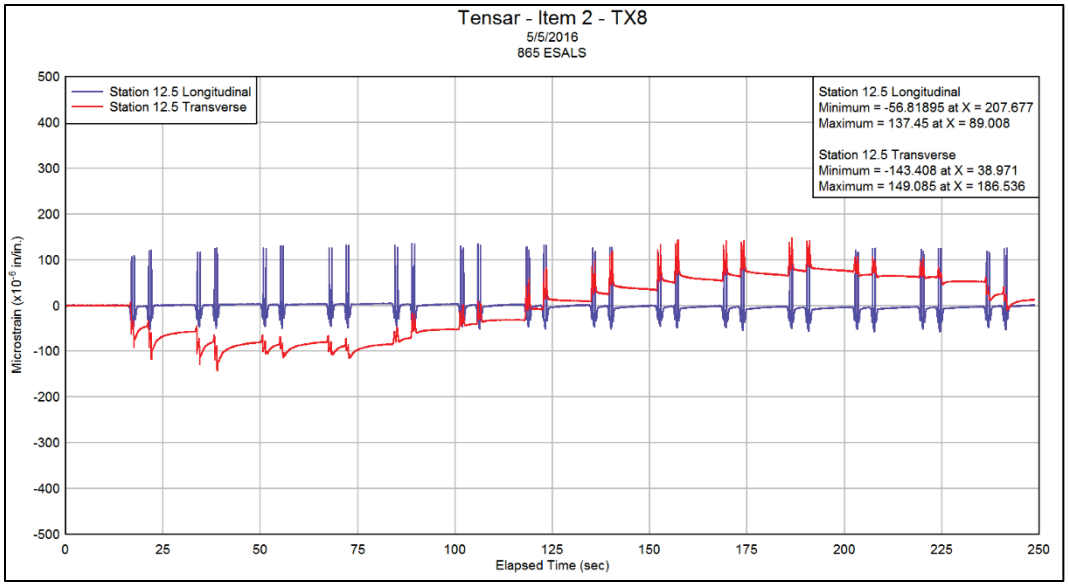

Tensar - Item 2 - TX8
5/3/2016
54 ESALS
Station 37 Longitudinal
Station 37 Transverse
Station 37 Longitudinal
Minimum = -54.2915 at X = 265.37
Maximum = 98.9885 at X = 49.547
Station 37 Transverse
Minimum = -39.34484 at X = 265.651
Maximum = 180.3142 at X = 147.496
Microstrain (x10-6 in/in.)
Elapsed Time (sec)

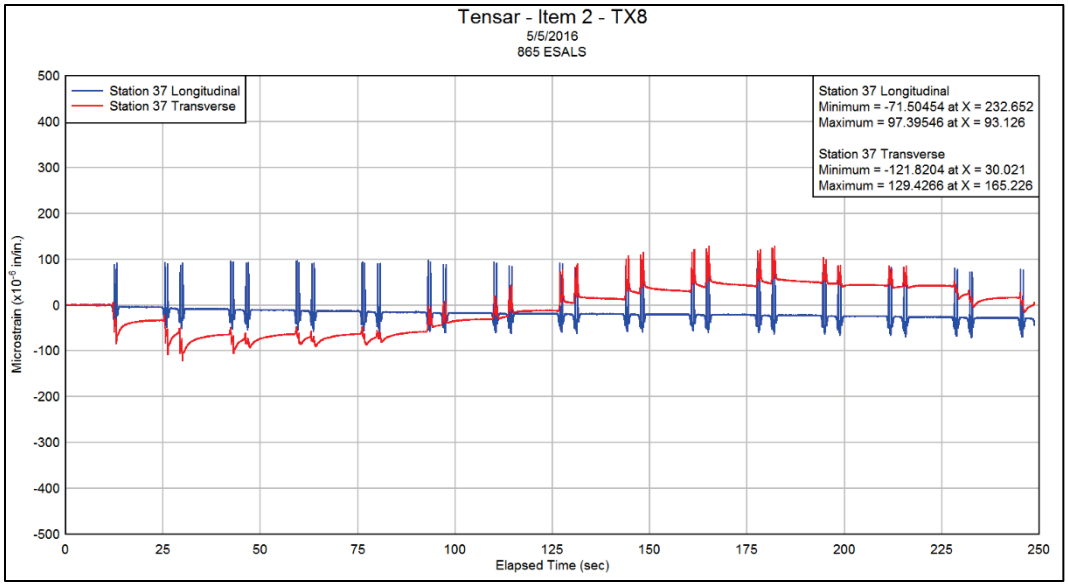

Tensar - Item 2 - TX8
5/4/2016
108 ESALS
Station 12.5 Longitudinal
Station 12.5 Transverse
Station 12.5 Longitudinal
Minimum = -55.62583 at X = 254.623
Maximum = 124.1192 at X = 96.898
Station 12.5 Transverse
Minimum = -92.59969 at X = 50.942
Maximum = 158.4723 at X = 220.801
Microstrain (x10-6 in/in.)
Elapsed Time (sec)

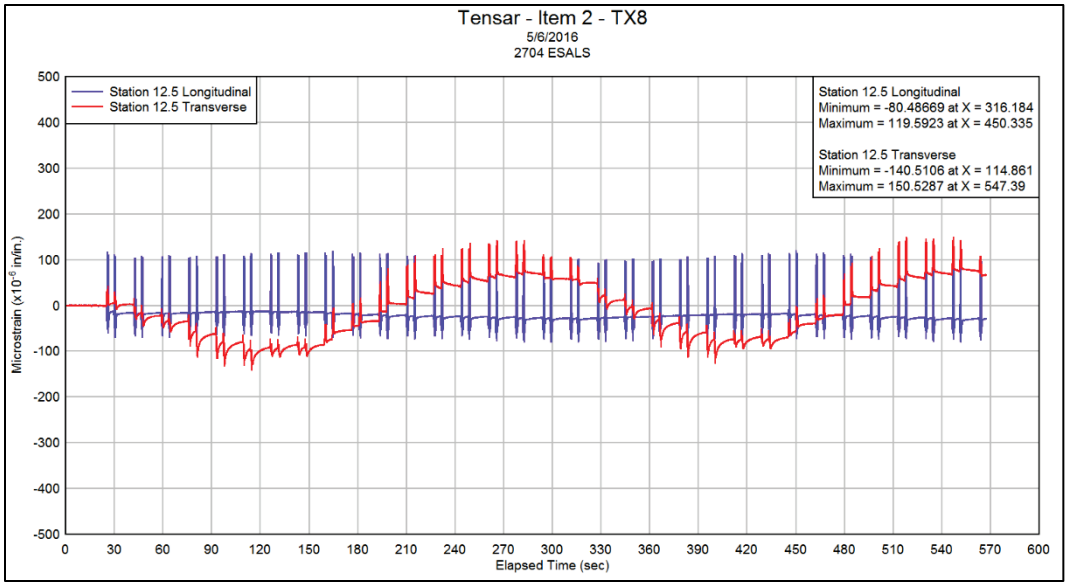

Tensar - Item 2 - TX8
5/4/2016
108 ESALS
Station 37 Longitudinal
Station 37 Transverse
Station 37 Longitudinal
Minimum = -58.75136 at X = 275.79
Maximum = 91.25864 at X = 41.951
Station 37 Transverse
Minimum = -98.7694 at X = 75.913
Maximum = 151.7506 at X = 194.168
Microstrain (x10-6 in/in.)
Elapsed Time (sec)

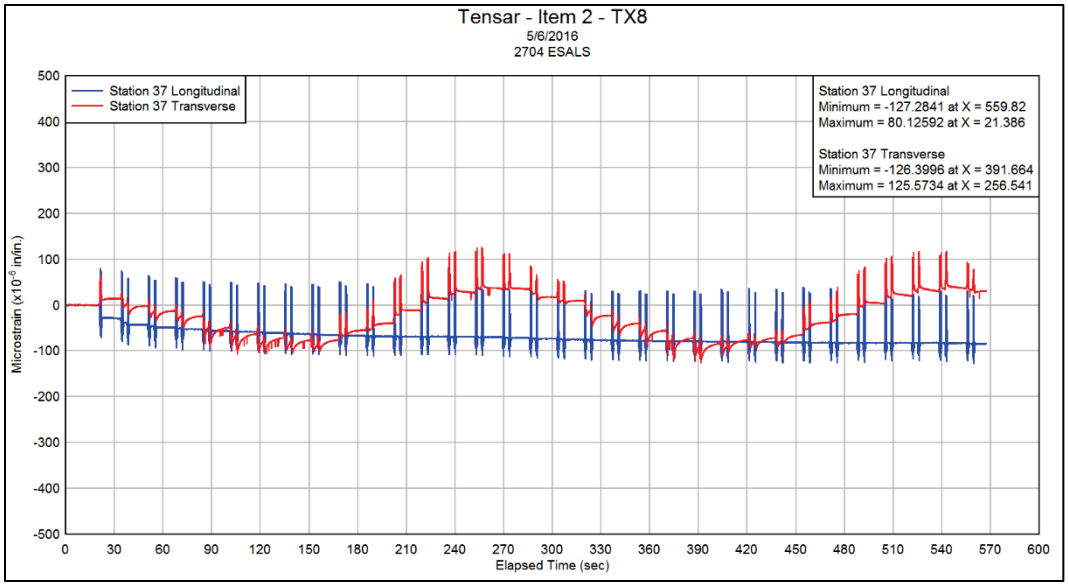

Tensar - Item 2 - TX8
5/4/2016
216 ESALS
Station 12.5 Longitudinal
Station 12.5 Transverse
Station 12.5 Longitudinal
Minimum = -52.54475 at X = 196.603
Maximum = 130.8312 at X = 314.717
Station 12.5 Transverse
Minimum = -99.46039 at X = 297.933
Maximum = 133.0803 at X = 398.997
Microstrain (x10-6 in/in.)
Elapsed Time (sec)

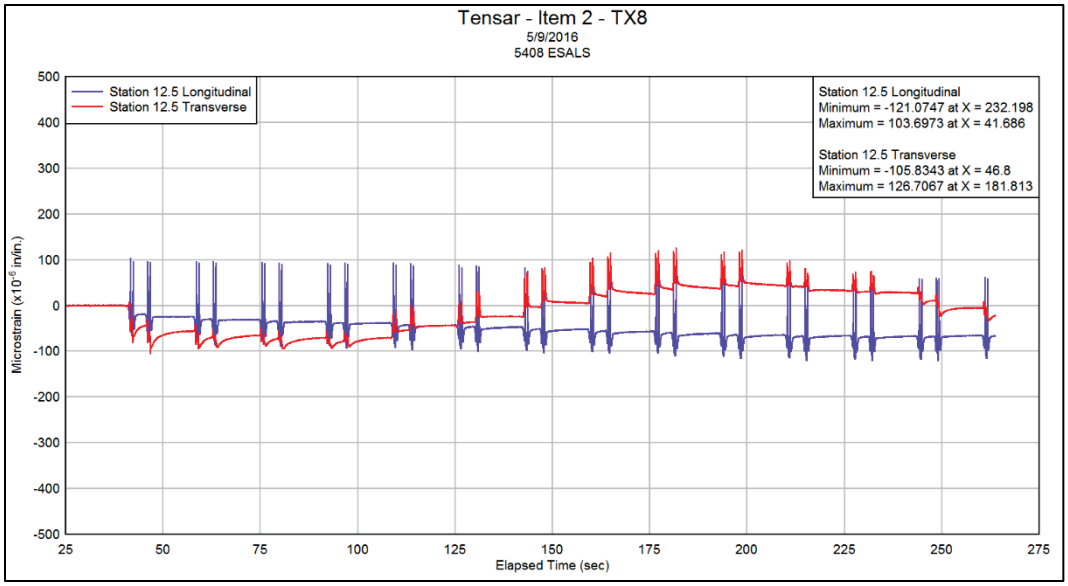

Tensar - Item 2 - TX8
5/4/2016
216 ESALS
Station 37 Longitudinal
Station 37 Transverse
Station 37 Longitudinal
Minimum = -54.73859 at X = 386.106
Maximum = 105.8114 at X = 170.479
Station 37 Transverse
Minimum = -91.85503 at X = 305.838
Maximum = 126.715 at X = 187.892
Microstrain (x10-6 in/in.)
Elapsed Time (sec)

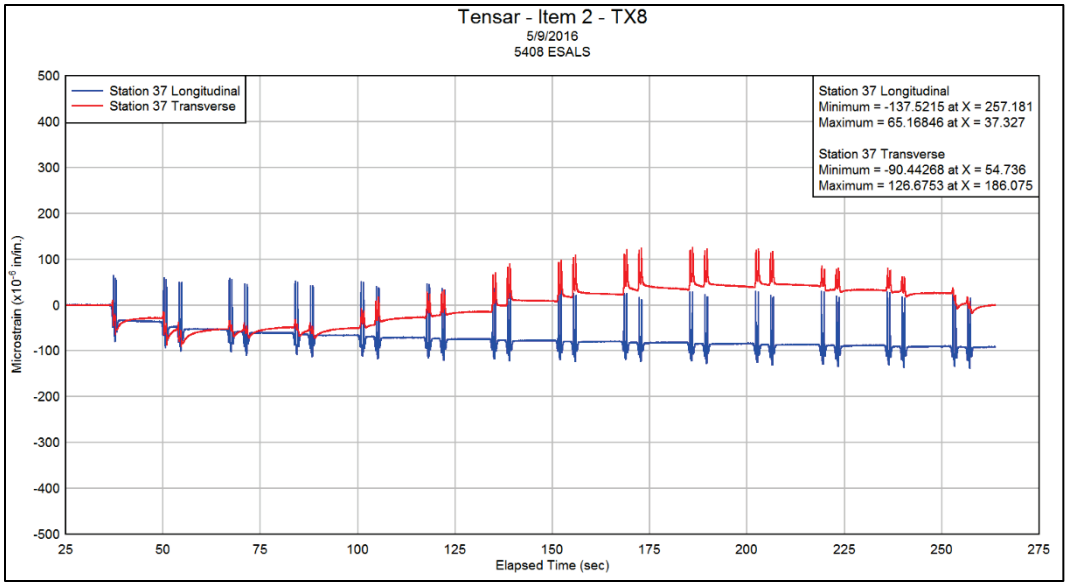

Tensar - Item 2 - TX8
5/5/2016
865 ESALS
Station 12.5 Longitudinal
Station 12.5 Transverse
Station 12.5 Longitudinal
Minimum = -56.81895 at X = 207.677
Maximum = 137.45 at X = 89.008
Station 12.5 Transverse
Minimum = -143.408 at X = 38.971
Maximum = 149.085 at X = 186.536
Microstrain (x10-6 in/in.)
Elapsed Time (sec)

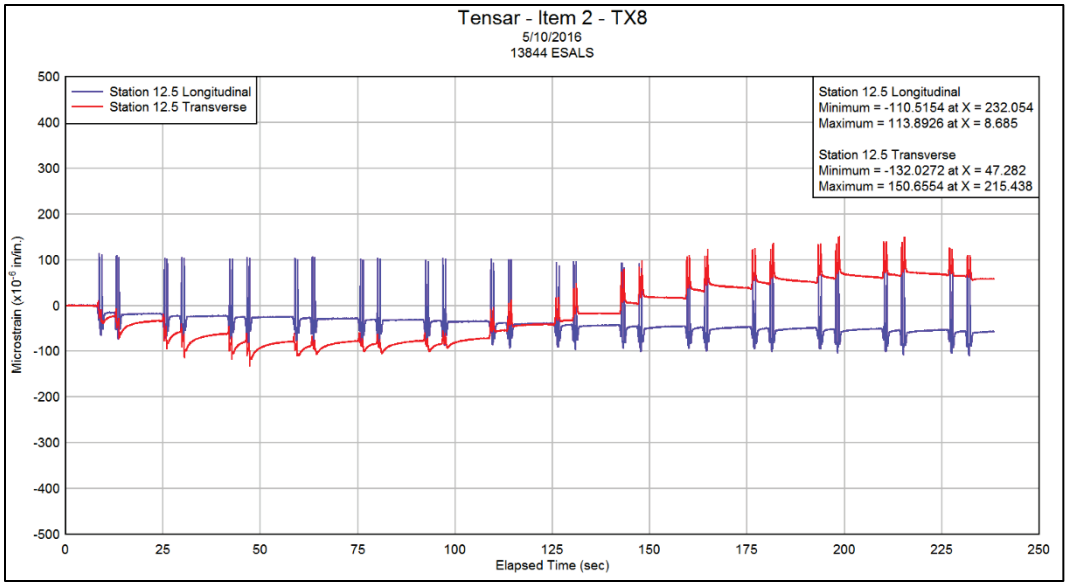

Tensar - Item 2 - TX8
5/5/2016
865 ESALS
Station 37 Longitudinal
Station 37 Transverse
Station 37 Longitudinal
Minimum = -71.50454 at X = 232.652
Maximum = 97.39546 at X = 93.126
Station 37 Transverse
Minimum = -121.8204 at X = 30.021
Maximum = 129.4266 at X = 165.226
Microstrain (x10-6 in/in.)
Elapsed Time (sec)

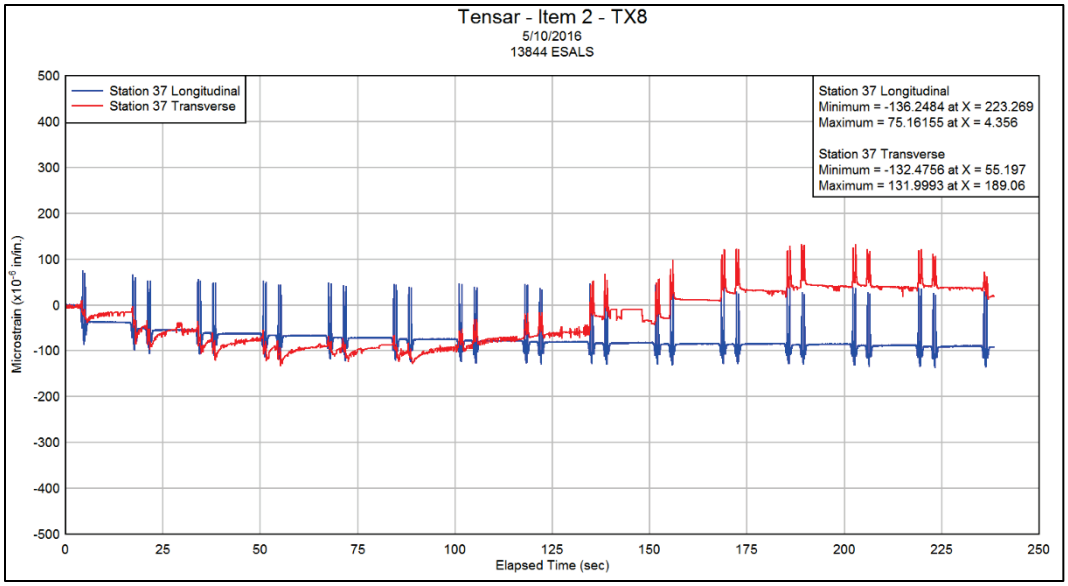

Tensar - Item 2 - TX8
5/6/2016
2704 ESALS
Station 12.5 Longitudinal
Station 12.5 Transverse
Station 12.5 Longitudinal
Minimum = -80.48669 at X = 316.184
Maximum = 119.5923 at X = 450.335
Station 12.5 Transverse
Minimum = -140.5106 at X = 114.861
Maximum = 150.5287 at X = 547.39
Microstrain (x10-6 in/in.)
Elapsed Time (sec)

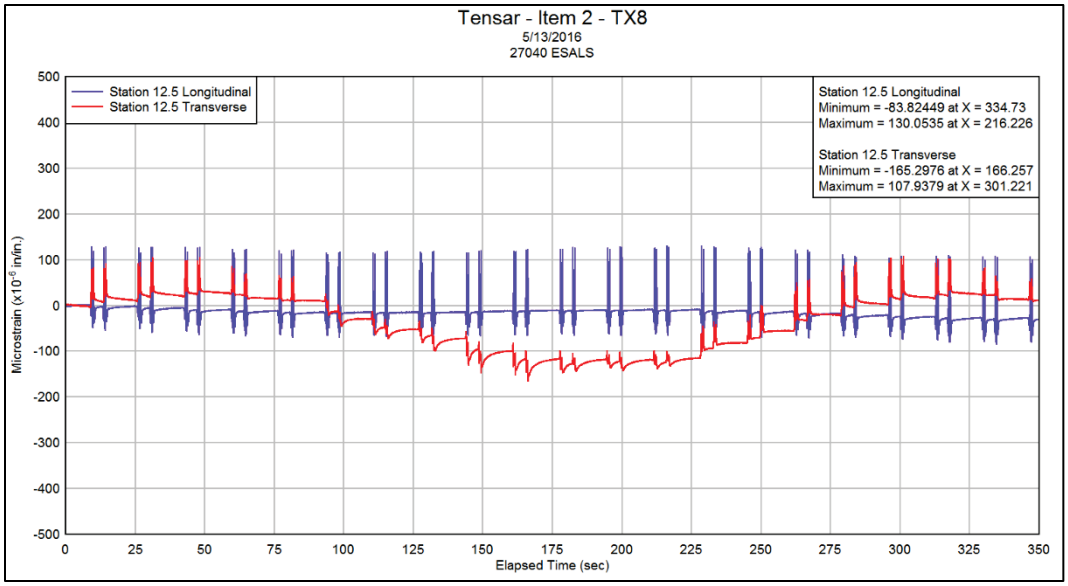

Tensar - Item 2 - TX8
5/6/2016
2704 ESALS
Station 37 Longitudinal
Station 37 Transverse
Station 37 Longitudinal
Minimum = -127.2841 at X = 559.82
Maximum = 80.12592 at X = 21.386
Station 37 Transverse
Minimum = -126.3996 at X = 391.664
Maximum = 125.5734 at X = 256.541
Microstrain (x10-6 in/in.)
Elapsed Time (sec)

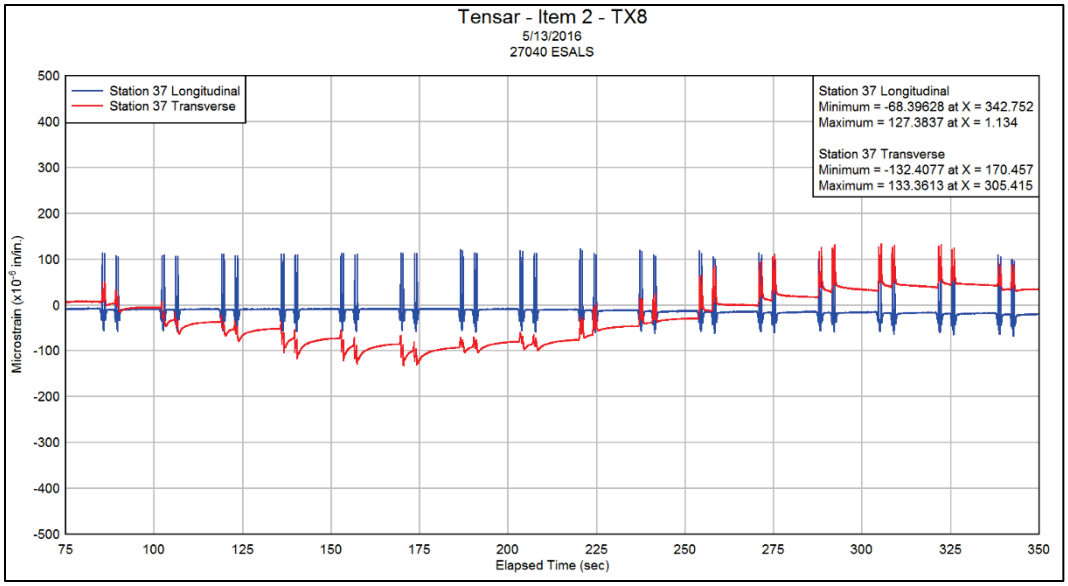

Tensar - Item 2 - TX8
5/9/2016
5408 ESALS
Station 12.5 Longitudinal
Station 12.5 Transverse
Station 12.5 Longitudinal
Minimum = -121.0747 at X = 232.198
Maximum = 103.6973 at X = 41.686
Station 12.5 Transverse
Minimum = -105.8343 at X = 46.8
Maximum = 126.7067 at X = 181.813
Microstrain (x10-6 in/in.)
Elapsed Time (sec)

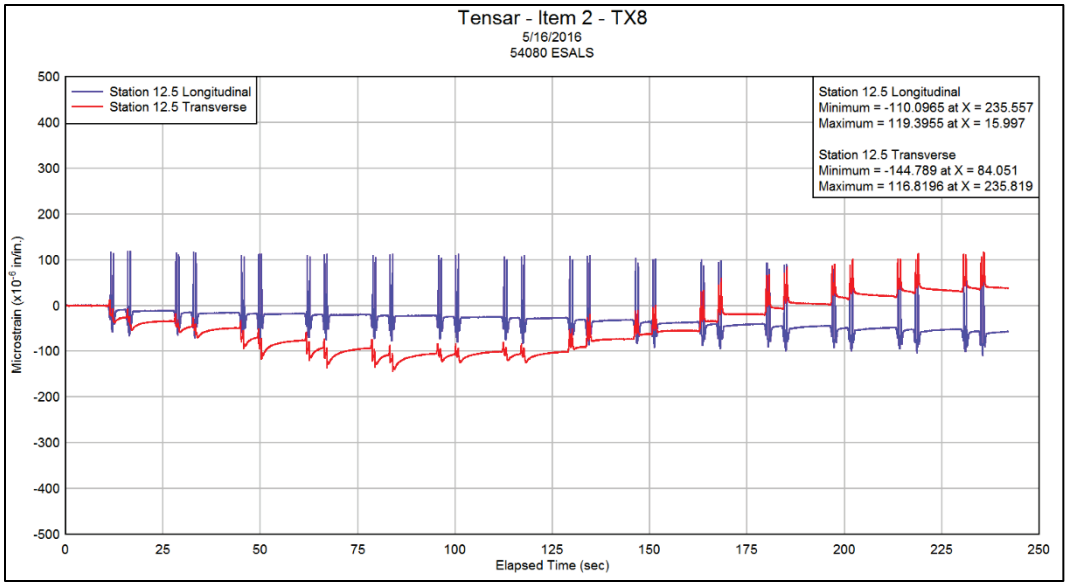

Tensar - Item 2 - TX8
5/9/2016
5408 ESALS
Station 37 Longitudinal
Station 37 Transverse
Station 37 Longitudinal
Minimum = -137.5215 at X = 257.181
Maximum = 65.16846 at X = 37.327
Station 37 Transverse
Minimum = -90.44268 at X = 54.736
Maximum = 126.6753 at X = 186.075
Microstrain (x10-6 in/in.)
Elapsed Time (sec)

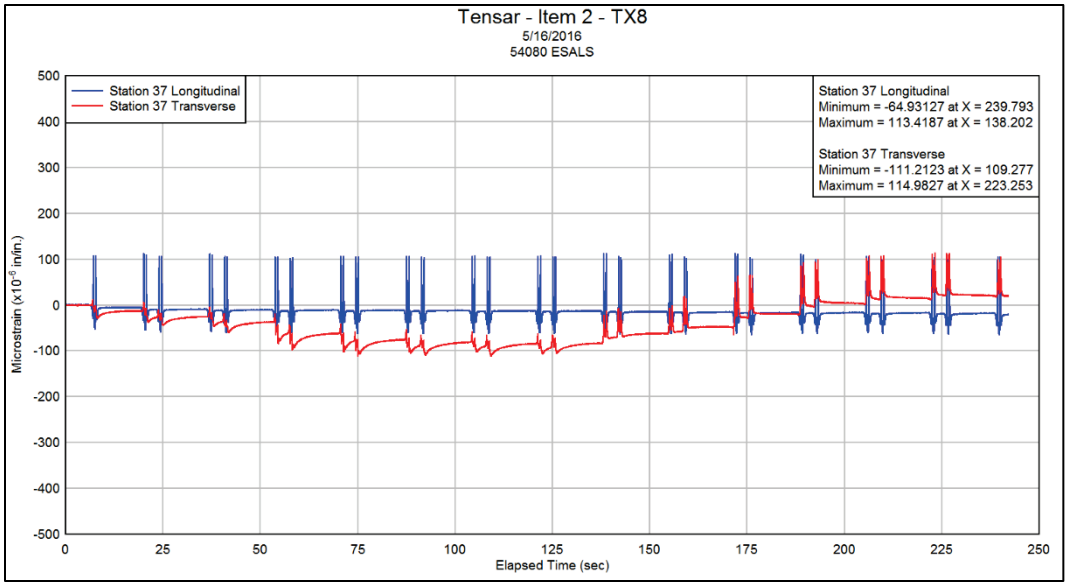

Tensar - Item 2 - TX8
5/10/2016
13844 ESALS
Station 12.5 Longitudinal
Station 12.5 Transverse
Station 12.5 Longitudinal
Minimum = -110.5154 at X = 232.054
Maximum = 113.8926 at X = 8.685
Station 12.5 Transverse
Minimum = -132.0272 at X = 47.282
Maximum = 150.6554 at X = 215.438
Microstrain (x10-6 in/in.)
Elapsed Time (sec)

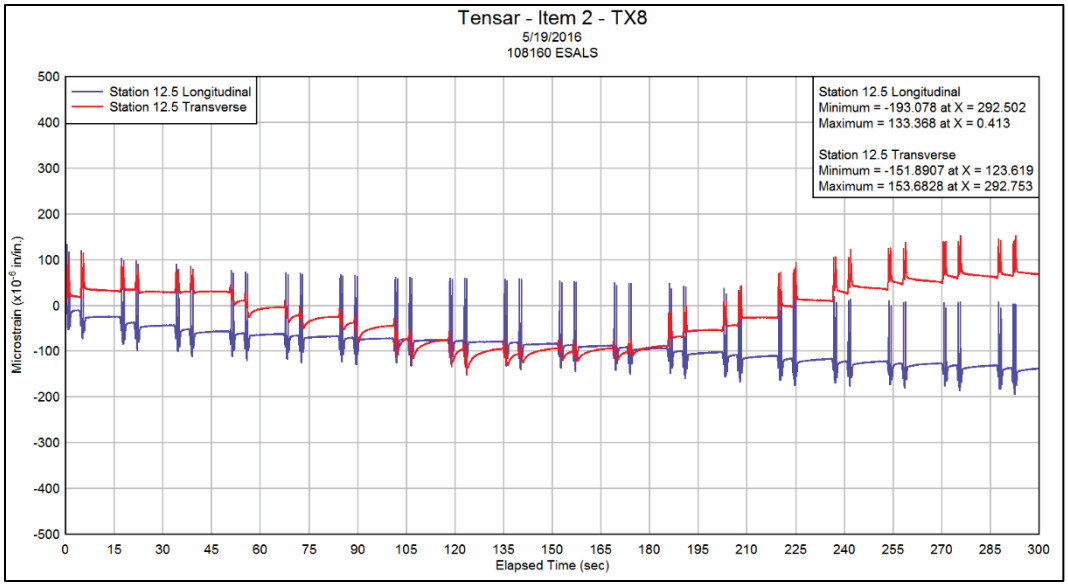

Tensar - Item 2 - TX8
5/10/2016
13844 ESALS
Station 37 Longitudinal
Station 37 Transverse
Station 37 Longitudinal
Minimum = -136.2484 at X = 223.269
Maximum = 75.16155 at X = 4.356
Station 37 Transverse
Minimum = -132.4756 at X = 55.197
Maximum = 131.9993 at X = 189.06
Microstrain (x10-6 in/in.)
Elapsed Time (sec)

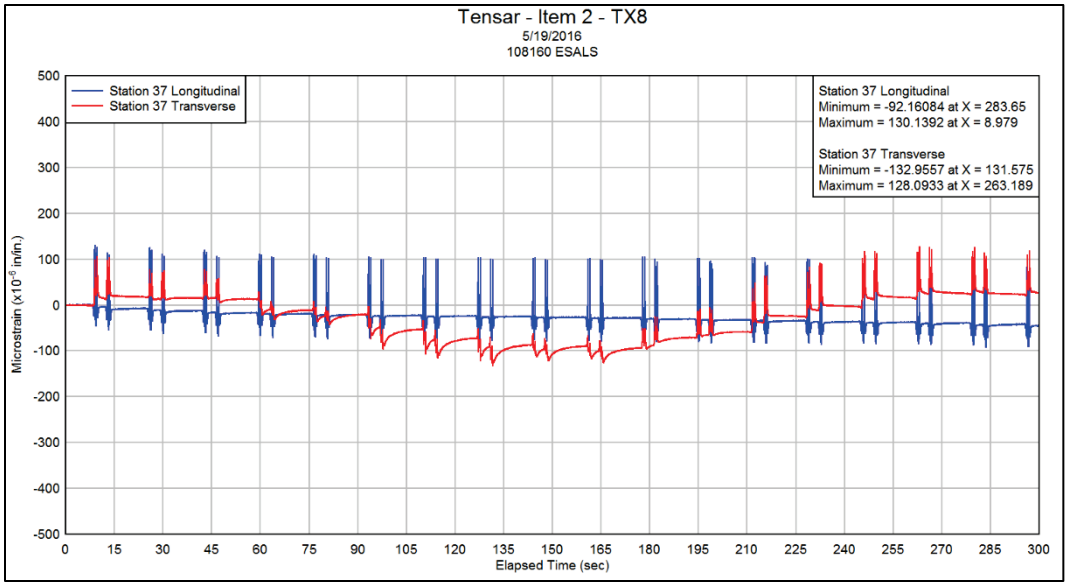

Tensar - Item 2 - TX8
5/13/2016
27040 ESALS
Station 12.5 Longitudinal
Station 12.5 Transverse
Station 12.5 Longitudinal
Minimum = -83.82449 at X = 334.73
Maximum = 130.0535 at X = 216.226
Station 12.5 Transverse
Minimum = -165.2976 at X = 166.257
Maximum = 107.9379 at X = 301.221
Microstrain (x10-6 in/in.)
Elapsed Time (sec)

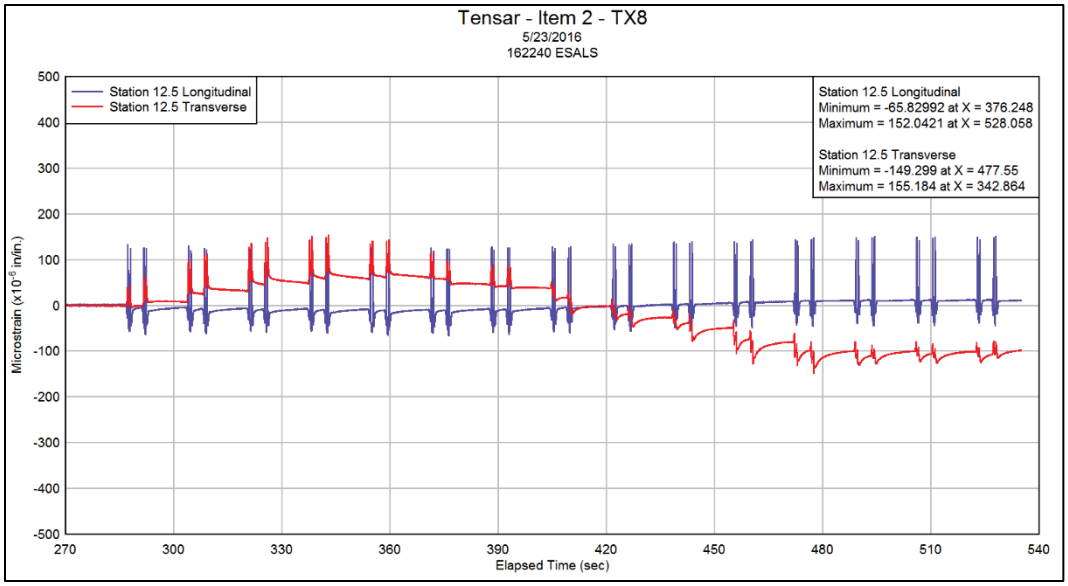

Tensar - Item 2 - TX8
5/13/2016
27040 ESALS
Station 37 Longitudinal
Station 37 Transverse
Station 37 Longitudinal
Minimum = -68.39628 at X = 342.752
Maximum = 127.3837 at X = 1.134
Station 37 Transverse
Minimum = -132.4077 at X = 170.457
Maximum = 133.3613 at X = 305.415
Microstrain (x10-6 in/in.)
Elapsed Time (sec)

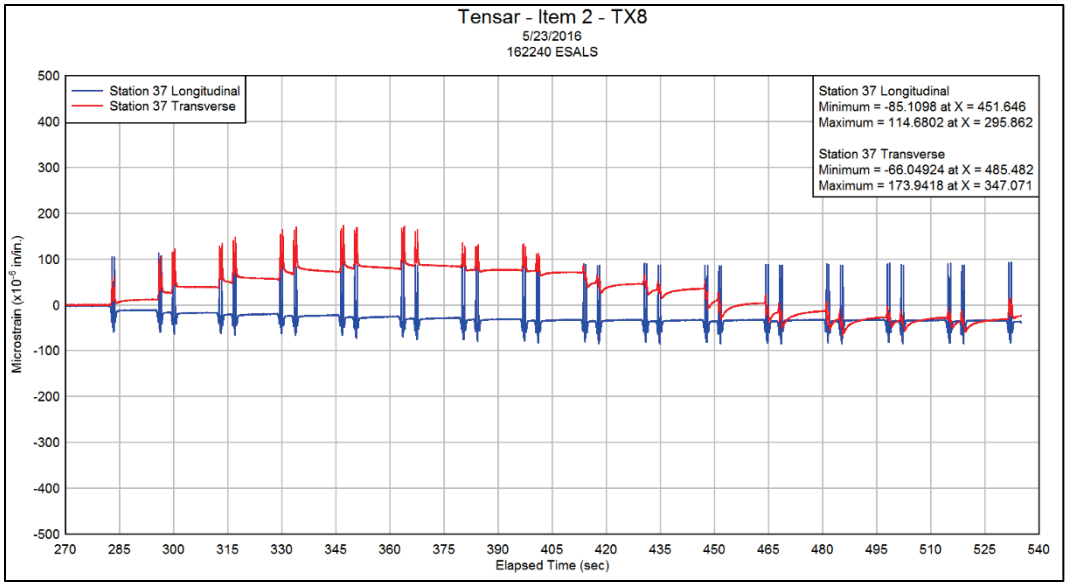

Tensar - Item 2 - TX8
5/16/2016
54080 ESALS
Station 12.5 Longitudinal
Station 12.5 Transverse
Station 12.5 Longitudinal
Minimum = -110.0965 at X = 235.557
Maximum = 119.3955 at X = 15.997
Station 12.5 Transverse
Minimum = -144.789 at X = 84.051
Maximum = 116.8196 at X = 235.819
Microstrain (x10^-6 in/in.)
Elapsed Time (sec)

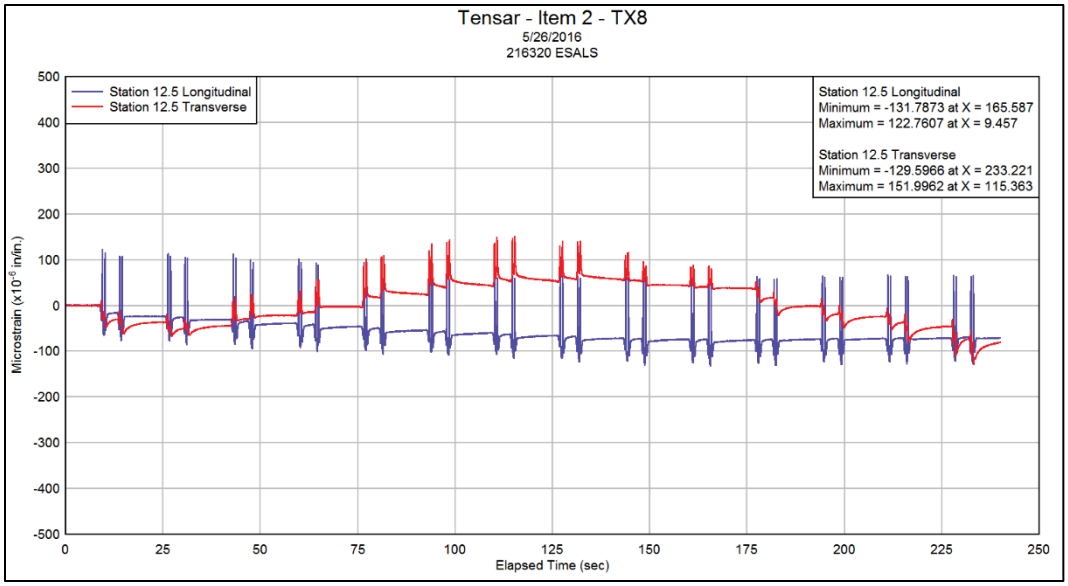

Tensar - Item 2 - TX8
5/16/2016
54080 ESALS
Station 37 Longitudinal
Station 37 Transverse
Station 37 Longitudinal
Minimum = -64.93127 at X = 239.793
Maximum = 113.4187 at X = 138.202
Station 37 Transverse
Minimum = -111.2123 at X = 109.277
Maximum = 114.9827 at X = 223.253
Microstrain (x10^-6 in/in.)
Elapsed Time (sec)

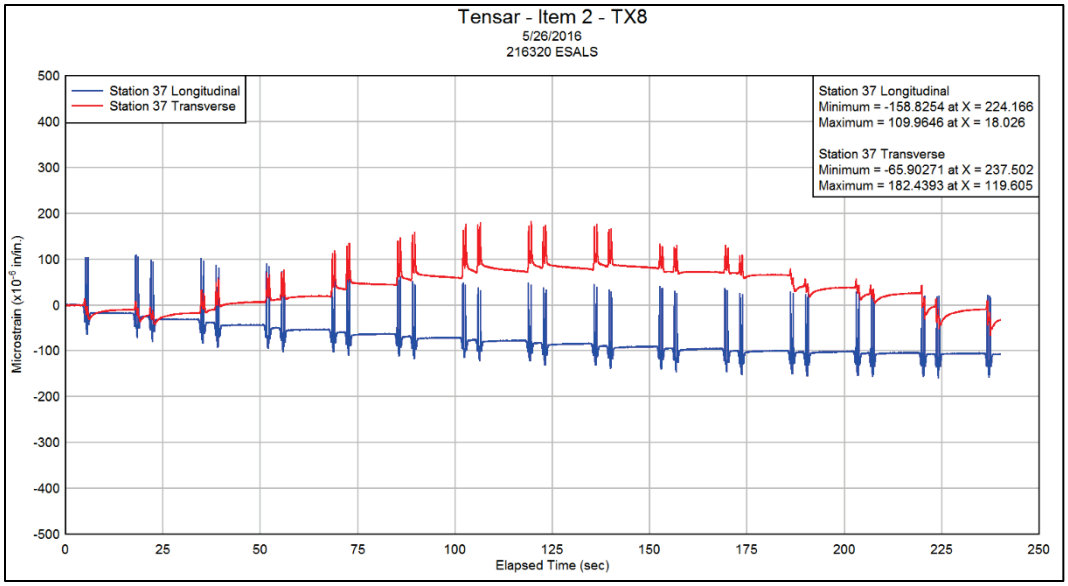

Tensar - Item 2 - TX8
5/19/2016
108160 ESALS
Station 12.5 Longitudinal
Station 12.5 Transverse
Station 12.5 Longitudinal
Minimum = -193.078 at X = 292.502
Maximum = 133.368 at X = 0.413
Station 12.5 Transverse
Minimum = -151.8907 at X = 123.619
Maximum = 153.6828 at X = 292.753
Microstrain (x10^-6 in/in.)
Elapsed Time (sec)

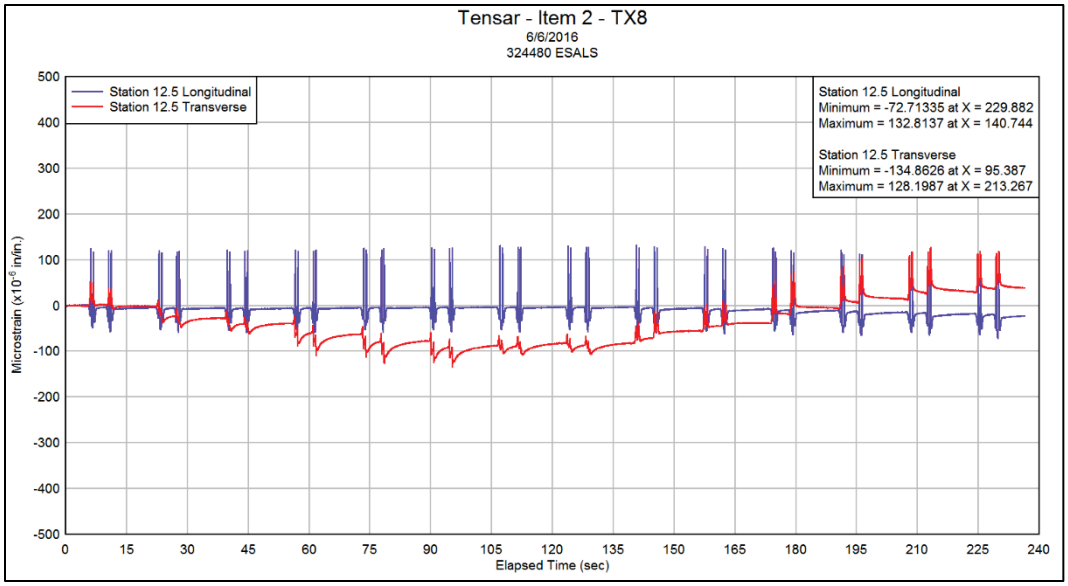

Tensar - Item 2 - TX8
5/19/2016
108160 ESALS
Station 37 Longitudinal
Station 37 Transverse
Station 37 Longitudinal
Minimum = -92.16084 at X = 283.65
Maximum = 130.1392 at X = 8.979
Station 37 Transverse
Minimum = -132.9557 at X = 131.575
Maximum = 128.0933 at X = 263.189
Microstrain (x10^-6 in/in.)
Elapsed Time (sec)

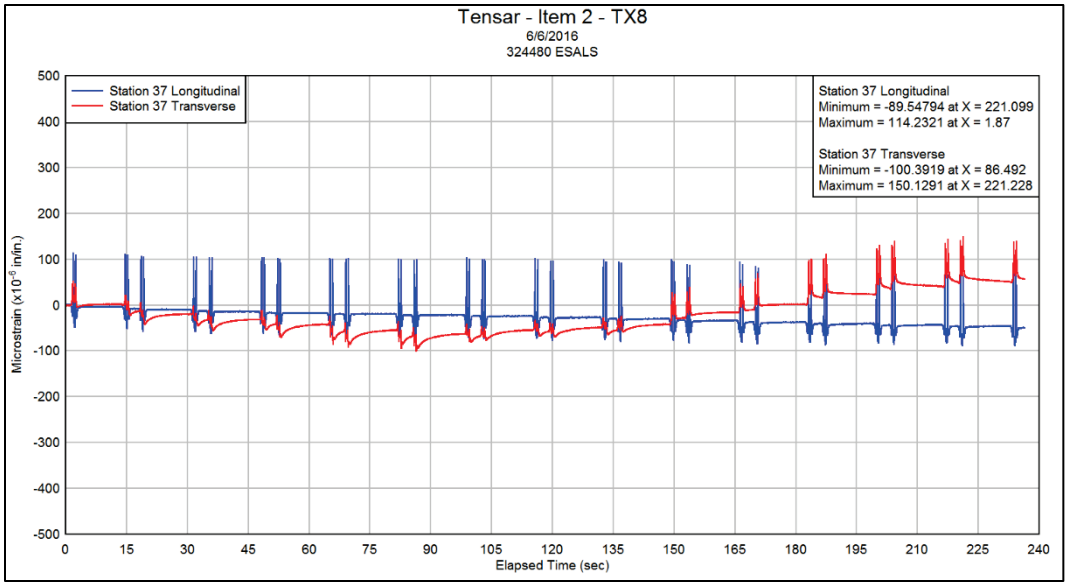

Tensar - Item 2 - TX8
5/23/2016
162240 ESALS
Station 12.5 Longitudinal
Station 12.5 Transverse
Station 12.5 Longitudinal
Minimum = -65.82992 at X = 376.248
Maximum = 152.0421 at X = 528.058
Station 12.5 Transverse
Minimum = -149.299 at X = 477.55
Maximum = 155.184 at X = 342.864
Microstrain (x10-6 in/in.)
Elapsed Time (sec)

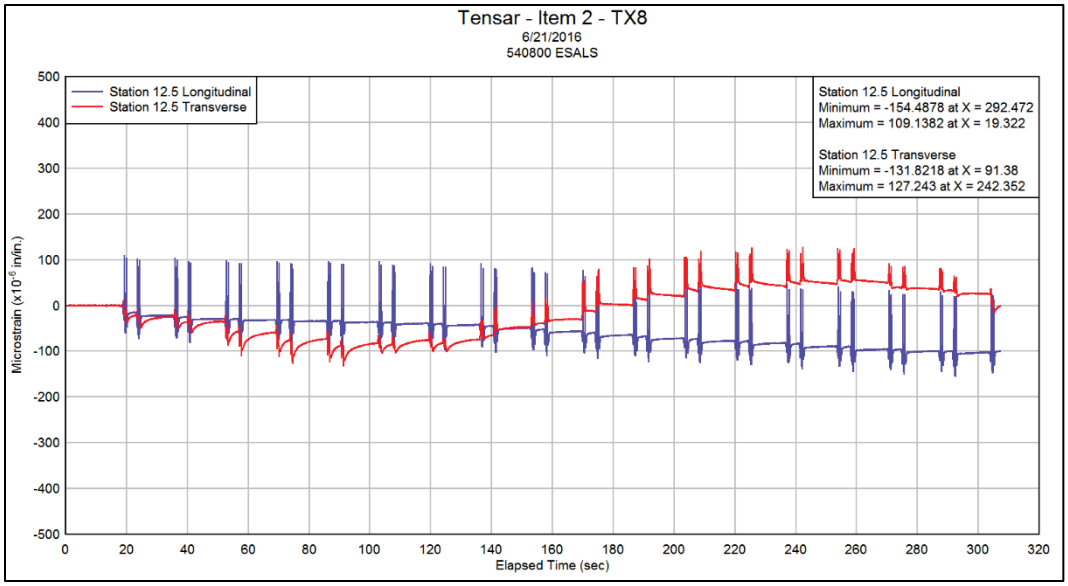

Tensar - Item 2 - TX8
5/23/2016
162240 ESALS
Station 37 Longitudinal
Station 37 Transverse
Station 37 Longitudinal
Minimum = -85.1098 at X = 451.646
Maximum = 114.6802 at X = 295.862
Station 37 Transverse
Minimum = -66.04924 at X = 485.482
Maximum = 173.9418 at X = 347.071
Microstrain (x10-6 in/in.)
Elapsed Time (sec)

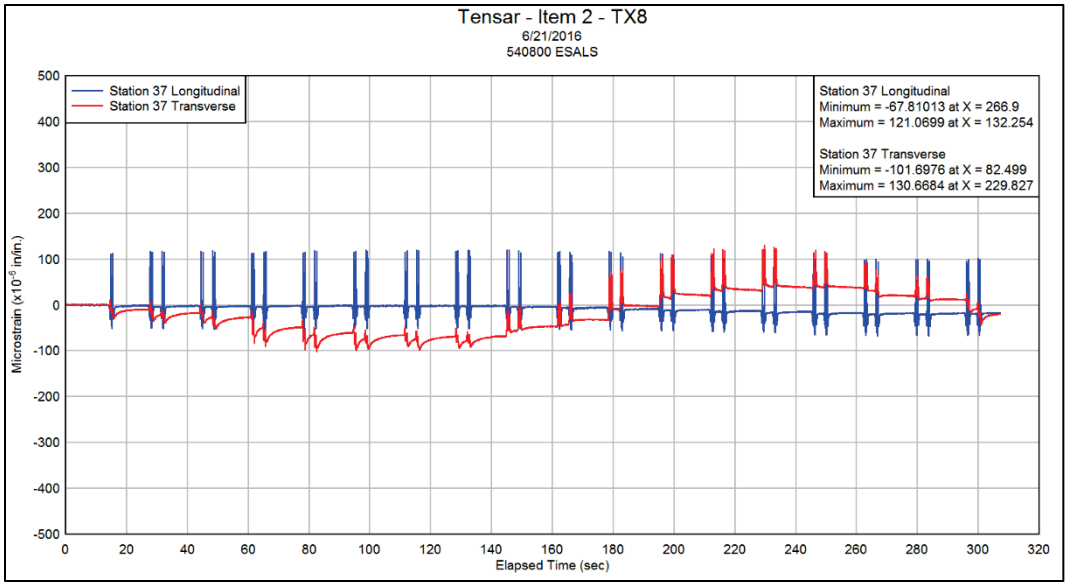

Tensar - Item 2 - TX8
5/26/2016
216320 ESALS
Station 12.5 Longitudinal
Station 12.5 Transverse
Station 12.5 Longitudinal
Minimum = -131.7873 at X = 165.587
Maximum = 122.7607 at X = 9.457
Station 12.5 Transverse
Minimum = -129.5966 at X = 233.221
Maximum = 151.9962 at X = 115.363
Microstrain (x10-6 in/in.)
Elapsed Time (sec)

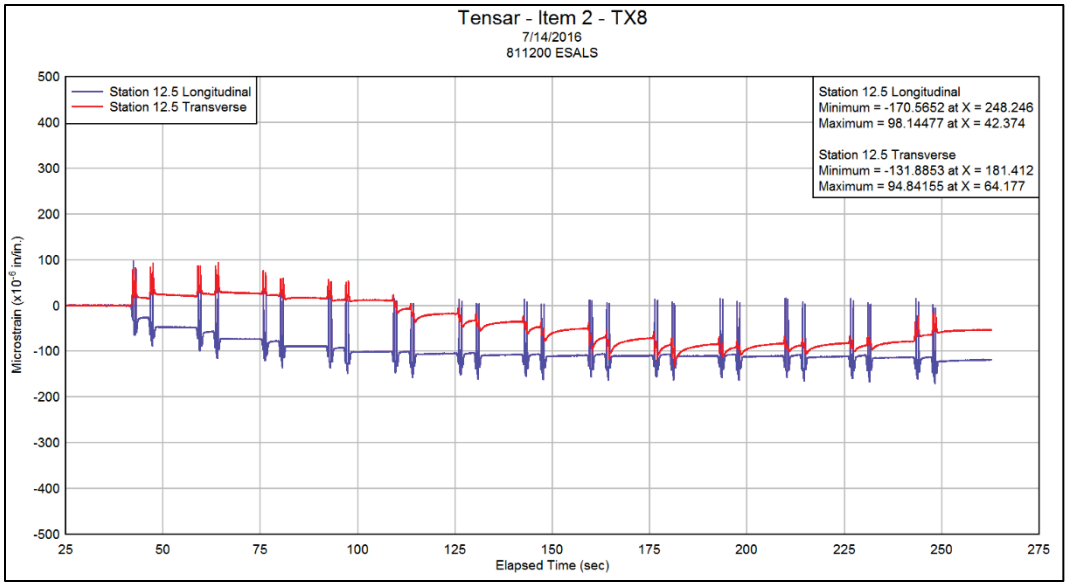

Tensar - Item 2 - TX8
5/26/2016
216320 ESALS
Station 37 Longitudinal
Station 37 Transverse
Station 37 Longitudinal
Minimum = -158.8254 at X = 224.166
Maximum = 109.9646 at X = 18.026
Station 37 Transverse
Minimum = -65.90271 at X = 237.502
Maximum = 182.4393 at X = 119.605
Microstrain (x10-6 in/in.)
Elapsed Time (sec)

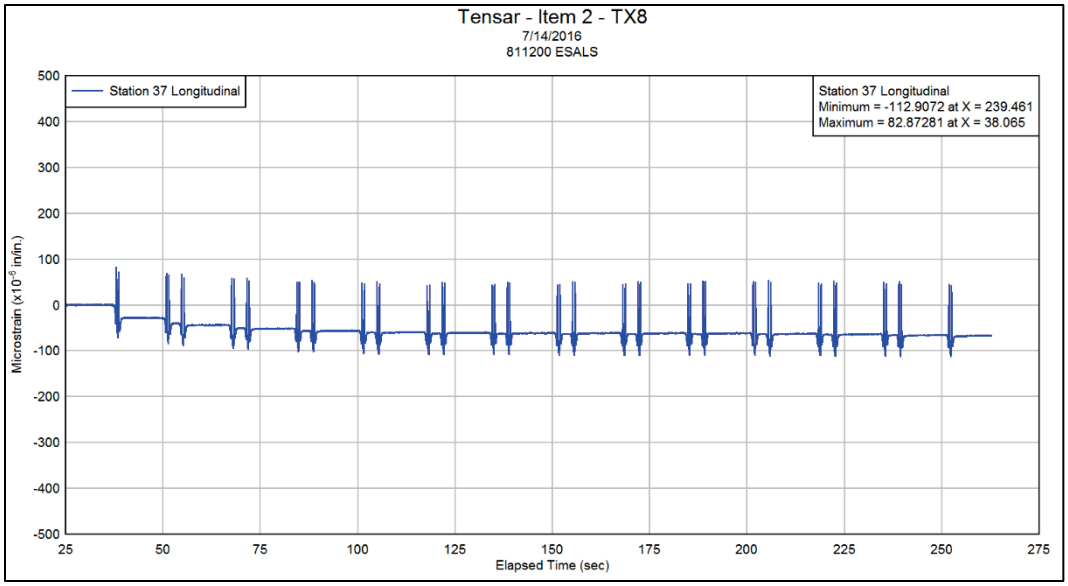

Tensar - Item 2 - TX8
6/6/2016
324480 ESALS
Station 12.5 Longitudinal
Station 12.5 Transverse
Station 12.5 Longitudinal
Minimum = -72.71335 at X = 229.882
Maximum = 132.8137 at X = 140.744
Station 12.5 Transverse
Minimum = -134.8626 at X = 95.387
Maximum = 128.1987 at X = 213.267
Microstrain (x10-6 in/in.)
Elapsed Time (sec)


Tensar - Item 2 - TX8
6/6/2016
324480 ESALS
Station 37 Longitudinal
Station 37 Transverse
Station 37 Longitudinal
Minimum = -89.54794 at X = 221.099
Maximum = 114.2321 at X = 1.87
Station 37 Transverse
Minimum = -100.3919 at X = 86.492
Maximum = 150.1291 at X = 221.228
Microstrain (x10-6 in/in.)
Elapsed Time (sec)


Tensar - Item 2 - TX8
6/21/2016
540800 ESALS
Station 12.5 Longitudinal
Station 12.5 Transverse
Station 12.5 Longitudinal
Minimum = -154.4878 at X = 292.472
Maximum = 109.1382 at X = 19.322
Station 12.5 Transverse
Minimum = -131.8218 at X = 91.38
Maximum = 127.243 at X = 242.352
Microstrain (x10^-6 in/in.)
Elapsed Time (sec)


Tensar - Item 2 - TX8
6/21/2016
540800 ESALS
Station 37 Longitudinal
Station 37 Transverse
Station 37 Longitudinal
Minimum = -67.81013 at X = 266.9
Maximum = 121.0699 at X = 132.254
Station 37 Transverse
Minimum = -101.6976 at X = 82.499
Maximum = 130.6684 at X = 229.827
Microstrain (x10^-6 in/in.)
Elapsed Time (sec)


Tensar - Item 2 - TX8
7/14/2016
811200 ESALS
Station 12.5 Longitudinal
Station 12.5 Transverse
Station 12.5 Longitudinal
Minimum = -170.5652 at X = 248.246
Maximum = 98.14477 at X = 42.374
Station 12.5 Transverse
Minimum = -131.8853 at X = 181.412
Maximum = 94.84155 at X = 64.177
Microstrain (x10-6 in/in.)
Elapsed Time (sec)


Tensar - Item 2 - TX8
7/14/2016
811200 ESALS
Station 37 Longitudinal
Station 37 Longitudinal
Minimum = -112.9072 at X = 239.461
Maximum = 82.87281 at X = 38.065
Microstrain (x10-6 in/in.)
Elapsed Time (sec)

# REPORT DOCUMENTATION PAGE

*Form Approved*
*OMB No. 0704-0188*

Public reporting burden for this collection of information is estimated to average 1 hour per response, including the time for reviewing instructions, searching existing data sources, gathering and maintaining the data needed, and completing and reviewing this collection of information. Send comments regarding this burden estimate or any other aspect of this collection of information, including suggestions for reducing this burden to Department of Defense, Washington Headquarters Services, Directorate for Information Operations and Reports (0704-0188), 1215 Jefferson Davis Highway, Suite 1204, Arlington, VA 22202-4302. Respondents should be aware that notwithstanding any other provision of law, no person shall be subject to any penalty for failing to comply with a collection of information if it does not display a currently valid OMB control number. **PLEASE DO NOT RETURN YOUR FORM TO THE ABOVE ADDRESS.**

| 1. REPORT DATE *(DD-MM-YYYY)* | 2. REPORT TYPE | 3. DATES COVERED *(From - To)* |
|---|---|---|
| June 2017 | Final | |

**4. TITLE AND SUBTITLE**

Full-Scale Accelerated Testing of Multi-axial Geogrid Stabilized Flexible Pavements

**5a. CONTRACT NUMBER**

**5b. GRANT NUMBER**

**5c. PROGRAM ELEMENT NUMBER**

**6. AUTHOR(S)**

W. Jeremy Robinson, P.E., Jeb S. Tingle, and Gregory J. Norwood, P.E.

**5d. PROJECT NUMBER**
151098

**5e. TASK NUMBER**

**5f. WORK UNIT NUMBER**

**7. PERFORMING ORGANIZATION NAME(S) AND ADDRESS(ES)**

Geotechnical and Structures Laboratory
U.S. Army Engineer Research and Development Center
3909 Halls Ferry Road
Vicksburg, MS 39180-6199

**8. PERFORMING ORGANIZATION REPORT NUMBER**

ERDC/GSL TR-17-9

**9. SPONSORING / MONITORING AGENCY NAME(S) AND ADDRESS(ES)**

Tensar International Corporation
Alpharetta, GA

**10. SPONSOR/MONITOR'S ACRONYM(S)**

**11. SPONSOR/MONITOR'S REPORT NUMBER(S)**

**12. DISTRIBUTION / AVAILABILITY STATEMENT**

Approved for public release; distribution is unlimited.

**13. SUPPLEMENTARY NOTES**

**14. ABSTRACT**

The U.S. Army Engineer Research and Development Center (ERDC) constructed a full-scale test section to evaluate the performance of geogrid-stabilized highway pavements. The test section consisted of two pavements composed of 3 in. of hot mix asphalt over a crushed limestone base course over a 6 CBR subgrade. One section was stabilized with Tensar's TX5 multi-axial geogrid, and the second section was stabilized with a developmental geogrid referred to as TX8. Each section was instrumented with moisture probes, pore-water pressure probes, temperature probes, earth pressure cells, and asphalt strain gauges. Simulated truck traffic was applied using a heavy vehicle simulator (HVS) to evaluate the rutting performance and collect instrumentation response data. This report summarizes the material characterization and construction techniques, instrumentation response, and performance response of each section under simulated truck traffic. Comparisons are drawn to previous sections constructed and trafficked at ERDC without geogrids utilizing similar construction techniques and material properties.

**15. SUBJECT TERMS**

Geogrid
Base stabilization
Pavements – Performance
Pavements – Testing
Effective structural coefficient
Pavements, Flexible
Heavy vehicle simulator
Geogrids
Soil stabilization

| 16. SECURITY CLASSIFICATION OF: | | | 17. LIMITATION OF ABSTRACT | 18. NUMBER OF PAGES | 19a. NAME OF RESPONSIBLE PERSON |
|---|---|---|---|---|---|
| a. REPORT | b. ABSTRACT | c. THIS PAGE | | | 19b. TELEPHONE NUMBER *(include area code)* |
| Unclassified | Unclassified | Unclassified | | 113 | |